uOttawa

L'Université canadienne
Canada's university

FACULTÉ DES ÉTUDES SUPÉRIEURES ET POSTOCTORALES

uOttawa

L'Université canadienne
Canada's university

FACULTY OF GRADUATE AND POSDOCTORAL STUDIES

Carmen Estey

AUTEUR DE LA THÈSE / AUTHOR OF THESIS

M.Sc. (Biochemistry)

GRADE / DEGREE

Department of Biochemistry

FACULTÉ, ÉCOLE, DÉPARTEMENT / FACULTY, SCHOOL, DEPARTMENT

Mitochondrial Uncoupling and Remodelling During Caloric Restriction : Implications for Oxidative Stress and Aging

TITRE DE LA THÈSE / TITLE OF THESIS

Mary-Ellen Harper

DIRECTEUR (DIRECTRICE) DE LA THÈSE / THESIS SUPERVISOR

CO-DIRECTEUR (CO-DIRECTRICE) DE LA THÈSE / THESIS CO-SUPERVISOR

Ilona Skerjanc

Jean-Michel Weber

Gary W. Slater

Le Doyen de la Faculté des études supérieures et postdoctorales / Dean of the Faculty of Graduate and Postdoctoral Studies

Mitochondrial uncoupling and remodelling during caloric restriction: Implications for oxidative stress and aging

M.Sc. Thesis of Carmen M. Estey

Supervisor: Mary-Ellen Harper, Ph.D.

A thesis submitted to the Faculty of Graduate and

Postdoctoral Studies in partial fulfilment of the

requirements for the degree of Masters of Science, Biochemistry

Faculty of Medicine

Department of Biochemistry, Microbiology, and Immunology

University of Ottawa

Ottawa, ON, Canada

Your file Votre référence
ISBN: 978-0-494-65501-6
Our file Notre référence
ISBN: 978-0-494-65501-6

ABSTRACT

The *'uncoupling to survive'* theory suggests that mitochondrial uncoupling protects cells from reactive oxygen species (ROS), thereby slowing aging. Caloric restriction (CR) mitigates aging; mechanisms may involve mitochondrial remodelling such that ROS production is decreased. It is unclear how uncoupling protein 3 (UCP3) in skeletal muscle is involved. Objective: To characterize effects of short-term 40% CR in wildtype (Wt) and UCP3 transgenic (UCP3 Tg) mice that possess uncoupled mitochondria. Hypothesis: In an uncoupled system, CR provides no further ROS protection. Approaches: Muscle mitochondrial and whole body assessments of UCP3's contribution to uncoupling and oxidative stress. Results: UCP3 Tg mice had lower body ($P<0.001$) and muscle weight ($P<0.01$), increased energy expenditure ($P=0.12$), similar body composition, increased proton leak ($P<0.05$), and decreased ROS production ($P<0.05$). In Wt mice, 1 mo CR mitigated ROS production ($P<0.05$), increased proton leak ($P<0.05$), decreased oxidative capacity ($P<0.01$), and increased UCP3 ($P<0.05$) protein levels. Such changes were not observed in UCP3 Tg mice. Overall, findings indicate that uncoupling in muscle does not reflect a pre-adaptation to CR. Rather, uncoupling delays the adaptive mitochondrial remodelling normally induced by short-term CR.

ACKNOWLEDGEMENTS

I would like to take this opportunity to thank those who have been instrumental in helping me complete my MSc degree at the University of Ottawa.

- Thank you Dr. Mary–Ellen Harper, my supervisor, for seeing something in me that no one before had. You believed in me and helped me accomplish something I never even imagined I could. Your constant support, endless encouragement and invaluable guidance are greatly appreciated and will never be forgotten. I will take all this with me as I move forward in my career and in life.

- Thank you Dr. Erin Seifert for the extensive amount of support you have given me along the way. I have learned so much from you and you have been such an outstanding colleague and friend. I do not know if I could have been here today without everything you have done for me. Words cannot express my gratitude and appreciation.

- Thank you Jian Xuan, Mahmoud Salkhordeh and Linda Jui for the constant technical assistance you provided to me.

- Thank you Dr. Ross Milne, Dr. Thomas Moon and Dr. Michael McBurney, my thesis advisory committee members, for your valuable time, support, and insight.

- Thank you to all the current and former Harper lab members especially Cynthia Moffat for always being there and motivating me whenever it was needed. I know the friendship we have made will last a lifetime.

- Thank you to my family and, of course, Mike for surrounding me with so much love and support. Your constant encouragement and understanding is what allowed me to be where I am today. Mike, I sincerely appreciate everything you have done for me and am extremely excited to become your wife and spend the rest of our lives together!

TABLE OF CONTENTS

LIST OF ABBREVIATIONS

A

ADP	adenosine 5'-diphosphate
AL	*ad libitum*
AMP	adenosine 5'-monophosphate
ANOVA	analysis of variance
ANT	adenine nucleotide translocase
ATP	adenosine 5'-triphosphate
A.U.	arbitrary units

B

BAT	brown adipose tissue
BM	basic medium
BMR	basal metabolic rate
BSA	bovine serum albumin
BW	body weight

C

CAT	carboxyatractylate
CO_2	carbon dioxide
CoA	coenzyme A
Complex I	NADH-CoQ reductase or NADH dehydrogenase
Complex II	succinate dehydrogenase
Complex III	cytochrome bc1 complex or CoQ-cytochrome c reductase
Complex IV	cytochrome c oxidase
Complex V	ATP synthase
COX	cytochrome c oxidase
CR	calorie restriction
CuZnSOD	copper zinc superoxide dismutase
cyt b	cytochrome b
cyt c	cytochrome c

D

DAB	diaminobenzidine
ddH_2O	deionized distilled water
DNA	deoxyribonucleic acid

E

e^-	electron

ECL	enhanced chemiluminescence
e.g.,	example
EGTA	ethylene glycol-bis tetraacetic acid
ETC	electron transport chain
ETF	electron transferring flavoprotein
ETF:QOR	electron transferring flavoprotein:quinine oxidoreductase

F

$FADH_2$	flavin adenine nucleotide dinucleotide (reduced form)
FCCP	carbonyl cyanide-p-trifluoromethoxyphenylhydrazone
Fe^{2+}	ferrous iron
Fe^{3+}	ferric iron
Fe-S	iron-sulfur

G

g	centrifugal force
g	gram
GDP	guanosine diphosphate
GPx	glutathione peroxidase
gWAT	gonadal white adipose tissue

H

H_2O	water
H_2O_2	hydrogen peroxide
4-HNE	4-hydroxy-2,3,-trans-nonenal
H^+	hydrogen
h	hours
HEPES	hydroxyethyl piperazine ethane sulfonic acid
HIF-1α	hypoxia-inducible factor 1-alpha
HM	homogenizing medium
HRP	horseradish peroxidase

I

i.e.	in other words
iBAT	interscapular brown adipose tissue
IGF-1R	insulin-like growth factor type 1 receptor gene
IgG	immunoglobulin G
IM	incubation medium

J

JNK	Jun-N-terminal kinase

K

KCl	potassium chloride
kDa	kilodalton
KH_2PO_4	potassium dihydrogen orthophosphate
KO	knockout

L

L	litre

M

mg	milligram
$MgCl_2$	magnesium chloride
MIM	mitochondrial inner membrane
min	minute
mL	millilitre
mM	millimol/litre
MnSOD	manganese superoxide dismutase
mo	month
mRNA	messenger RNA
MsrA	methionine sulfoxide reductase-A (protein form)
MsrA	methionine sulfoxide reductase-A (gene)
mtDNA	mitochondrial DNA
mV	millivolt

N

n	sample size
Na_2CO3	sodium carbonate
$Na_2S_2O_4$	sodium dithionite
NAD^+	oxidized nicotinamide adenine dinucleotide
NADH	reduced nicotinamide adenine dinucleotide
NADPH	nicotinamide adenine dinucleotide phosphate
nm	nanometre
nmol	nanomol
NST	non-shivering thermogenesis

O

O	monoatomic oxygen
O_2	molecular (diatomic) oxygen
$O_2^{\bullet-}$	superoxide
O.C.T.	Optimal Cutting Temperature Compound
OH^-	hydroxyl ion
$OH^\bullet$	hydroxyl radical

P

P_i	inorganic phosphate
PC	palmitoylcarnitine
PHPA	p-hydroxyphenyl acetic acid
PMF	protonmotive force

Q

Q	ubiquinone
Q-cycle	ubiquinone cycle
QH_2	reduced ubiquinone
Q_i	'inner' ubiquinone binding site
Q_o	'outer' ubiquinone binding site

R

RCR	respiratory control ratio
RER	respiratory exchange ratio
ROS	reactive oxygen species
RNS	reactive nitrogen species

S

s	second
SDA	specific dynamic action
SDS	sodium dodecyl sulfate
SEM	standard error of the mean
SOD	superoxide dismutase
SOD1	superoxide dismutase isoform 1 (intermembrane space)
SOD2	superoxide dismutase isoform 2 (matrix)
SOD1$^{-/-}$	superoxide dismutase isoform 1 gene knockout
State 3	maximal phosphorylating respiration
State 4	maximal non-phosphorylating respiration

T

TBS	tris-buffered saline
TBST	tris-buffered saline + Tween 20
Tg	transgenic
Trx 2	thioredoxin 2
Trx 2$^{+/-}$	thioredoxin 2 heterozygous gene knockout
Tris	2-Amino-2-(hydroxymethyl)-1,3-propanediol
Tris-HCl	2-Amino-2-(hydroxymethyl)-1,3-propanediol, hydrochloride

U

ubiquinone	ubiquinol or coenzyme Q10
UCP3	uncoupling protein
UCP1	uncoupling protein 1
UCP2	uncoupling protein 2
UCP3	uncoupling protein 3
UCP4	uncoupling protein 4
UCP5	uncoupling protein 5
UCPs	uncoupling proteins
UCP3 Tg	transgenic mice overexpressing UCP3

V

V	volts
v/v	volume per volume
$\dot{V}CO_2$	whole body carbon dioxide production
$\dot{V}O_2$	whole body oxygen consumption
vs.	versus

W

wk	week
wks	weeks
Wt	wild-type
w/v	weight per volume

Symbols

α	alpha
~	approximately
β	beta
°C	degrees Celsius
>	greater than
<	less than
µg	microgram
µL	microlitre
µM	micromole/litre
±	plus or minus

LIST OF FIGURES

LIST OF TABLES

CHAPTER 1
INTRODUCTION

1.1 AGING AND AGE–RELATED DISEASES

Throughout time humans have sought to preserve the characteristics of youth. For example, in 1512 a Spanish explorer named Ponce de Leon left his homeland in Puerto Rico and travelled around the Florida coast in search for the 'Fountain of Youth'. Ponce de Leon believed that if he sampled water from every river and lake he and his men could find, one would contain the power to grant him eternal youth (Finkel, 2003). While we now know that aging is inevitable, extensive research continues in attempts to find ways to prolong healthy lifespan. Lifespan is a general term that includes both maximum lifespan and average life expectancy (also referred to as 'mean lifespan') (Fontana and Klein, 2007). Maximum lifespan refers to the age at which 0% of the population being studied is living (Fontana, 2006), whereas, average life expectancy is the age at which 50% of the population is living (Gates et al., 2007).

Aging is a multi–dimensional, highly complex process (Weinert and Timiras, 2003) that includes a post-reproductive, physiological decline in overall body function and physical structure due to progressive changes at the organ, cellular and molecular level. Aging involves gradual changes in body composition, including decreased muscle mass (termed 'sarcopenia') and bone density and increased accumulation of abdominal fat content (Fontana and Klein, 2007; Looker et al., 1997; Roubenoff, 2000; Seidell et al., 1988). Due to such adverse changes, body

functions including muscle strength, as well as cardiopulmonary, renal and immune function, and vision and hearing all decline with age (Fontana and Klein, 2007; Lakatta, 2003; Lindeman et al., 1985; Schmidt et al., 1973). Many additional physical changes are associated with aging, including wrinkled skin and greying hair.

With advancing age, the organism becomes predisposed to disease. These 'age–related diseases' include atherosclerosis, diabetes, kidney disease, hypertension, cancer and arthritis. However, many diseases and disorders are completely distinct from the aging process, such as asthma (Hill et al., 1981; Tantisira et al., 2008). The age–related predisposition to disease may reflect an overall inability of the organism to maintain a proper homeostatic balance due to the functional and physical changes that occur with age. As a result, the organism becomes less resistant to stress and more susceptible to disease.

Canada's seniors, individuals aged 65 years or older, are the fastest growing population group in the country. In 1921, 1 out of every 20 Canadians belonged to the senior population, as compared to 1 in 8 in 2001. By the year 2041, it has been estimated that Canada's senior population will reach 1 in 4 (Canada, 2002). Therefore our population as a whole has been rapidly getting older.

One reason why our population is getting older is an increase in maximal lifespan. In 1997, the average life expectancy at birth for both men and women was estimated to be 76 and 81 years, respectively. In 2041, the predicted increase in life expectancy for both men and women is 5 years (Canada, 2002). This expected increase is attributed to improvements in the treatment of age-related diseases and prevention of diseases in the younger population. Therefore, research that focuses

on age-related diseases and the specific mechanisms of aging is extremely important to maximize health in a rapidly aging population.

Calorie restriction (CR) refers to a decrease in energy intake without a reduction in the intake of essential vitamins, minerals and other dietary components (Fontana and Klein, 2007). Interestingly, CR is the only known intervention to prolong both mean and maximum lifespan, delay aging and age-related diseases, and improve overall health in all species studied thus far including humans (Fontana et al., 2004). Despite extensive research, the specific mechanisms whereby CR is able to delay aging remain poorly understood. The research presented herein seeks to better understand such mechanisms in skeletal muscle.

1.2 WHY DO WE AGE?

1.2.1 The *oxidative stress theory of aging*

A number of theories have sought to explain why we age (Weinert and Timiras, 2003). In 1956, Denham Harman first described the *free radical theory of aging* (Harman, 1956) which has since been modified to the *oxidative stress theory of aging* (Finkel and Holbrook, 2000) and remains one of the most widely accepted explanations of the aging process to date. This theory posits that our cells, organs and tissues become damaged due to oxidative stress, which results in aging and eventual death of the organism (Finkel and Holbrook, 2000). Oxidative stress refers to damage caused by both reactive oxygen species (ROS) and reactive nitrogen species (RNS).

1.2.2 What are ROS?

ROS are formed during normal oxidative metabolism. These oxygen-derived molecules are highly reactive because most types of ROS have an unpaired electron. The following three reactions show four types of ROS and how they are produced:

(a) $O_2 + e^- \rightarrow O_2^{\bullet -}$

(b) $2\ O_2^{\bullet -} + 2H^+ \xrightarrow{SOD} H_2O_2$

(c) $Fe^{2+} + H_2O_2 \rightarrow Fe^{3+} + OH^{\bullet} + OH^-$

Reaction (a) shows that when oxygen (O_2) acts as an electron (e^-) acceptor, superoxide ($O_2^{\bullet -}$) can be formed. Superoxide is one type of ROS and is highly reactive, but unstable and therefore short-lived. Reaction (b) shows that superoxide can be metabolized to another, less reactive, type of ROS, hydrogen peroxide (H_2O_2). This reaction is catalyzed by superoxide dismutase (SOD) which is one type of detoxifying enzyme. H_2O_2 is more stable than $O_2^{\bullet -}$ (half-life: 0.05 s at 0.1 mM), and thus can act as a biological effector. Furthermore, in the presence of ferrous iron (Fe^{2+}), H_2O_2 can be broken down into two further types of ROS, a hydroxyl radical ($OH^{\bullet}$) and a hydroxyl ion (OH^-) (reaction c: the Fenton reaction). Therefore,

there are four common types of ROS; $O_2^{\bullet-}$, H_2O_2, $OH^{\bullet}$ and OH^- which vary in their degree of reactivity and stability.

1.2.2.1 Intracellular location of ROS generation

The primary sources of ROS generation within most cell types are the mitochondria. Mitochondria are referred to as the 'powerhouses' of the cell because it is within these organelles that the cellular energy currency in the form of adenosine triphosphate (ATP), is produced. Traditionally, mitochondria have been viewed as independent, 'sausage-shaped' organelles; however, over the last 10 years it has become increasingly appreciated that mitochondria exist as a dynamic reticulum whose morphology is regulated by fission and fusion events (Mannella et al., 1997). Mitochondria have two membranes: an outer membrane and an inner membrane. The mitochondrial outer membrane is semi-permeable, whereas, the mitochondrial inner membrane (MIM) is highly selectively permeable requiring specialized transport mechanisms to allow molecules to pass through. The MIM forms folds, or cristae, thereby increasing its surface area. The area between the outer and inner membrane is referred to as the mitochondrial intermembrane space, whereas the area enclosed by the inner membrane is the mitochondrial matrix.

It is estimated that 0.2-2% of cellular oxygen consumed during oxidative phosphorylation via the electron transport chain (ETC) produce ROS (Chance et al., 1979). The ETC is located within the MIM and is composed of four integral membrane enzyme complexes referred to as complexes I, II, III and IV (Figure 1). These complexes shuttle electrons, obtained from reducing equivalents (reduced

Figure 1. Schematic representation of the electron transport chain (ETC). The ETC is located within the mitochondrial inner membrane and is composed of complexes I-IV. NADH and $FADH_2$ feed into complex I and II respectively and electrons are transferred via ubiquinone (Q) to complex III and then to cytochrome c (cyt c). Upon arriving at complex IV the electrons participate in respiration. During the transfer of electrons through the ETC, a protonmotive force (PMF) of ~ 200 mV is generated across the inner membrane, the dissipation of which drives the formation of ATP by the ATP synthase. ATP is then shuttled to the intermembrane space via the adenine nucleotide translocase (ANT), ultimately providing energy to the rest of the cell.

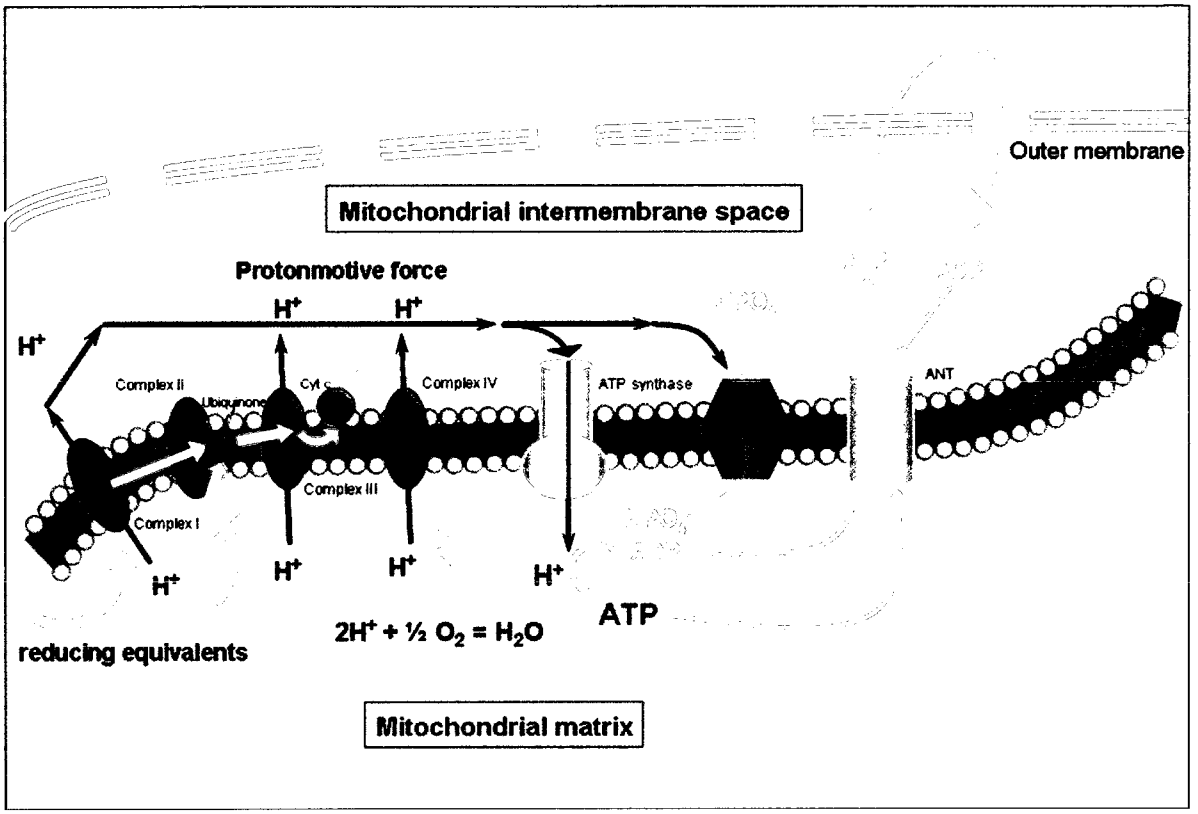
Outer membrane
Mitochondrial intermembrane space
Protonmotive force
H+
H+
H+
Complex II
Ubiquinone
Cyt c
Complex IV
ATP synthase
ANT
Complex III
Complex I
H+
H+
H+
H+
2H+ + ½ O2 = H2O
ATP
reducing equivalents
Mitochondrial matrix

nicotinamide adenine dinucleotide, NADH; and reduced flavin adenine dinucleotide, $FADH_2$), via a series of redox reactions. Oxygen acts as the final electron acceptor in a reaction that produces water at complex IV. NADH and $FADH_2$ produced from the oxidation of proteins, carbohydrates and fats feed into complex I and II respectively. Additionally, the acyl-coA dehydrogenase complex, which is one enzyme involved in fatty acid oxidation, is capable of feeding reducing equivalents into the ETC via the electron transferring flavoprotein:quinine oxidoreductase (ETF:QOR). All electrons are transferred to ubiquinone (Q) where they are then shuttled through complex III to cytochrome c (cyt c) and subsequently to complex IV. Electrons are transferred through the chain via a series of hemes, flavoproteins and iron-sulphur (Fe-S) proteins. During the transfer of electrons through the ETC, a protonmotive force (PMF) of ~ 200 mV is generated across the inner membrane, the dissipation of which drives the formation of ATP from adenosine diphosphate (ADP) and inorganic phosphate (P_i) by the ATP synthase (complex V). ATP is then exported from the mitochondrial matrix to the cytosol via the adenine nucleotide translocase (ANT), ultimately providing energy to the cell.

As detailed below, superoxide is formed when electrons leak from the ETC. More specifically, this occurs mainly at complex I and complex III (Barja, 1999).

1.2.2.2 Sites of ROS production

One location within the ETC where ROS can be produced is at complex I. Figure 2 (adapted from: (Muller et al., 2004)) depicts the structure of complex I as inferred by cryoelectron microscopy (Grigorieff, 1998); an x-ray structure has not yet

Figure 2. Complex I of the electron transport chain (ETC). Detailed schematic view of complex I of the ETC showing how electrons flow through the complex, where rotenone binds and where superoxide ($O_2^{\bullet-}$) is thought to be produced (Muller et al., 2004).

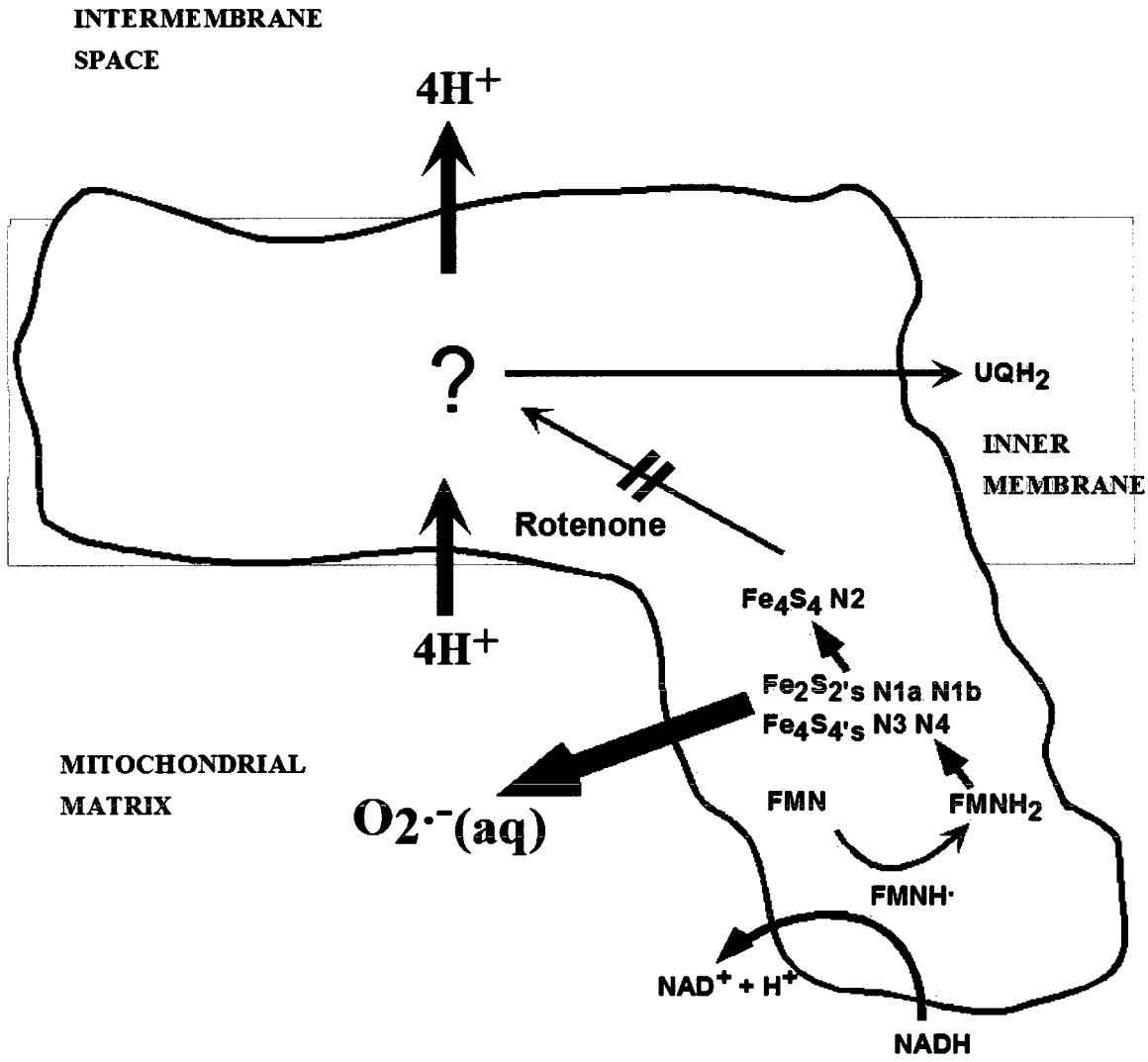
INTERMEMBRANE
SPACE
4H+
?
UQH2
INNER
MEMBRANE
Rotenone
4H+
Fe4S4 N2
Fe2S2's N1a N1b
Fe4S4's N3 N4
MITOCHONDRIAL
MATRIX
O2·-(aq)
FMN
FMNH2
FMNH·
NAD+ + H+
NADH

been elucidated. One portion of the complex appears to reside within the MIM and the remaining portion appears to extend into the mitochondrial matrix forming a distinct 'upside-down' L shape. At complex I, NADH is oxidized to NAD^+, with subsequent flow of electrons to Q from which they are shuttled to complex III. Rotenone is a complex I inhibitor that is thought to bind within complex I at the junction between the portion of the complex that spans the MIM and the portion that extends into the matrix; however, the precise binding site of rotenone is unknown. When rotenone is present, the flow of electrons to Q is prevented; consequently, the electrons fully reduce the Fe-S centres present in the matrix arm of complex I. The Fe-S centres may then donate electrons to oxygen, subsequently forming superoxide within the matrix (Muller et al., 2004).

The other key site within the ETC where ROS can be produced is at complex III, for which a crystal structure has been resolved (Zhang et al., 1998). Complex III is composed of two monomers, one of which is depicted in Figure 3 (adapted from: (Muller et al., 2004)). Each monomer is composed of eleven different subunits, three of which are important for the transfer of electrons through the complex (cytochrome b, Rieske Fe - S protein, and cytochrome c_1). Cytochrome b (cyt b) has two specific locations that are able to bind Q; Q_o and Q_i ('o' and 'i' refer to inner and outer–side of the MIM respectively). Electrons are shuttled through this complex via the Q-cycle, ultimately leading to the transfer of electrons to complex IV via cyt c and the formation of fully reduced ubiquinone (QH_2) (Andreyev et al., 2005). Antimycin A is a complex III inhibitor which binds at the Q_i site of cyt b (Figure 3: modified from (Muller et al., 2004)). The binding of antimycin A promotes the formation of a semiquinone molecule, a partially reduced Q with an unpaired

Figure 3. Complex III of the electron transport chain (ETC). Detailed schematic view of one monomer of complex III of the ETC. The red subunit is cytochrome b, the yellow subunit is the Rieske iron sulphur (Fe–S) protein, and the blue subunit is cytochrome c_1. Q_o and Q_i are both ubiquinone binding sites. The majority of complex III spans the mitochondrial inner membrane, indicated by the area between the two red horizontal lines. The top portion of the Rieske Fe–S protein and cytochrome c_1 extend into the intermembrane space; whereas, the bottom of cytochrome c_1 and b extend slightly into the mitochondrial matrix. Electrons flow through this complex via the Q-cycle which ultimately leads to the shuttling of electrons to complex IV via cytochrome c (located near cytochrome c_1: not shown in the figure) and the formation of fully reduced ubiquinone. Antimycin binds at the Q_i site of cyt b and promotes the formation of a semiquinone molecule which can react with oxygen to form superoxide (modified from Muller et al., 2004).

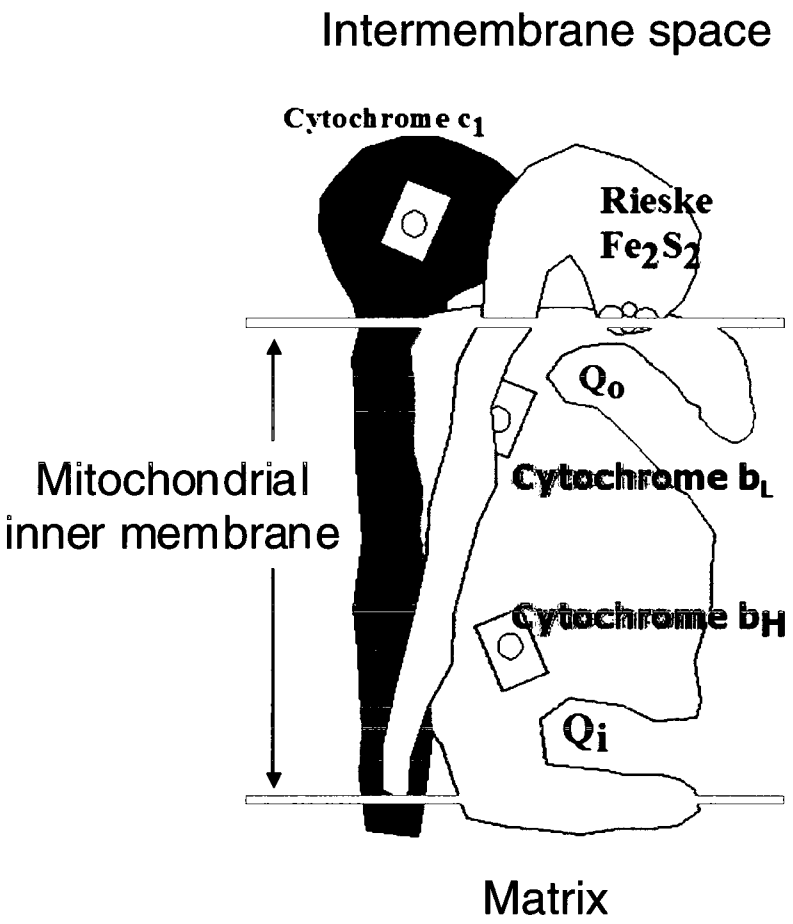
Intermembrane space
Cytochrome c_1
Rieske
Fe_2S_2
Q_o
Cytochrome b_L
Mitochondrial
inner membrane
Cytochrome b_H
Q_i
Matrix

electron. Due to its unpaired electron, semiquinone is able to react with oxygen, consequently forming superoxide. The topology of ROS production at complex III is not as well accepted as that of complex I. The traditional view has been that the majority of superoxide produced at complex III is released into the matrix (Turrens, 1997); however, after the crystal structure of complex III was solved, it was shown that the Q_o site (one possible site of ROS production) is located next to the intermembrane space (Figure 3) (Iwata et al., 1998; Zhang et al., 1998). Subsequent studies have indeed convincingly shown that superoxide generated at complex III can be released into the intermembrane space (Muller et al., 2004; St-Pierre et al., 2002). However, the majority of the superoxide generated at complex III seems to be released into the matrix (Muller et al., 2004; St-Pierre et al., 2002).

1.2.2.3 Conditions favouring ROS production

An important condition that favours mitochondrial ROS production is a highly reduced state of the ETC; that is, when PMF is high (Kushnareva et al., 2002). Such a highly reduced state could arise, *in vivo*, when electron (or reducing equivalent) supply exceeds ETC capacity. *In vitro*, physical inhibition of the respiratory chain, for example by rotenone or antimycin, will result in a highly reduced state of the complexes (Kushnareva et al., 2002; St-Pierre et al., 2002). It follows, therefore, that increased flux through the ETC, as occurs when ATP demand is high, is less conductive to ROS formation. Indeed, it has been shown that levels of superoxide produced by isolated mitochondria can be reduced by 70% if PMF is decreased by only 10 mV (Miwa et al., 2003). This study, and others,

highlight the importance of ROS production on mitochondrial PMF (Hansford et al., 1997; Korshunov et al., 1997; Votyakova and Reynolds, 2001). Non–phosphorylating oxygen consumption, which occurs in mitochondria due to 'proton leak', is thought to mitigate superoxide generation (discussed below). Mechanisms that increase proton leak would thus mitigate ROS formation (see section 1.4.1).

An increase in oxygen availability can also favour ROS production, thereby increasing the chances that oxygen will act as an electron acceptor (Turrens, 2003). Interestingly, hypoxia is also associated with increased ROS production (Guzy et al., 2005). Finally, through mechanisms that remain poorly understood, fatty acids seem to promote ROS production (St-Pierre et al., 2002).

1.2.2.4 Functional role of ROS

Low levels of ROS play important roles in cell signalling pathways. For example, it has been demonstrated that when cells are in a hypoxic state mitochondrial ROS production increases, leading to stabilization of the transcription factor hypoxia–inducible factor 1–α (HIF–1α) and the subsequent cellular adaptation to low oxygen levels (Brunelle et al., 2005). ROS can also play an important role in regulating immune responses. Macrophages and neutrophils contain a nicotinamide adenine dinucleotide phosphate (NADPH) oxidase which is a membrane–bound enzyme complex. Once activated during an inflammatory response, ROS are produced and have antimicrobial and tumoricidal functions (*i.e.* the 'oxidative burst') (Droge, 2002). ROS are also involved in many other cellular processes such as regulating vascular tone, cell adhesion, and programmed cell death (Droge, 2002).

Overall, at low concentrations, ROS play important roles in many physiological cellular processes.

ROS at high levels can lead to cellular dysfunction through an effect on lipids, proteins and DNA. For example, ROS can react with cell membranes resulting in a change in the biophysical properties of the membranes. As depicted in Figure 4 (adapted and modified from (Brand et al., 2004)) superoxide produced by the ETC is converted to a hydroxyl radical through the Fenton reaction, as previously described (section 1.2.2). The hydroxyl radical can react with the hydrogen in polyunsaturated fatty acyl chains present in the membrane to produce a carbon–centred phospholipid fatty acyl radical. This radical can then react with oxygen forming a phospholipid fatty acyl peroxyl radical. Ultimately, this leads to a cascade of lipid peroxidation causing damage to the membrane and the release of reactive alkenals such as 4–hydroxyl–2–nonenal (4–HNE). Additionally, released 4-HNE can react with proteins forming adducts that modify protein structure and function (Brand et al., 2004). ROS can also induce oxidative damage within DNA by promoting strand breaks, and/or by modifying bases and nucleotides which has been implicated in cancer development (Wiseman and Halliwell, 1996). Mitochondrial DNA (mtDNA) is highly susceptible to ROS-induced damage, thus leading to decreased mitochondrial function and integrity (Finkel and Holbrook, 2000; Sanz et al., 2006). Therefore, ROS are able to cause direct damage to cellular components.

1.2.2.5 ROS defence mechanisms

Several antioxidant defence mechanisms, in the form of detoxifying enzymes,

Figure 4. Schematic representation of 4–hydroxy–2–nonenal production. Superoxide ($O_2^{\bullet-}$) produced by the electron transport chain (ETC) is converted to hydrogen peroxide (H_2O_2) by superoxide dismutase in the mitochondrial matrix (MnSOD). By combing with iron (Fe^{2+}), H_2O_2 is then converted to a hydroxyl radical ($^{\bullet}OH$). $^{\bullet}OH$ can acquire a hydrogen (H) from polyunsaturated fatty acyl chains present in the membrane which subsequently produces a carbon–centred phospholipid fatty acyl radical. This radical can then react with oxygen (O_2) forming a phospholipid fatty acyl peroxyl radical. Ultimately this leads to a cascade of lipid peroxidation causing damage to the membrane and the release of reactive alkenals such as 4–hydroxyl–2–nonenal (4–HNE). Released 4-HNE can then react with proteins to form adducts which could modify protein function. The reactive portion of 4–HNE is shown in grey and consists of an aldehyde group and a double bond (Brand et al., 2004). Figure adapted and modified from (Brand et al., 2004).

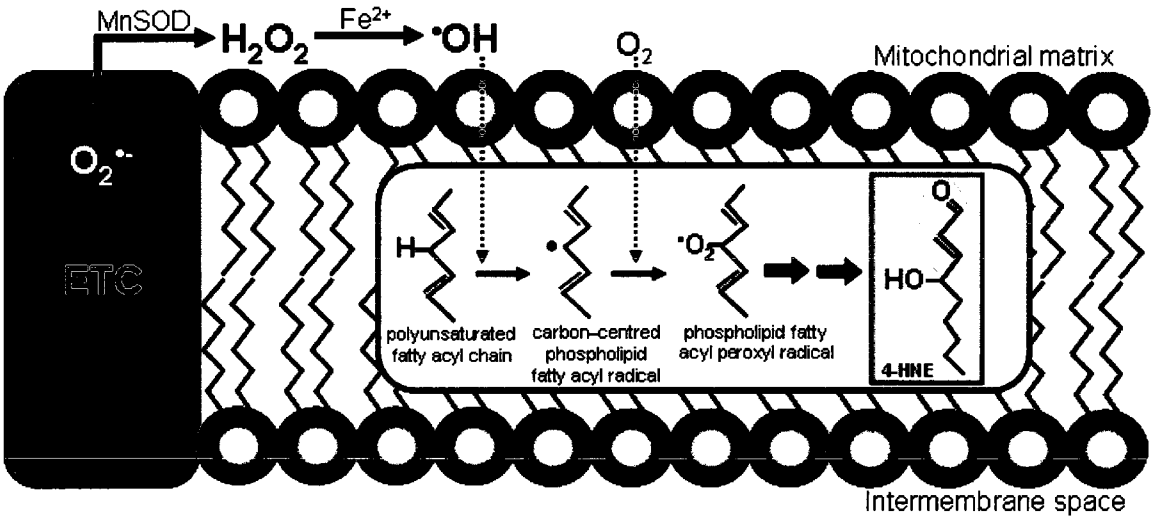
MnSOD
H_2O_2
Fe^{2+}
$^{\bullet}OH$
O_2
Mitochondrial matrix
$O_2^{\bullet-}$
ETC
H
$^{\bullet}O_2$
HO
O
polyunsaturated fatty acyl chain
carbon-centred phospholipid fatty acyl radical
phospholipid fatty acyl peroxyl radical
4-HNE
Intermembrane space

exist thereby dampening the pathological effects of ROS. In skeletal muscle, such enzymes include SOD and glutathione peroxidase (GPx). As described above, superoxide can be converted to H_2O_2 through the action of SOD, resulting in a less toxic form of ROS due to the absence of an unpaired electron. There are two isoforms of SOD: CuZnSOD (SOD1) is present in both the cytoplasm and in the mitochondrial intermembrane space, and MnSOD (SOD2) is present in the mitochondrial matrix (Okado-Matsumoto and Fridovich, 2001). GPx is present in both the mitochondrial matrix and the cytoplasm. GPx converts H_2O_2 into water (Halliwell, 1999). Catalase can also convert H_2O_2 to water, and is found in peroxisomes; however, peroxisomes are not abundant in skeletal muscle (Hulbert et al., 2007). Thioredoxin 2 (Trx2) is another antioxidant enzyme which is present in mitochondria and is responsible for repairing oxidative damage to proteins, namely cystein residues (Lillig and Holmgren, 2007). In skeletal muscle, SOD and GPx are considered to be the most important antioxidant enzymes.

Although not a detoxifying enzyme *per se*, it is hypothesized that uncoupling protein 3 (UCP3), a protein that is found within the MIM in skeletal muscle, is thought to prevent ROS production within this tissue. Therefore, UCP3 could potentially be another mechanism by which muscle is protected against the pathological effects of ROS. A detailed discussion surrounding UCP3's ability to detoxify ROS is presented in section 1.4.3.

Like UCP3, the adenine nucleotide translocase (ANT), also located within the MIM, is not a detoxifying enzyme *per se*. However, ANT can mitigate ROS formation by an inducible proton leak, which it mediates (see section 1.4.1).

1.2.3 ROS, oxidative stress and aging

The level of oxidative stress within a cell is determined by the balance between ROS production and detoxification. The *oxidative stress theory of aging* holds that the gradual accumulation of ROS–induced damage over time is responsible for the physical and functional decline associated with increased age (Finkel and Holbrook, 2000). This progressive decline results in the organism's inability to overcome additional stress which then leads to, or worsens, pathology (Finkel and Holbrook, 2000).

Studies have shown that long–lived animals produce ROS at a lower rate compared to shorter–lived species. For example, the body size and metabolic rate of pigeons and rats are comparable; however, pigeons possess a maximum lifespan of 35 years whereas, that of a rat is only 4 years. Interestingly, mitochondria from pigeons produce much less ROS then mitochondria from rats (Barja et al., 1994). Similar results were also seen when comparing bats to shrews or mice (Brunet-Rossinni, 2004). ROS production in bat mitochondria was half to one third the amount of that produced in the rodents; bats possess a maximum lifespan of 34 years compared to 2 or 8 years for the shrew and mouse respectively. Furthermore, much evidence exists to support the idea that ROS production increases with age in a wide variety of species and tissue types (Antier et al., 2004; Bandy and Davison, 1990; Blackwell et al., 2004; Csiszar et al., 2002; Farmer and Sohal, 1989; Hamilton et al., 2001; Judge et al., 2005), including in human tissue (Jun et al., 1996; Martins Chaves et al., 2002). Together, the above results support a role for oxidative stress in determining the rate of aging. However, is the

accumulation of ROS–induced cellular damage, *per se*, over time responsible for the aging process? A number of studies have addressed this question using either knockout (KO) or transgenic (Tg) overexpressing models of important ROS antioxidant systems. If the *oxidative stress theory of aging* is in fact true, then eliminating vital ROS detoxifiers should result in increased oxidative stress and a shorter lifespan. It has been reported that mice lacking CuZnSOD (*Sod 1*$^{-/-}$) had higher levels of oxidative damage within skeletal muscle compared to age–matched controls (Muller et al., 2006). This resulted in an accelerated age–associated decline in muscle mass and function that is reminiscent of age–related sarcopenia observed in normal human aging (Thomas, 2007). Using the same mouse model, Elchuri *et al.* determined that *Sod 1*$^{-/-}$ mice had a significantly lower mean and maximum lifespan with extensive liver oxidative damage compared to controls (Elchuri et al., 2005). These observations have since been confirmed in a separate study (Perez et al., 2009). Recently, it has been demonstrated that mice deficient in the Trx2 gene (*Trx2*$^{+/-}$) have increased oxidative stress in liver compared to wild–type (Wt) littermates (Perez et al., 2008). Mitochondria isolated from a variety of tissues from *Trx2*$^{+/-}$ mice including from liver and skeletal muscle showed higher levels of ROS production and an overall decrease in mitochondrial ATP production and ETC function compared to controls. In a follow up study, it was established that the *Trx2*$^{+/-}$ mice had a 16% decrease in maximum lifespan and a slight (7%) decrease in mean lifespan (Perez et al., 2009). Although this small difference was not statistically significant, the authors acknowledged that this difference could become significant with a larger sample size. Methionine sulfoxide reductase–A (MsrA) is another important ROS antioxidant enzyme that is responsible for repairing

oxidized methionine groups within proteins. Moskovitz *et al.* have shown that mice lacking the *MsrA* gene are also more highly susceptible to oxidative stress in a variety of tissues and exhibit a shorter lifespan compared to Wt mice (Moskovitz et al., 2001). Evidence to support the *oxidative stress theory of aging* also exists in yeast and drosophila KO models of important antioxidant enzymes (Koc et al., 2004; Longo et al., 1996; Phillips et al., 1989; Reveillaud et al., 1994; Wawryn et al., 1999).

Further support for the *oxidative stress theory of aging* comes from studies in which important ROS antioxidants have been overexpressed in a variety of species with the overall hypothesis that by doing so oxidative stress levels would be attenuated resulting in a prolonged, healthier life. Mice overexpressing SOD2 have been shown to have decreased levels of mitochondrial superoxide production and an increased maximum lifespan (Hu et al., 2007). Furthermore, it has been demonstrated that mice overexpressing human catalase targeted to mitochondria had less ROS production and overall oxidative damage compared to controls (Schriner et al., 2005). Additionally, the catalase–overexpressing mice had an extended, healthier lifespan in that cataract development and cardiac pathology were delayed compared to controls. These are two pathologies that have been associated with normal human aging (Finkel and Holbrook, 2000). Similar results have also been found with the overexpression of a variety of ROS antioxidants in Drosophila (Chavous et al., 2001; Parkes et al., 1998; Ruan et al., 2002; Sohal et al., 1995; Sun et al., 2002; Sun et al., 2004; Sun and Tower, 1999), yeast (Harris et al., 2003; Koc et al., 2004) and flies (Spencer et al., 2003). Therefore, despite its recent questioning (Perez et al., 2009), much evidence exists in support of the *oxidative stress theory of aging.*

1.3 OTHER PATHWAYS THAT MAY CONTROL AGING

Significant attempts have been made to delay aging and promote a healthier lifespan. In 1993, a ground-breaking study was conducted by Kenyon *et al.*, who mutated the gene homologous to the mammalian insulin-like growth factor type 1 receptor gene (*IGF-1R*) in *C. elegans* (Kenyon et al., 1993). This mutation allowed the nematodes to out-live the Wt controls by more than 2-fold. A similar effect was seen in *Drosophila* (Tatar et al., 2001). In mice, Holzenberger *et al.* inactivated one of the *IGF-1R* alleles and found that females lived ~ 30% longer than controls (Holzenberger et al., 2003). On the other hand, mutated male mice were glucose intolerant and did not live longer than their controls. It has been discovered that female and male mice lacking the adipose tissue specific insulin receptor had an 18% increase in lifespan (Bluher et al., 2003). However, when insulin signalling was disrupted in hepatocytes, mice developed insulin resistance and glucose intolerance (Michael et al., 2000). Wang *et al.* showed that activation of the Jun–N–terminal kinase (JNK) pathway in *Drosophila* lead to increased lifespan (Wang et al., 2005). In mice, however, high levels of JNK activity were associated with diabetes (Hirosumi et al., 2002) and atherosclerosis (Ricci et al., 2004). Thus in these experimental systems, targeted perturbation of a single pathway tended to be associated, at least in mammals, with deleterious effects on physiology at some stage in life, and possibly in a gender–specific manner.

1.4 CALORIE RESTRICTION

Calorie restriction (CR) refers to a decrease in energy intake in the absence of malnutrition; that is, without decreasing the intake of essential vitamins, minerals and other dietary components. Interestingly, CR is the only known intervention to consistently prolong both mean and maximum lifespan, delay aging and age-related diseases, and improve overall health in all species studied thus far (*e.g.*, flies, nematodes, spiders, fish, mice, rats, and dogs) (Austad, 1989; Comfort, 1963; Klass, 1977; Weindruch et al., 1986). Despite only minimal research on the effects of CR in monkeys (Kemnitz et al., 1994; Lane et al., 1996; Lane et al., 1995) and humans (Fontana et al., 2004; Heilbronn et al., 2006; Walford et al., 1999), preliminary studies suggest the same beneficial effects. In a very recent study, Colman *et al.* demonstrated that CR in rhesus monkeys slows aging and delays the onset of several age–related pathologies including diabetes, cancer, and cardiovascular disease (Colman et al., 2009). In addition, improved brain function was also seen in CR monkeys compared to controls. Despite extensive research, the specific mechanism whereby CR is able to delay aging and promote healthy lifespan is still poorly understood.

The one well known and consistent effect of CR is a reduction in overall mitochondrial ROS production and cellular oxidative damage (Asami et al., 2008; Bevilacqua et al., 2004, 2005; Lass et al., 1998; Pamplona et al., 2002), observations consistent with the *oxidative stress theory of aging*. Since mitochondria are the main producers of ROS, these organelles have been linked to the underlying mechanisms of CR, and mitochondrial remodelling is increasingly

acknowledged as an important factor (Guarente, 2008). The idea that mitochondria become significantly remodelled during CR derives from observations such as altered mitochondria content and composition, including alterations in mitochondrial proteins, lipids and DNA (Bevilacqua et al., 2004, 2005; Bua et al., 2004; Civitarese et al., 2007; Pamplona et al., 2002). Similarly, CR–induced changes in both mitochondrial dynamics and function are also consistent with this notion (Barazzoni et al., 2005; Bevilacqua et al., 2004, 2005; Guarente, 2008; Marzetti et al., 2008). Mitochondrial remodelling with CR and how this relates to increased healthy lifespan remain poorly understood; the research presented herein seeks to better understand this notion.

1.4.1 The *'uncoupling to survive'* theory

One mechanism that may explain how CR prolongs lifespan and delays aging is described by the *'uncoupling to survive'* theory, a sub–theory of the *oxidative stress theory of aging*. Uncoupled respiration in mitochondria refers to oxygen consumption in the absence of ATP production ('non–phosphorylating oxygen consumption'). This is depicted in Figure 5. Under most conditions, oxygen consumption at complex IV is coupled to the formation of ATP by complex V (ATP synthase). However, it has been known for approximately 20 years that this process is inefficient (Brand, 1990). Some of the protons that are pumped from the mitochondrial matrix into the intermembrane space return to the matrix by means other than the ATP synthase. When this occurs, the 'leaked' protons do not participate in ATP production; however, oxygen is still reduced at complex IV. This

Figure 5. Schematic representation of mitochondrial uncoupling. Oxygen consumption at complex IV is not perfectly coupled to the formation of ATP via the ATP synthase. Some of the protons contributing to the PMF can revert back into the mitochondrial matrix through an alternate route, other then the ATP synthase. The 'leaked' protons do not participate in ATP production; however, oxygen consumption continues. This process is called proton leak, and the wasted energy is released as heat. Basal proton leak refers to leak that occurs within mitochondria under non-phosphorylating conditions and is primarily mediated by ANT. Inducible proton leak refers to leak processes that are activated by, for example, fatty acids or 4-HNE.

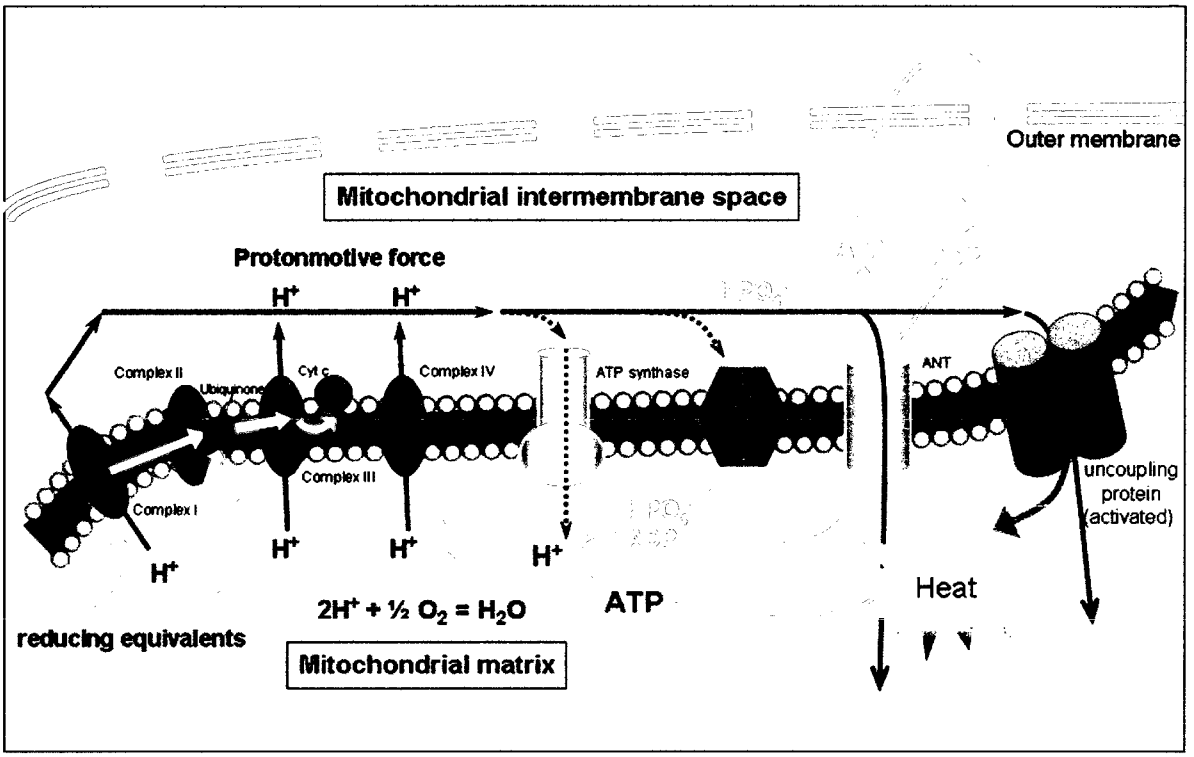
Outer membrane
Mitochondrial intermembrane space
Protonmotive force
H+
H+
Complex II
Ubiquinone
Cyt c
Complex IV
ATP synthase
ANT
Complex III
Complex I
uncoupling
protein
(activated)
H+
H+
H+
H+
2H+ + ½ O2 = H2O
ATP
Heat
reducing equivalents
Mitochondrial matrix

process is also known as proton leak, or mitochondrial uncoupling and the potential energy of the PMF is released as heat (Brown, 1992; Nicholls, 1974). When ATP demand is high, the majority of the protons return to the matrix via the ATP synthase. However, when ATP demand is decreased, as would occur in muscle at rest, the contribution from proton leak processes to oxygen consumption is increased. It has been estimated that up to ~ 25% of the resting metabolic rate of a rat may be due to proton leak (Rolfe and Brand, 1997).

Two types of proton leak have been defined: 'basal' and 'inducible'. Although the mechanism is not entirely understood, ANT is responsible for ~ 50% of proton leak in skeletal muscle mitochondria (Brand et al., 2005). Carboxyatractylate (CAT) is a classic inhibitor of ANT. The majority of ANT–mediated proton leak is not inhibited by CAT (Brand et al., 2005). Such CAT-insensitive proton leak is termed 'basal' proton leak and is not due to ADP/ATP exchange or activation of ANT (Brand et al., 2005). Yet, ANT activation also leads to proton leak. Such activators include fatty acids (Andreyev et al., 1989; Andreyev et al., 1988; Brand et al., 2005; Shabalina et al., 2006), alkenals (Echtay et al., 2003), adenine monophosphate (AMP) (Cadenas et al., 2000) and the need for ADP/ATP exchange during oxidative phosphorylation. Such activated ANT-mediated proton leak is inhibited by CAT (Brand et al., 2005) and is termed 'inducible' proton leak. Uncoupling proteins can also mediate inducible proton leak (see next section).

As stated above, ROS production is increased when PMF is high. When mitochondria are slightly uncoupled, PMF is partially dissipated, thereby decreasing the possibility of ROS formation. As described above, the *oxidative stress theory of aging* posits that ROS are the key molecules responsible for age-associated loss of

function. Therefore, uncoupling of mitochondria could promote less ROS production, and over time, less oxidative damage, which in turn, would mitigate aging processes. This is the basis for the *'uncoupling to survive'* theory (Brand, 2000).

1.4.2 Uncoupling proteins

Despite extensive research on uncoupling proteins (UCPs), there remains controversy regarding their physiological function and mechanism of action. The first uncoupling protein to be identified was uncoupling protein 1 (UCP1), also known as thermogenin (Bouillaud et al., 1985; Bouillaud et al., 1986). This 32 kDa, MIM protein was discovered during the mid-1970's and is expressed exclusively in brown adipose tissue (BAT). UCP1 is responsible for non-shivering thermogenesis (NST) in BAT, the process of heat production through a fatty acid-activated mitochondrial proton leak process (Nicholls and Locke, 1984).

More recently, four proteins with significant homology to UCP1 were discovered: UCP2 and UCP3 in 1997, UCP4 in 1998, and UCP5 in 1999. At the amino acid level, UCP4 and UCP5 are 30% homologous to UCP1; whereas, UCP2 and UCP3 are 50% and 57% homologous, respectively (Boss et al., 1997; Fleury et al., 1997; Gimeno et al., 1997; Gong et al., 1997; Vidal-Puig et al., 1997). Due to the high sequence similarity to UCP1, it was initially thought that the physiological role of UCP2 and UCP3 would also be thermogenic uncoupling. Very little is known about UCP4 and UCP5 and, to date, the specific function of UCP2 and UCP3 is still

speculative. The research presented herein focuses on UCP3 and its proposed function in mediating proton leak and mitigating ROS production during CR.

1.4.3 Uncoupling protein 3 (UCP3)

The 34 kDa UCP3 protein is selectively expressed in skeletal muscle and, at lower levels, in heart and BAT (Bezaire et al., 2007). UCP3 is the only uncoupling protein to be expressed at the protein level in skeletal muscle. As mentioned previously, due to UCP3's high sequence homology to UCP1, it was originally hypothesized that UCP3's primary physiological function would be NST through mitochondrial uncoupling specifically in skeletal muscle. However, many studies have shown that UCP3 does not mediate this function. For example, Cadenas *et al.* showed that a 2–fold increase in UCP3 protein, induced by fasting, in rat skeletal muscle mitochondria is not associated with increased basal proton conductance (Cadenas et al., 1999). Additionally, mice lacking UCP3 protein had normal body temperature compared to controls even during cold exposure or when treated with a beta 3-adrenergic agonist. Therefore, the above studies and others (Bezaire et al., 2001) have provided evidence against the hypothesis that UCP3 induces basal uncoupling and contributes to NST in skeletal muscle.

Another proposed function of UCP3 is protection from ROS (reviewed in (Bezaire et al., 2007)). UCP3 has been linked to decreased ROS production and oxidative stress in a number of studies. It has been shown that skeletal muscle mitochondria isolated from mice lacking UCP3 possessed greater levels of ROS production (Vidal-Puig et al., 2000). Additionally, it has been demonstrated that

mice lacking UCP3 have higher levels of oxidative damage compared to controls (Brand et al., 2002). Decreased ROS production has also been shown in muscle cells overexpressing physiological levels of UCP3 protein (MacLellan et al., 2005). It has been hypothesized that the mechanism by which UCP3 attenuates ROS production is through a small degree of uncoupling induced by UCP3 upon its activation by by–products of lipid peroxidation, such as 4–HNE (reviewed in (Brand and Esteves, 2005)). This activated 'mild' uncoupling would decrease mitochondrial PMF, subsequently mitigating ROS formation.

This proposed mechanism has gained much support, at least at the *in vitro* level. Echtay *et al.* have shown that exogenously produced superoxide, generated by xanthine and xanthine oxidase, in skeletal muscle mitochondria resulted in increased mitochondrial uncoupling (Echtay et al., 2002). The increase in proton conductance was abolished when GDP, an inhibitor of UCP3, was added. Also shown was the dependence of the increased proton leak on the presence of fatty acids. Skeletal muscle mitochondria isolated from mice lacking UCP3 did not possess increased proton leak in the presence of superoxide compared to controls. In another study, Brand and colleagues (Echtay et al., 2003) showed that 4–HNE and other structurally related compounds induce a similar GDP–sensitive proton leak in skeletal muscle mitochondria. This increased proton conductance was again absent in mice lacking UCP3. In a follow–up study, Talbot *et al.* endogenously generated superoxide in mitochondria isolated from rat skeletal muscle mitochondria (Talbot et al., 2004). Superoxide was induced at complex I by allowing the mitochondria to respire on succinate as the substrate. Under these conditions, GDP inhibited the proton conductance and superoxide production was enhanced. The

addition of rotenone and an antioxidant similarly inhibited the GDP–sensitive proton leak and ROS production was reduced. This latter study avoided the criticisms of using non–physiological levels of superoxide to activate UCP3 by allowing mitochondria to endogenously produce superoxide.

Evidence does however exist against the above hypothesis. Mitochondria from SOD2 overexpressing mice were shown to have decreased ROS production and oxidative damage (Silva et al., 2005). Since these mice were already protected from extensive ROS production and damage, it was thought that under conditions in which ROS production was significantly elevated, mitochondria from SOD2 mice would have a smaller GDP–inhibitable proton leak compared to Wt mice. However, while skeletal muscle mitochondria from mice overexpressing SOD2 possessed a proton leak that was sensitive to GDP, the degree of this inhibition was similar to that in Wt mice. Recently, Parker *et al.* have provided evidence against the specificity of GDP for UCP3 (Parker et al., 2008). In the latter study, it was shown that mitochondria isolated from mouse skeletal muscle lacking UCP3 in fact possessed a GDP–sensitive proton leak. Additionally, UCP3 specific proton conductance activated by endogenously produced superoxide was not inhibited by GDP and was strongly attenuated when carboxyatractylate (CAT) was added, a known inhibitor of ANT. Therefore, Parker and colleagues concluded that GDP is not specific for UCP3, as it can inhibit proton conductance by ANT as well. The possible non–specificity of GDP to UCP3 raises a fundamental concern surrounding previous studies that have utilized GDP as a tool to reveal an activated UCP3-mediated proton conductance. Evidence also exists against the idea that UCP3 mitigates ROS production and decreases oxidative stress. For example, Brand and

colleagues have shown that skeletal muscle mitochondria from mice overexpressing UCP3 do not possess lower levels of oxidative damage compared to controls (Brand et al., 2002).

Thus, there remains much controversy over the physiological function of UCP3 and its specific mechanism, and the need for further research is evident.

1.4.4 CR, uncoupling and aging

The *'uncoupling to survive'* theory proposes that uncoupling of mitochondria, via proton leak, promotes less ROS production, and over time, less oxidative damage results in a slower aging process and increased lifespan (Brand, 2000).

CR has been associated with increased mitochondrial proton leak (*i.e.* a change in overall mitochondrial function). Lambert *et al.* showed that liver mitochondria from CR rats (4-month treatment period) possessed increased proton leak compared to controls. The increased proton leak observed was also associated with decreased ROS production (Lambert and Merry, 2004). Consistent with these results are studies that were conducted in our laboratory with mitochondria isolated from skeletal muscle of rats that underwent short–term (2 week and 2 month) or medium-term (6 month) CR (Bevilacqua et al., 2004). Results from these studies showed that mitochondria from rats exposed to short-term CR had a lower PMF, increased oxygen consumption and marked decreases in ROS production and oxidative stress compared to controls.

Therefore, the above data show that short–term CR may promote an increase in mitochondrial proton leak. Because uncoupling would result in lower ROS

production rates and oxidative damage, uncoupling may be a mechanism activated by CR that underlies the anti-aging effects of CR.

1.5 OBJECTIVES

An association exists between UCP3 protein expression levels and body weight (BW). Therefore, UCP3 has been suggested to play a role in whole body energy balance. Studies from our laboratory have reported a lower BW phenotype in mice overexpressing physiological levels (~ 2-fold increase) of UCP3 protein (Costford et al., 2008; Costford et al., 2006). UCP3 overexpression in muscle has also been shown to induce increased uncoupling in skeletal muscle mitochondria (Clapham et al., 2000), which could explain the BW phenotype.

Based on the above results, it was of interest to assess the level of mitochondrial uncoupling in skeletal muscle mitochondria from our UCP3 Tg mice. Pilot studies indicated that our UCP3 Tg mice had increased mitochondrial proton leak compared to age-matched controls. The level of mitochondrial ROS production is highly dependent on proton leak processes. Therefore, it was predicted that our UCP3 Tg mice would possess decreased skeletal muscle mitochondrial ROS production. Again, this was confirmed in pilot experiments.

Based on the preliminary observations of increased mitochondrial proton leak and decreased ROS production in UCP3 Tg mice compared to Wt mice, it was of interest to investigate this model in the context of CR. Given that short-term CR has been shown to cause uncoupling in skeletal muscle mitochondria, thereby mitigating ROS production and oxidative stress (Bevilacqua et al., 2004), it was hypothesized

that this would be observed in mitochondria from Wt mice subjected to CR. However, it was predicted that CR would have little impact on ROS production and oxidative stress in an already uncoupled system (*i.e.* mitochondria from UCP3 Tg mice). Such results would provide support for mitochondrial uncoupling as an important mechanism that mediates some of the effects of CR.

To address the hypothesis, we characterized the effects of a 2 week (wk) and 1 month (mo) 40% CR treatment in Wt and UCP3 Tg mice on whole body energetics and composition, and on skeletal muscle mitochondrial energetics and ROS metabolism. Skeletal muscle was chosen as the primary tissue of investigation based on the well known effects of aging to induce sarcopenia, with subsequent impairment in muscle strength (Evans, 1995; Marzetti et al., 2008). Moreover, muscle possesses the ability to oxidize fuel at extremely high rates by virtue of its high mass per BW and is an important site for insulin-stimulated glucose disposal. However, with age, fuel oxidation capacity in this tissue decreases (Marzetti et al., 2008). Therefore, studies of the effects of CR on muscle are of interest as muscle is highly susceptible to several degenerative processes associated with aging; yet, it is a tissue of fundamental importance for locomotion and metabolic health.

CHAPTER 2
METHODS AND MATERIALS

2.1 MEASUREMENTS IN 2 WEEK AND 1 MONTH CALORIE RESTRICTED WT AND UCP3 TG C57BL/6J MICE

2.1.1 Animals

Male C57BL/6J wild–type (Wt) and UCP3 transgenic (UCP3 Tg) mice were used in this study. The UCP3 Tg mice were originally provided by Dr. John Clapham at GlaxoSmithKline (Harlow, UK). The human α–skeletal muscle actin promoter was used to drive tissue-specific expression of the human UCP3 transgene in skeletal muscle (Clapham et al., 2000). Importantly, the UCP3 Tg mice used in this study, from our colony, have been backcrossed 10 generations into the C57BL/6J background to minimize any genetic background differences between the two groups of mice.

2.1.2 Calorie restriction protocol

A schematic representation of the 2 wk and 1 mo CR protocol is outlined in Figure 6. 8 wk old Wt and UCP3 Tg mice were housed in groups of 2-4 mice per cage from weaning. During this time, mice were allowed free access to water and standard rodent chow (Harlan; 2018). At 7 wks of age, Wt and UCP3 Tg mice were housed individually and continued to be fed the standard chow diet. At 8 wks of age, Wt and UCP3 Tg mice entered into the food intake portion of the study. The

Figure 6. Schematic representation of the 2 wk and 1 mo calorie restriction protocol. 8 wk old Wt and UCP3 Tg mice were provided with a defined control diet (Research Diets D01092701; New Brunswick, NJ: see Table 1 for diet composition) until 12 wks of age. During this 4 wk period individual body weight and daily food intake measurements were determined twice a wk (1 mo food intake). At 12 wks of age, Wt and UCP3 Tg mice were randomly divided into control (*ad libitum*; AL) or calorie restricted (CR) groups. CR mice were switched to a 40% CR diet (Research Diets D01092701; New Brunswick, NJ) and were given 40% less of this diet than their average daily food intake. AL mice were given the average of their daily food intake and remained on the AL diet. The 2 wk and 1 mo CR interventions were terminated at 14 or 16 wks of age, respectively, and mice were sacrificed. Two days prior to sacrifice, whole body energy consumption was determined by IC in each mouse over a 24 h period. At sacrifice, organ and fat pad weights were measured and muscle was prepared for later histological determination of mitochondrial content. Skeletal muscle mitochondria were also isolated for functional determinations of ROS production; non-phosphorylating, maximal phosphorylating and maximal uncoupled respiration; and proton leak (in 1 mo CR only). Mitochondria were also frozen at -80°C for later determinations of protein expression by Western blotting. Abbreviations: mitos; mitochondria, RCR; respiratory control ratio, ROS; reactive oxygen species, IC; indirect calorimetry

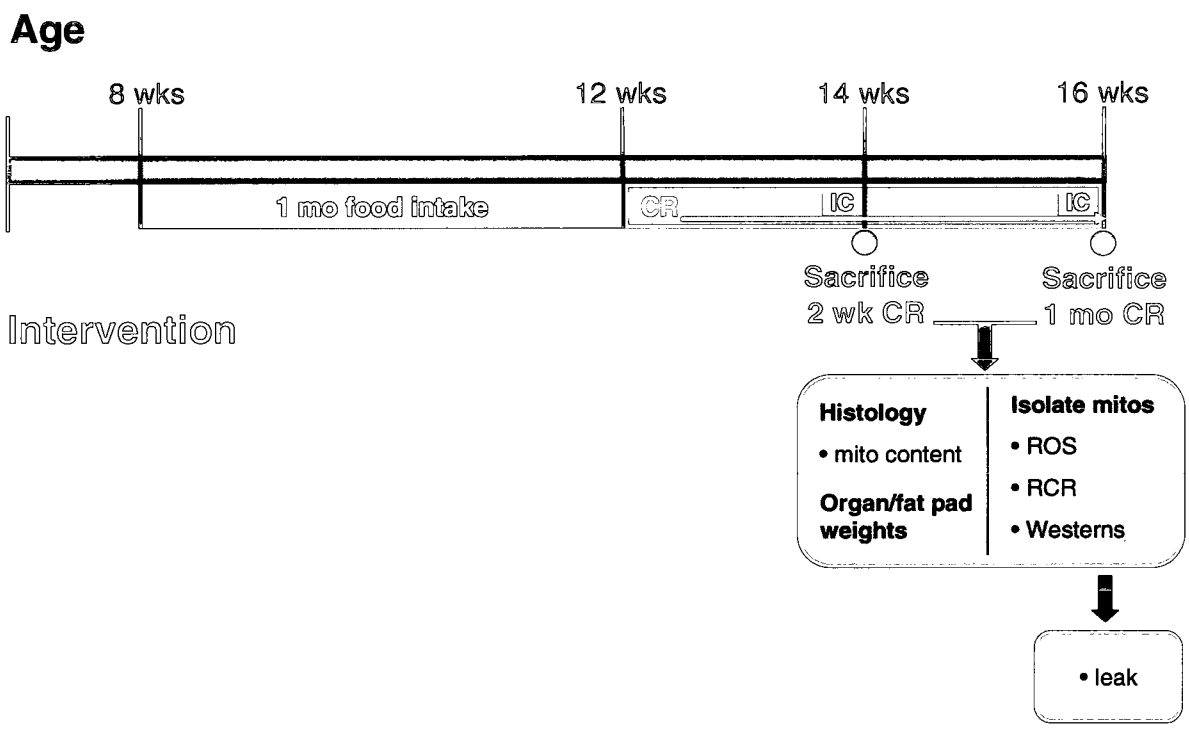
Age
8 wks
12 wks
14 wks
16 wks
1 mo food intake
CR
IC
IC
Sacrifice
2 wk CR
Sacrifice
1 mo CR
Intervention
Histology
• mito content
Organ/fat pad weights
Isolate mitos
• ROS
• RCR
• Westerns
• leak

purpose of housing mice individually one wk prior to the beginning of the food intake study was to acclimate each mouse to living on its own. At this point, all mice were switched from the standard rodent chow to the control rodent chow diet (see next section). To commence the food intake study, each mouse was placed in a new cage to eliminate possible rodent chow carry over. Each mouse was given ~ 25 grams (g) of the control diet (see next section), and was permitted *ad libitum* feeding during this portion of the study. Until 12 wks of age, BW and food intake were determined twice per wk. At the end of the food intake study, mice were randomly divided into either control (*ad libitum*: AL) or calorie restricted (CR) treatment groups. Mice entering into the AL group remained on the control diet and were given an average of their daily food intake for the treatment period. Mice entering into the CR group were switched to a 40% CR diet (see next section), based again on the food intake results collected from each mouse during the previous food intake studies. The duration of this subsequent intervention was 2 wks or 1 mo. Therefore, mice were 14 or 16 wks of age at sacrifice. On any given experimental day either two Wt or two UCP3 Tg mice were sacrificed: one having been AL-fed and the other CR-fed.

During the study, all mice were given free access to water, and were kept at 24°C with light-dark cycle from 06:00-18:00. All animal work including feeding and BW measurements took place from 16:00-16:30 and cages were changed every two wks. All mice were cared for according to the principles and guidelines of the Canadian Council on Animal Care and the Institute of Laboratory Animal Resources (National Research Council). Approval of this study came from the Animal Care Committee of the University of Ottawa.

2.1.3 Composition of diets

The specific compositions of the control and CR diets are summarized in Table 1. The control (or AL) diet was an AIN-93M purified, defined mature rodent diet (D01092701: Research Diets, New Brunswick, NJ); whereas, the CR diet was a modified version of the AL diet (D01092702: Research Diets, New Brunswick, NJ). In order to produce the CR diet, the carbohydrate (corn starch and maltodextrin) component was decreased compared to the AL diet, causing a 40% increase in protein, fat, vitamins and minerals. Consequently, the imposed 40% decrease in food intake during the CR period offset the increase in these dietary components. Thus only the carbohydrate component of the diet was reduced to produce a 40% reduction in calories in the CR diet. Therefore, the intake of essential vitamins, minerals and other nutrients in the CR mice was as in the control diet.

2.1.4 Indirect calorimetry

Two days prior to sacrifice, mice were placed in a customized 4-chamber Oxymax open-circuit indirect calorimeter (Columbus Instruments, Columbus, OH). To acclimate the mice to this new environment, each mouse was placed individually in a 2.5 L respiration chamber at 09:00. All mice were allowed free access to water and were given any left over food from the previous day's feeding. Measurements were started at 14:00. For the indirect calorimetry experiments, mice were maintained at 24°C with lights on from 06:00 to 18:00. Airflow of 0.5 L/min was maintained. Readings that were taken between 14:00-16:00 were ignored during

Table 1. Composition of both the control and CR diets (Research Diets D01092701 and D01092702, respectively; New Brunswick, NJ). During the 2 wk or 1 mo CR intervention, AL mice were given the control diet. The amount of food given was equal to the average of their daily food intake determined during the 1 mo food intake study. CR mice were given 40% less of the CR diet then their average daily food intake on the control diet during the 1 mo food intake study. By feeding the CR group 40% less, only the carbohydrate component (corn starch and maltodextrin, in bold) of the CR diet was decreased. To avoid malnutrition, all essential vitamins, minerals and nutrients were maintained within the CR group.

	Control Diet		CR diet	
Ingredient	*gm %*	*kcal %*	*gm %*	*kcal %*
protein	14	15	23	24
carbohydrate	73	76	56	60
fat	4	9	6	16
Total		100		100
kcal/gm	3.85		3.76	
Diet composition after 40% correction of CR diet				
	Control Diet		CR diet	
Ingredient	*gm*	*kcal*	*gm*	*kcal*
casein, 80 mesh	140	560	140	560
L-cystine	1.8	7.2	1.8	7.2
corn starch	495.7	1982.8	**187.5**	**750**
maltodextrin 10	125	500	**50**	**200**
sucrose	100	400	100	400
cellulose, BW200	50	0	50	0
soybean oil	40	360	40	360
t-butylhydroquinone	0.008	0	0.008	0
mineral mix (S10022M)	35	0	35	0
vitamin mix (V10037)	10	40	10	40
choline bitartrate	2.5	0	2.5	0
Total	**1000**	**3850**	**616.8**	**2317**

data analysis, as mice were allowed a 2 h acclimation period to the calorimeter. Mice were then fed at 16:00.

Indirect calorimetry readings (60 s per chamber, 4 chambers) were obtained every 9 min, over a 24 h period (16:00-16:00) with a sample line-purge time of 2 min. The final BW of each mouse was recorded after the 24 h data collection period. Readings included whole body oxygen consumption ($\dot{V}O_2$), or energy expenditure, and CO_2 ($\dot{V}CO_2$) production measurements. The respiratory exchange ratio (RER) was calculated as the ratio of CO_2 production to oxygen consumption. RER provides an indication of the type of fuel being oxidized by an animal: an RER that is closer to 0.7 is indicative of increased fat catabolism; whereas, an RER closer to 1 indicates that the mouse is largely oxidizing carbohydrates. $\dot{V}O_2$ can be subcategorized into: basal metabolic rate (BMR), exercise-induced thermogenesis, thermoregulatory thermogenesis and the specific dynamic action (SDA) of ingested food. BMR represents all of the energy expended at rest needed to maintain normal basal body functions; whereas, SDA represents the energy expended for processes involved in feeding (*i.e.* digestion and absorption). Thermoregulatory thermogenesis is increased when animals are in a cold environment (*i.e.* a temperature that is lower than the animal's thermoneutrality temperature). The level of energy expended during thermoregulation, SDA and exercise is variable while the BMR remains relatively constant.

2.1.5 Collection of muscle samples for histology

All mice were sacrificed between 08:00 and 08:30 on any given experiment

day. At the beginning of each mouse dissection, a small muscle sample from the *vastus lateralis* was quickly transferred to an ice-cold, plastic histology cassette containing Optimal Cutting Temperature Compound (O.C.T. compound: Tissue-Tek). Once the tissue was submerged in O.C.T. compound, the cassette was promptly transferred to isopentane (2-Methylbutane: Sigma) that had been cooled on dry ice for ~ 30 min. The O.C.T. compound containing the muscle tissue froze instantly once it came in contact with the cold isopentane solution. The cassette was then wrapped in chilled aluminum foil, and was transferred to -80°C. The *vastus lateralis* was chosen as it contains a mix of different fiber types (Staron et al., 2000). This sample was then used for later enzyme histochemical analysis (see section 2.1.11).

2.1.6 Organ and fat pad weights

Individual tissues were dissected and weighed to assess the effects of CR. From each mouse the heart, liver and kidneys along with the gonadal white adipose tissue (gWAT) and interscapular brown adipose tissue (iBAT) were dissected and placed on ice. Each organ and fat pad was blotted dry and subsequently weighed.

2.1.7 Isolation of skeletal muscle mitochondria

Isolation of skeletal muscle mitochondria was performed using a modified method of Chappell and Perry (Chappell and Perry, 1954). All media were ice-cold, and the procedure done on ice to mitigate degradation processes. Skeletal muscle

from the forelimbs, hind limbs and the pectoral region was quickly dissected and placed in ice-cold basic medium (BM: 140 mM KCl, 20 mM HEPES, 5 mM $MgCl_2$, 1 mM EGTA; pH 7.0 at 25°C) and were then cleaned of any visible connective tissue and fat. Removal of fat was important because an excess of fat may cause mitochondrial uncoupling which would adversely affect experimental results. Also, removing any obvious connective tissue allowed for easier release of the mitochondria during the homogenization steps. The muscle was then blotted dry and weighed then minced for 2 min on a Teflon cutting board. The minced muscle was then placed in 15 volumes of homogenizing medium (HM: BM supplemented with 1 mM ATP and 1% BSA (w/v)) and one unit of protease (Subtilisin A: Sigma) per g of tissue was added to the muscle suspension. Tissue was then homogenized using a glass/Teflon Potter-Elvehjem tissue grinder and fractioned by centrifugation at 800 *g* (9 min, 4°C). The supernatant was collected and respun at 12,000 *g* (8 min, 4°C). The resulting pellet was resuspended in BM and incubated on ice for 5 min to allow myofibrillar re-polymerization. Samples were spun at 800 *g* (9 min, 4°C), the supernatant was collected and then spun at 12,000 *g* (8 min, 4°C). The final pellet was resuspended in ~ 200 µL of BM depending on the size of the pellet.

Two mitochondrial isolations were carried out on each experimental day: either from Wt AL and Wt CR mice or from UCP3 Tg AL and UCP3 Tg CR mice. The two mouse dissections were staggered by ~ 20 min and the order of sacrifice (either an AL or CR mouse) was alternated on each experiment day. A small sample (~ 30 µL) of isolated mitochondria from each preparation was frozen down at -80°C immediately after the final pellet was resuspended in BM. This sample was then used for later Western blot determinations (see section 2.1.10).

2.1.7.1 Protein concentration of isolated skeletal muscle mitochondria

Immediately after the final mitochondrial pellet was resuspended in BM, the protein concentration of each sample was determined using a modified Lowry protein assay (Schacterle and Pollack, 1973) with BSA as the standard. The final BSA concentration of the standard curve ranged from 0-24 µg/mL; the assay was linear in this range. Each mitochondrial sample was diluted 1:200 in duplicate using ddH_2O. The protein assay was carried out in duplicate of each diluted sample; therefore, the protein concentration of each mitochondrial sample was determined in quadruplicate to ensure accuracy. The absorbance of all standards and samples were read at 650 nm using a Beckman DU-50 spectrophotometer. The standard curves were generated by plotting absorbance *vs.* µg of protein and the protein concentration of each sample was well within the standard curve.

2.1.8 Oxygen consumption determinations in isolated skeletal muscle mitochondria

The respiratory control ratio (RCR) was assessed by measuring oxygen consumption using a Hansatech Clark-type oxygen electrode (Norfolk, UK). RCR is determined by measuring state 3 (maximal phosphorylating oxygen consumption) and state 4 (non-phosphorylating oxygen consumption) of the isolated mitochondria, and dividing the former by the latter.

Mitochondria in the magnetically stirred Clark oxygen electrode chamber (0.25 mg mitochondria/mL) were maintained at 37°C and suspended in incubation media (IM: 120 mM KCl, 5 mM HEPES, 5 mM $MgCl_2$, 1 mM EGTA, 5 mM KH_2PO_4

and 0.3% BSA (w/v); pH 7.4 at 25°C). Malate (2.5 mM) and pyruvate (5 mM) were added as energy substrates, and ADP (200 μM) was added to stimulate state 3 respiration. Oligomycin (8 μg/mg mitochondria) was added to inhibit ATP synthase, and the chemical uncoupler carbonyl cyanide–p-trifluoromethoxyphenylhydrazone (FCCP; 3 μM) was added to maximally uncouple the mitochondria. Pilot experiments determined that these concentrations of reagents were saturating.

RCR determinations were performed in duplicate for all mitochondrial preparations. Well coupled mitochondria have an RCR value > 6. Additional determinations included state 3 oxygen consumption rates, state 4 oxygen consumption rates and maximal FCCP-uncoupled oxygen consumption rates, and rates were converted to nmol O/(mg protein*min). Prior to rate determinations the oxygen electrode was calibrated by allowing 1 mL of IM to reach equilibrium with air for 7 min at 37°C. This corresponding reading represented the 100% air saturation value. A small amount of sodium dithionite ($Na_2S_2O_4$) was then added to the chamber and the stabilized signal represented 0% air saturation. Previous studies have determined oxygen solubility in our IM (409 nmol O/mL (Reynafarje et al., 1985)), and so, this value was divided by the difference between 100% and 0% air saturation. Oxygen consumption values were then converted to nmol O/(mg protein*min).

2.1.9 ROS production capacity of isolated skeletal muscle mitochondria

2.1.9.1 The PHPA/HRP assay

The p-hydroxyphenyl acetic acid (PHPA)/horseradish peroxidase (HRP) assay (Hyslop and Sklar, 1984) was employed to measure H_2O_2 emission, used as a measure of ROS formation. H_2O_2 reacts with PHPA in the presence of the enzyme HRP to form a fluorescent dimer. Dimer formation can be followed as an increase in fluorescence. H_2O_2 was thus detected by measuring fluorescence (excitation: 320 nm; emission: 400 nm) using a temperature-controlled microplate fluorescence reader (FL x 800, Biotek), at 37°C.

PHPA (167 µg/mL), HRP (9 units/mL), SOD (20 units/0.3 mL: to convert all superoxide to H_2O_2), and isolated mitochondria (0.1 mg mitochondria/0.3 mL) were added to each well containing warmed incubation medium (IM: 120 mM KCl, 5 mM HEPES, 5 mM $MgCl_2$, 1 mM EGTA, 5 mM KH_2PO_4 and 0.3% BSA (w/v); pH 7.4 at 25°C). Depending on the experimental conditions, the following were also added: antimycin A (5 µM: complex III inhibitor), rotenone (5 µM: complex I inhibitor), and oligomycin (8 µg/mg mitochondria: ATP synthase inhibitor). Readings were collected following temperature re–equilibration to 37°C. A 3 min incubation time was used in which four basal readings were recorded; then, the substrate, palmitoylcarnitine (PC: 18 µM), pyruvate/malate (5 mM pyruvate, 2.5 mM malate) or succinate (10 mM) was added and mixed. Readings under each condition were collected in duplicate and each experiment was run for 20-25 min, taking a fluorescence reading every 1 min.

H_2O_2 production was determined as nmol H_2O_2/min/mg mitochondria by the use of a standard curve. Standard curves were generated in the presence of mitochondria because mitochondria quench the fluorescence; thus, values of H_2O_2 would be underestimated if mitochondria were not included in the standard curve.

Artifactual rates of H_2O_2 production have been reported with reagents alone (St-Pierre et al., 2002). Thus, pilot experiments determined whether any of the reagents, or combinations of reagents, in the absence of mitochondria, would generate an increase in fluorescence. None of the reagents were found to generate a change in fluorescence with time.

2.1.9.2 Site–specific ROS determinations

ROS formation at different sites along the mitochondrial electron transport chain was followed through the use of different combinations of substrates and inhibitors. Pyruvate/malate is primarily an NADH-linked substrate and thus reducing equivalents feed into complex I; this mimics the situation which occurs with glucose oxidation. Succinate is converted to fumarate by complex II (*i.e.* succinate dehydrogenase) with formation of $FADH_2$ which feed directly into the ubiquinone pool. PC is a fatty acid substrate and contributes both NADH and $FADH_2$.

To determine the level of superoxide produced at complex I, the specific complex I inhibitor, rotenone, was used. Therefore, the level of superoxide produced at complex I was determined using both a fatty acid substrate (PC) and a non–lipid substrate (pyruvate/malate).

To determine the level of superoxide produced at complex III, the specific complex III inhibitor, antimycin A, was used. Therefore, the level of superoxide produced at complex III was measured using a fatty acid substrate (PC) and a non-lipid substrate (succinate). Rotenone was used in the latter condition to block any superoxide produced at complex I due to backflow of electrons from the complex II-linked substrate.

In order to determine the level of superoxide produced while the mitochondria respired in their basal state (*i.e.* low ATP demand, and no specific ETC inhibitors present), oligomycin was used with PC as the mitochondrial substrate.

2.1.10 Western blotting

Previously frozen mitochondrial suspensions from Wt/UCP3 Tg AL and Wt/UCP3 Tg CR mice were diluted to 4 mg/mL with ddH_2O, were combined 6:1 with sample loading buffer (2% SDS, 50 mM Tris-HCl (pH 6.8), 25% glycerol (w/v), 0.2% bromophenol blue (w/v), and 14.4 mM β-mercaptoethanol) and were electrophoresed in a 12% polyacrylamide gel. Western blotting was then used to detect levels of UCP3, ANT, MnSOD and of 4-HNE protein adducts. The level of 4-HNE protein adducts within a cell provides a measure of oxidative damage (Tsai et al., 1998).

On the day of the experiment, all samples were boiled for 5 min and were loaded at 30 µg of protein per lane for 4-HNE and UCP3, or 15 µg of protein per lane for MnSOD and ANT. The Page Ruler Prestained Protein Ladder (Fermentas Life Sciences) served as the molecular weight marker. Proteins were

electrophoresed at 150 V, for ~ 1 h, at room temperature, and then transferred onto a nitrocellulose membrane in Tris/glycine buffer (25 mM Tris base, 192 mM glycine, and 0.1% SDS) at 120 V for 40 min at room temperature. Following protein transfer, gels were stained with Coomassie blue (40% methanol, 10% acetic acid and 0.1% (w/v) Coomassie)), then destained (25% methanol and 7.5% acetic acid) to improve band resolution.

Membranes were blocked for 1 h, at room temperature, with 5% skim milk diluted in Tris-buffered saline (TBS) plus 0.1% (v/v) Tween-20 (TBST). Membranes were then probed overnight at 4°C with one of the following primary antibodies (diluted in TBST): MnSOD (1:2,000; rabbit polyclonal IgG (FL-222): sc-30080, Santa Cruz Biotechnology), 4–HNE (1:2,500; rabbit polyclonal IgG: 393206, Calbiochem), ANT (1:4,000; goat polyclonal IgG (N-19): sc-9299, Santa Cruz Biotechnology) and UCP3 (1:1,000; rabbit polyclonal IgG, Abcam). Following 3 X 10 min washes with TBST, membranes were incubated in the appropriate secondary antibody, diluted in TBST + 5% skim milk at room temperature for 1 h: goat anti-rabbit IgG-HRP (1:1000; sc-2030, Santa Cruz Biotechnology), donkey anti-goat IgG-HRP (1:1000; sc-2033, Santa Cruz Biotechnology). Secondary antibodies were conjugated to HRP. Following the incubation, membranes were washed for 3 X 10 min with TBST. Protein bands were detected by enhanced chemiluminescence (ECL RPN 2109: Amersham Pharmacia Biotech) and subsequent exposure onto film (Polaroid Polapan–667) or imaging using the Typhoon imaging system (Typhoon Trio, GE Healthcare). Band intensity was quantified as the integrated pixel intensity using ImageJ software (NIH). Coomassie stained gels were used as protein loading controls; gels were scanned, and pixel intensity of a series of bands was determined

as above. The rationale for the use of Coomassie stained proteins was that numerous mitochondrial protein levels are altered with CR, making it difficult to select one specific protein as the loading control (Sreekumar et al., 2002).

2.1.11 Mitochondrial content

Previously frozen skeletal muscle pieces from the *vastus lateralis* of Wt and UCP3 Tg AL/CR mice (section 2.1.5) were used to determine mitochondrial content by histochemical determination of cytochrome c oxidase (COX) activity (Dubowitz, 2007). *In vivo*, COX accepts electrons from cyt c and subsequently reduces oxygen producing H_2O. In the presence of active COX (within the tissue sample) and exogenous reduced cyt c, COX accepts an electron from cyt c. Exogenous diaminobenzidine (DAB) then donates an electron to oxidized cyt c which then becomes reduced. Consequently, oxidized DAB undergoes polymerization which causes it to become osmophillic ('salt-loving'). As a result, DAB precipitates and forms dark deposits on the surface of the mitochondrial inner membrane (Kugler et al., 1988; Seligman et al., 1968).

COX staining was carried out following procedures as described (Dubowitz, 2007). Briefly, frozen sections were cut (10 µM thick) perpendicular to the muscle fibers at ~ -25°C, and were subsequently mounted onto glass slides. Sections were then incubated in 9 mL of a 0.1 M phosphate buffer (0.1 M sodium dihydrogen orthophosphate, 0.1 M disodium hydrogen orthophosphate, pH 7.4) containing 7.5 mg of 3,3'–diaminobenzidine tetrahydrochloride (DAB; Vector Lab, 5k-4105 (ImmPACT^{TM}DAB)) with addition of 1 mL of catalase c (4 mg/ mL ddH_2O; Sigma,

from bovine liver), 10 mg cytochrome c (Sigma, from horse heart) and 750 mg sucrose) for 3 h at 37–38°C. Sections were subsequently fixed in formol calcium (100 µL of 10% calcium chloride, 100 µl of 40% formaldehyde and 900 µl ddH_2O) for 15–20 min at room temperature, and then dehydrated in alcohol. Finally, sections were cleared of alcohol using xylene and were mounted using Permount (Fisher Scientific).

Slides were individually visualized by light microscopy using a 20X objective. To minimize differences in background intensity, images were captured using the same lighting and exposure settings. Images were analyzed by obtaining the integrated pixel density per muscle fiber along with the area of each muscle fiber using ImageJ software (NIH). The total integrated density for the whole region of muscle was normalized to the total area that was analyzed. For each image analysis, the integrated density values were corrected for background. It is important to note that the individual who performed the analysis was blinded to both the experimental groups and to the purpose of the experiment.

2.2 ADDITIONAL MEASUREMENTS IN 1 MONTH CALORIE RESTRICTED MICE

In addition to the experimental work described above, some further experiments were conducted in 1 mo CR mice, as detailed below.

2.2.1 Proton leak determinations in isolated skeletal muscle mitochondria

To measure the degree of proton leak at a given PMF in mitochondria from

Wt and UCP3 Tg mice (AL and CR), both PMF and oxygen consumption were measured in parallel, as outlined below. For all leak determinations, both an AL and a CR mouse from each of the two genotypes were tested on the same experimental day. Mice were sacrificed two at a time and isolations were carried out in tandem (either Wt or Tg AL/CR). An ~ 20 min delay occurred between mitochondrial isolations from the first and second set of mice and the order of sacrifice was alternated on each experimental day.

PMF was detected fluorometrically using safranin O (Akerman and Wikstrom, 1976). Excitation and emission were 485 nm and 580 nm, respectively. Safranin O (5 µM), rotenone (5 µM: to block complex I), nigericin (0.4 µg/mL: to convert the pH component of PMF to mV), oligomycin (8 µg/mg mitochondria: to induce state 4 respiration) and isolated mitochondria (0.1 mg mitochondria/0.3 mL) were added to each well containing warmed incubation medium (IM: 120 mM KCl, 5 mM HEPES, 5 mM $MgCl_2$, 1 mM EGTA, 5 mM KH_2PO_4 and 0.3% BSA (w/v); pH 7.4 at 25°C). Readings were initiated following temperature equilibration at 37°C. Four basal readings were made; then, succinate (10 mM) was added. Upon energization by succinate (recorded as a drop in fluorescence), the PMF was titrated by 5 successive 1 mM additions of malonate, a complex II inhibitor. Because the ATP synthase was inhibited by oligomycin, any drop in PMF (recorded as an increase in fluorescence) was due to mitochondrial proton leak. FCCP (0.3 µM) was then added to release all safranin O from the mitochondria. Each genotype comparison (AL or CR) was run in duplicate for 30 min. A fluorescence reading was taken every 30 s.

Oxygen consumption rates were converted to nmol O/(mg protein*min) after calibration of the oxygen electrode (see section 2.1.8). Mitochondrial proton leak curves were generated by plotting PMF for succinate and each of the 5 malonate titrations (arbitrary fluorescence units (A.U.)) *vs.* corresponding oxygen consumption values.

2.3 MATERIALS

All inhibitors (*e.g.,* oligomycin, antimycin A, rotenone, malonate, nigericin and FCCP), substrates (*e.g.,* succinate, malate, pyruvate and PC), enzymes (*e.g.,* SOD, subtilisin and HRP), ATP, ADP, PHPA, and BSA were all purchased from Sigma–Aldrich (St. Louis, MO). Primary antibodies including MnSOD and ANT were purchased from Santa Cruz Biotechnology (Santa Cruz, CA) whereas, those for UCP3 and 4–HNE were purchased from Abcam Inc. (Cambridge, MA) and Calbiochem (San Diego, CA), respectively. Secondary antibodies including goat anti–rabbit IgG–HRP and donkey anti–goat IgG–HRP were purchased from Santa Cruz Biotechnology.

2.4 STATISTICAL ANALYSIS

Comparisons between Wt AL and UCP3 Tg AL mice were analyzed by two–tailed, unpaired t–tests using Microsoft Office Excel 2003. To compare the CR effect in Wt and UCP3 Tg mice, two-way analysis of variance (ANOVA) (independent samples) were performed. The two grouping variables were diet (AL

vs. CR) and genotype (Wt *vs.* UCP3 Tg). Repeated measures two-way ANOVA was performed when comparing IC light-dark phase (repeated measure) and genotypes. When ANOVA was found to be significant, Bonferroni *post hoc* contrasts were performed (Graph Pad, La Jolla, CA). For clarity, only analyses of the diet-effect are presented, unless otherwise stated. Statistical significance was defined as a P value less than 0.05. All data are presented as mean ± standard error of the mean (SEM).

CHAPTER 3
RESULTS

3.1 CHARACTERIZATION OF UCP3 TG MICE

The first step of this study was to characterize UCP3 Tg mice at the whole body and skeletal muscle mitochondrial level, with particular emphasis on mitochondrial proton leak and ROS production. Therefore, results presented in this section are only from AL-fed Wt and UCP3 Tg mice, at 14 wks of age at sacrifice, unless otherwise stated.

3.1.1 Body weight phenotype

Table 2 shows the average BW, weights of individual tissues, as well as food intake results from Wt and UCP3 Tg mice. UCP3 Tg AL mice had a significantly lower BW compared to Wt AL mice ($P<0.001$). On average, UCP3 Tg mice weighed ~ 12% less then Wt mice. Interestingly, this difference in BW was not due to differences in daily food intake, as both genotypes consumed ~ 2.75 g of food each day. In terms of body composition, the BW discrepancy was attributed, at least in part, to decreased muscle weight in UCP3 Tg mice compared to Wt mice; UCP3 Tg mice had ~ 17% less muscle compared to Wt mice ($P<0.01$). In contrast, fat pad (gWAT and iBAT), heart, kidney and liver weights did not differ between genotypes.

Table 3 shows the average tissue weights from Wt and UCP3 Tg mice, expressed as a percentage of total BW. The percentages of liver, heart, kidney,

Table 2. Body weight and weights of individual tissues from Wt AL/CR and UCP3 Tg AL/CR at 14 wks of age (2 wk CR treatment). Values are presented as means ± SEM (n=8-12/group). Food intake values are based on the average daily food intake of Wt and UCP3 Tg mice during the 1 mo food intake period (n=21–23/group). The percent decrease with 2 wk CR treatment compared to AL for body weight and individual tissue weights from Wt and UCP3 Tg mice are also shown. UCP3 Tg AL mice weighed less then Wt controls due to less muscle weight. CR caused a decrease in body weight and in the weight of all tissues measured. *P<0.05, **P<0.01, ***P<0.001; two–way ANOVA, bonferroni post test (diet-effect). $^{\#\#}$P<0.01, $^{\#\#\#}$P<0.001; two–way ANOVA, bonferroni post test (genotype-effect). Abbreviations: gWAT; gonadal white adipose tissue, iBAT; interscapular brown adipose tissue.

2 week CR						
Organ (g)	Wt			UCP3 Tg		
	AL	CR	% decrease (CR *vs.* AL)	AL	CR	% decrease (CR *vs.* AL)
Liver	1.32 ± 0.03	0.82 ± 0.02***	38	1.21 ± 0.08	0.79 ± 0.03***	35
Kidney	0.31 ± 0.01	0.25 ± 0.01***	19	0.31 ± 0.02	0.24 ± 0.0***	23
Heart	0.13 ± 0.00	0.12 ± 0.00*	8	0.13 ± 0.00	0.11 ± 0.00**	15
gWAT	0.71 ± 0.08	0.31 ± 0.04***	56	0.65 ± 0.09	0.16 ± 0.02***	75
iBAT	0.18 ± 0.01	0.11 ± 0.00***	39	0.17 ± 0.01	0.09 ± 0.01***	47
Muscle	2.07 ± 0.11	1.83 ± 0.04*	12	1.71 ± 0.04##	1.43 ± 0.02**	16
Body weight	28.5 ± 0.6	21.3 ± 0.6***	25	25.0 ± 0.6###	18.5 ± 0.2***	26
Food intake (g/day)	2.72 ± 0.04			2.77 ± 0.05		

Table 3. Weights of individual tissues from Wt AL/CR and UCP3 Tg AL/CR at 14 wks of age (2 wk CR treatment) expressed as a percentage of total body weight. Values are presented as means ± SEM (n=8–10/group). There were no differences in body composition between Wt AL and UCP3 Tg AL mice. However, Wt and UCP3 Tg mice responded differently to CR. In Wt mice, liver, and gWAT weight/g BW decreased; whereas, muscle weight/g BW increased with CR. Kidney, heart and iBAT weight/g BW was unchanged with CR in Wt mice. In UCP3 Tg mice, CR caused a decrease in liver, kidneys, gWAT, iBAT and muscle weight/g BW; whereas heart weight/g BW was unchanged with CR. $^{\#}P<0.05$, $^{\#\#\#}P<0.001$; two–way ANOVA, bonferroni post test (genotype-effect). $^{*}P<0.05$, $^{**}P<0.01$, $^{***}P<0.001$; two–way ANOVA, bonferroni post test (diet-effect). Abbreviations: gWAT; gonadal white adipose tissue, iBAT; interscapular brown adipose tissue, BW; body weight.

2 week CR				
Organ (% of body weight)	Wt		UCP3 Tg	
	AL	CR	AL	CR
Liver	4.8 ± 0.13	3.9 ± 0.05**	4.8 ± 0.29	3.3 ± 0.23***
Kidney	1.1 ± 0.03	1.2 ± 0.02	1.2 ± 0.05	1.0 ± 0.05***
Heart	0.5 ± 0.03	0.6 ± 0.01	0.5 ± 0.02	0.5 ± 0.03
gWAT	2.6 ± 0.21	1.5 ± 0.16***	2.5 ± 0.24	0.7 ± 0.12***#
iBAT	0.6 ± 0.03	0.5 ± 0.02	0.7 ± 0.04	0.4 ± 0.03***###
Muscle	7.5 ± 0.30	8.8 ± 0.15**	6.9 ± 0.30	6.0 ± 0.25*###

gWAT, iBAT and muscle to total BW were similar between Wt and UCP3 Tg mice. Therefore, body composition was similar in these two genotypes.

3.1.2 Whole body energetics

Whole body $\dot{V}O_2$ from Wt AL and UCP3 Tg AL mice is plotted as a function of time in Figure 7. Data in Figure 7 (A) are from 14 wk and 16 wk old AL-fed mice. Analysis was subsequently performed on data averaged over each of the light and the dark phases (Figure 7 (B)). On a per mouse basis, $\dot{V}O_2$ was increased during the dark phase compared to the light phase in both genotypes (Figure 7 (A) and (B), $P<0.001$)). Also on a per mouse basis, average $\dot{V}O_2$ in Wt mice tended to be higher than in UCP3 Tg mice over the 24 h period (Figure 7 (A)); however, no differences in $\dot{V}O_2$/mouse were detected between genotypes when data was averaged over each of the light and dark phase (Figure 7 (B)).

Since no differences in body composition were detected between Wt and UCP3 Tg mice, whole body $\dot{V}O_2$ results could be divided through by BW without any complexities in interpretation related to changes in body composition (Figure 8). Figure 8 (A) shows average mass–adjusted $\dot{V}O_2$ for both genotypes over a 24 h period. As in Figure 7, average values for the light and dark phase were determined for analysis (Figure 8 (B)). Normalization to BW resulted in a tendency for higher $\dot{V}O_2$/g in UCP3 Tg mice compared to Wt mice during both the light and dark phase ($P=0.12$ and $P=0.10$, respectively).

The RER for Wt and UCP3 Tg mice is shown in Figure 9; as for $\dot{V}O_2$, data from 14 and 16 wk old AL mice have been included. In both genotypes, RER

Figure 7. Combined whole body oxygen consumption (VO_2) in Wt AL and UCP3 Tg AL mice at 14 and 16 wks of age. Values are expressed per mouse and are presented as means ± SEM (n=14/group). (A) Mean VO_2 plotted over a 24 h period (16:00-16:00). Some error bars are within the symbol. (B) Mean VO_2 in the light (06:00-18:00) and dark (18:00-06:00) phase for both Wt AL and UCP3 Tg AL mice. In both Wt and UCP3 Tg mice, VO_2 increased in the dark phase compared to the light phase (***$P<0.001$; two–way ANOVA, bonferroni post test). No significant differences in VO_2 were detected between genotypes in either the light or dark phase.

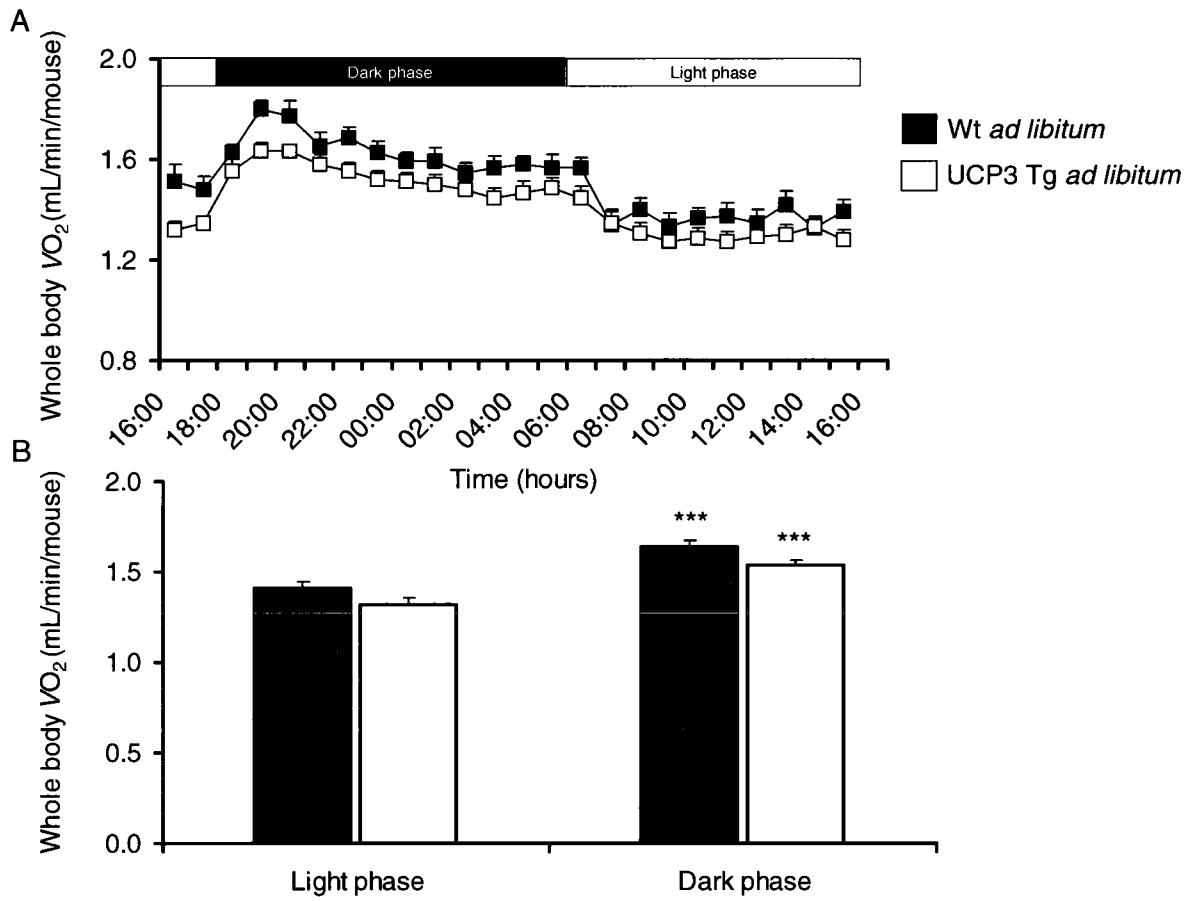
A
Whole body VO_2 (mL/min/mouse)
2.0
1.6
1.2
0.8
Dark phase
Light phase
16:00
18:00
20:00
22:00
00:00
02:00
04:00
06:00
08:00
10:00
12:00
14:00
16:00
Time (hours)
Wt ad libitum
UCP3 Tg ad libitum
B
Whole body VO_2 (mL/min/mouse)
2.0
1.5
1.0
0.5
0.0
***
***
Light phase
Dark phase

Figure 8. Combined whole body oxygen consumption (VO_2) in Wt AL and UCP3 Tg AL mice expressed per gram (g) of total body weight at 14 and 16 wks of age. Values are presented as means ± SEM (n=14/group). (A) Mean VO_2 plotted over a 24 h period (16:00-16:00). Some error bars are within the symbol. (B) Mean VO_2 in the light (06:00-18:00) and dark (18:00-06:00) phase for both Wt AL and UCP3 Tg AL mice. In both Wt and UCP3 Tg mice, VO_2 increased in the dark phase compared to the light phase (***P<0.001; two–way ANOVA, bonferroni post test). There was a trend for increased VO_2 in UCP3 Tg mice compared to Wt mice in the light and dark phase (P=0.12 and P=0.10, respectively; two–way ANOVA, bonferroni post test).

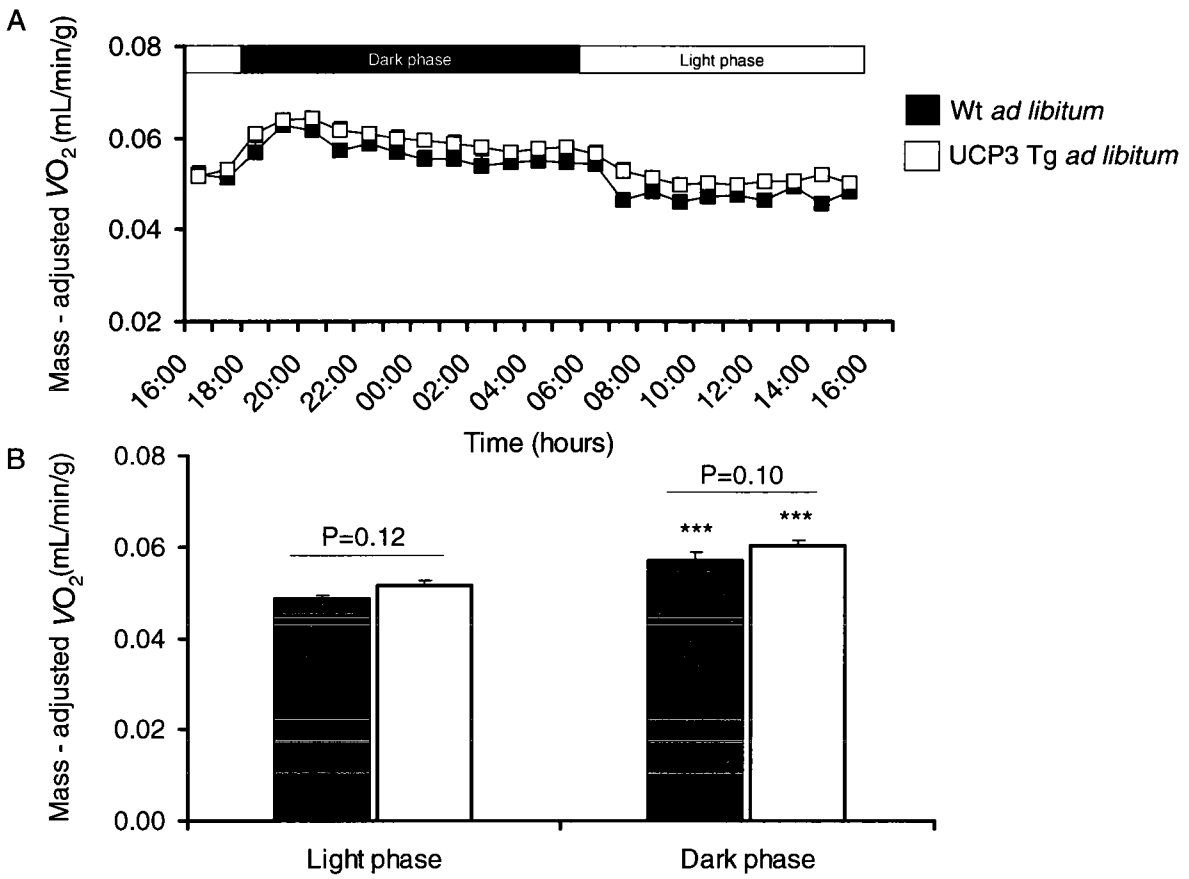
A
Mass - adjusted VO_2(mL/min/g)
0.08
0.06
0.04
0.02
Dark phase
Light phase
Wt *ad libitum*
UCP3 Tg *ad libitum*
16:00
18:00
20:00
22:00
00:00
02:00
04:00
06:00
08:00
10:00
12:00
14:00
16:00
Time (hours)
B
Mass - adjusted VO_2(mL/min/g)
0.08
0.06
0.04
0.02
0.00
P=0.12
P=0.10
***
***
Light phase
Dark phase

Figure 9. Combined respiratory exchange ratio (RER) in Wt AL and UCP3 Tg AL mice at 14 and 16 wks of age. Values are presented as means ± SEM (n=14/group). An RER closer to 1 indicates carbohydrate metabolism; whereas, an RER closer to 0.7 indicates fat metabolism. (A) Mean RER plotted over a 24 h period (16:00-16:00). Some error bars are within the symbol. (B) Mean RER values in the light (06:00-18:00) and dark phase (18:00-06:00) for both Wt AL and UCP3 Tg AL mice. In both Wt and UCP3 Tg mice, RER increased in the dark phase compared to the light phase (***$P<0.001$; two–way ANOVA, bonferroni post test). UCP3 Tg mice possessed higher RER values toward the end of the light phase and in the dark phase.

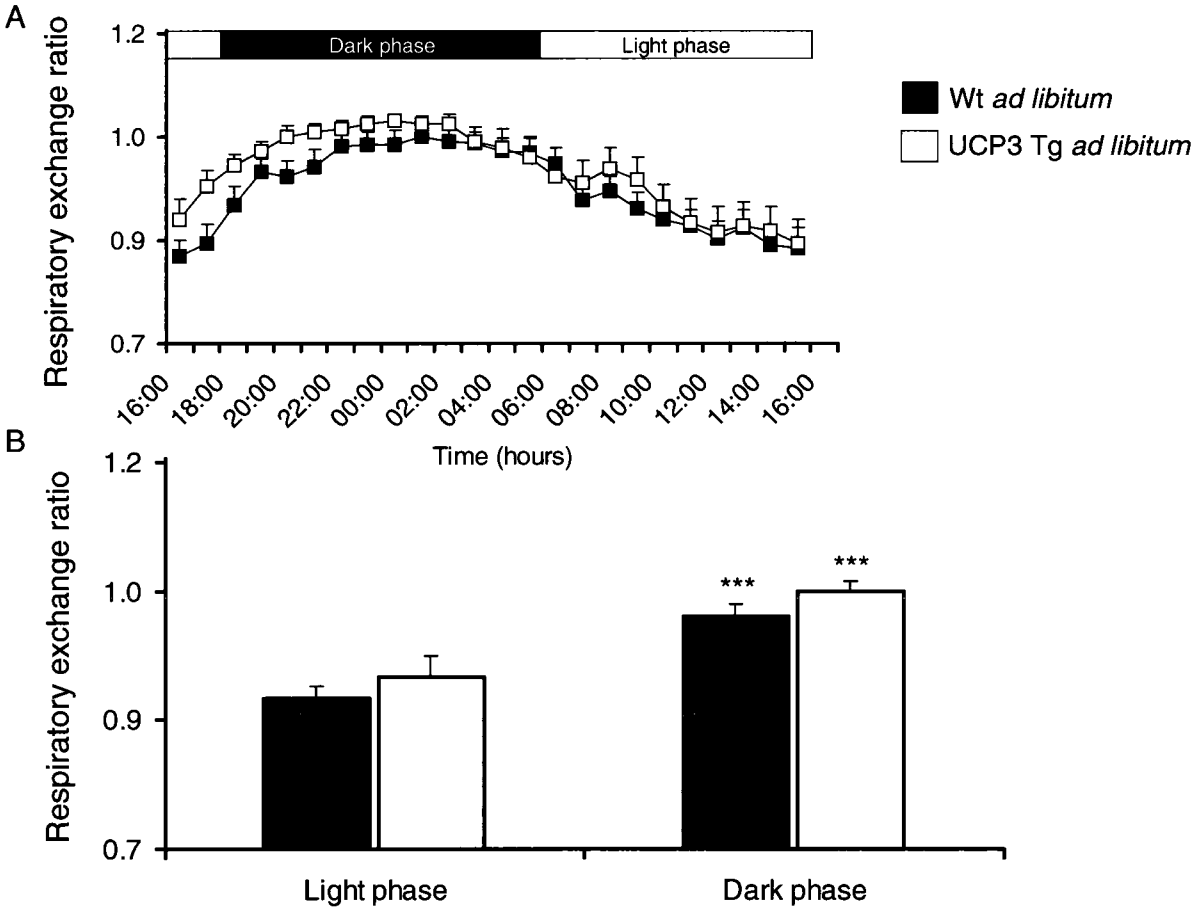
A
Respiratory exchange ratio
1.2
1.0
0.9
0.7
Dark phase
Light phase
Wt ad libitum
UCP3 Tg ad libitum
16:00
18:00
20:00
22:00
00:00
02:00
04:00
06:00
08:00
10:00
12:00
14:00
16:00
Time (hours)
B
Respiratory exchange ratio
1.2
1.0
0.9
0.7
***
***
Light phase
Dark phase

increased during the dark phase compared to the light phase ($P<0.001$, Figure 9 (A) and (B)). Toward the end of the light phase and during the first hours of the dark phase, RER tended to be higher in UCP3 Tg mice compared to Wt mice (Figure 9 (A)). However, differences between the genotypes were not significant when the values were averaged over each of the light and dark phases (Figure 9 (B)).

3.1.3 Mitochondrial content

Mitochondrial content was determined by measuring COX activity in skeletal muscle sections from Wt and UCP3 Tg mice (Figure 10). Data presented in Figure 10 are from AL-fed Wt and UCP3 Tg mice at 14 and 16 wks of age. No differences in COX activity were detected between Wt and UCP3 Tg mice, suggesting similar mitochondrial content in the two genotypes.

3.1.4 Mitochondrial UCP3 protein expression

UCP3 protein expression levels in isolated skeletal muscle mitochondria from Wt and UCP3 Tg AL mice are shown in Figure 11. Mitochondria from UCP3 Tg mice possessed an ~ 250% increase in UCP3 protein compared to mitochondria from Wt mice ($P<0.0005$).

3.1.5 Mitochondrial bioenergetics

Proton leak in isolated skeletal muscle mitochondria from Wt AL and UCP3

Figure 10. Mitochondrial content in skeletal muscle from Wt AL and UCP3 Tg AL mice. Values (means ± SEM) were obtained from AL-fed 14 and 16 wk old mice. Mitochondrial content was determined by histochemical activity of cytochrome c oxidase (COX; complex IV of the mitochondrial electron transport chain). Top: example of COX activity from Wt AL and UCP3 Tg AL muscle sections. Bottom: quantification of COX activity in Wt AL and UCP3 Tg AL muscle sections (n=8-11/group). No differences in mitochondrial content were detected between Wt and UCP3 Tg mice. Abbreviations: OD; optical density.

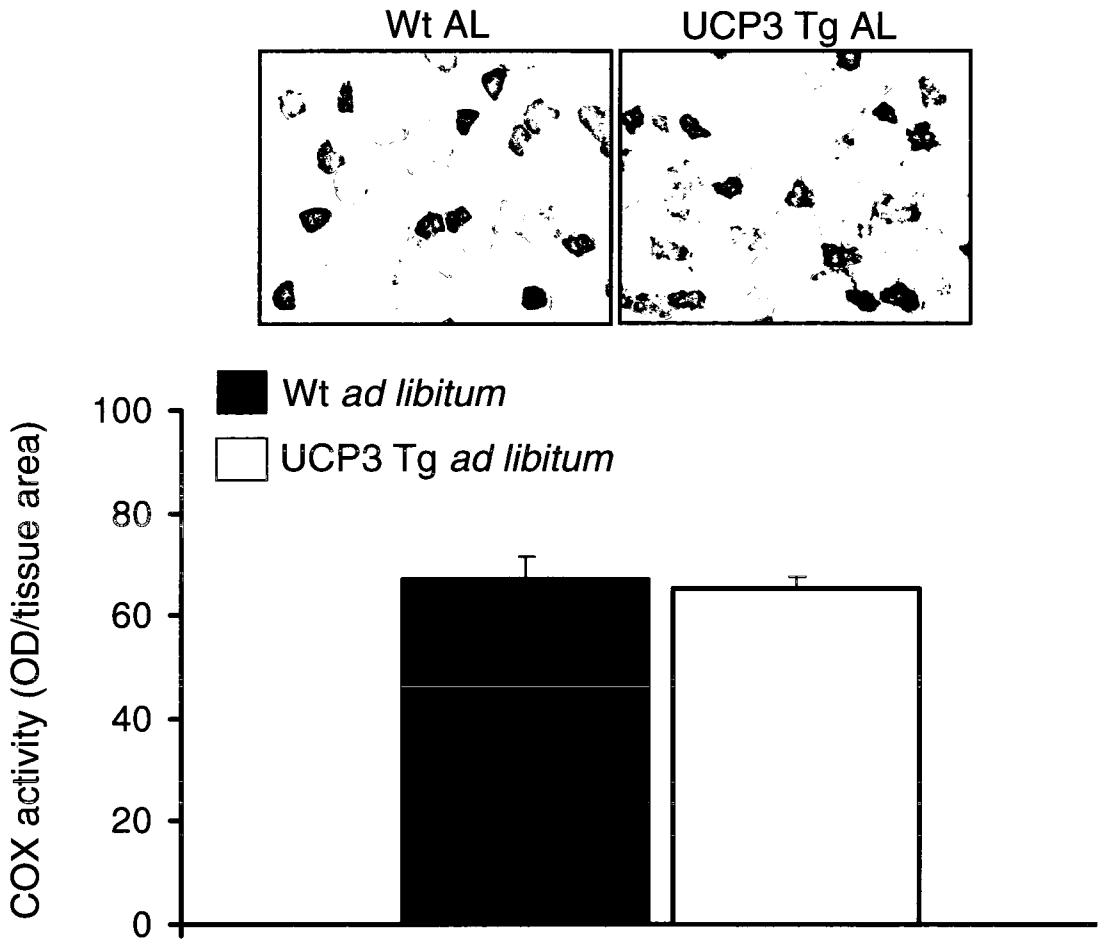
Wt AL
UCP3 Tg AL
Wt ad libitum
UCP3 Tg ad libitum
COX activity (OD/tissue area)
100
80
60
40
20
0

Figure 11. Quantification of UCP3 protein in isolated skeletal muscle mitochondria from Wt AL and UCP3 Tg AL mice at 14 wks of age. Representative Western blot and corresponding Coomassie stained gel for UCP3, 34 kDa (top panel). Each lane corresponds to mitochondria from a different mouse and protein was loaded at 30 μg. Samples were run on the same gel; the break represents different areas of the same blot/gel. UCP3 protein bands were quantified by densitometry (bottom panel). UCP3 Tg values were expressed relative to the average Wt value (100%); values are means ± SEM (n=8/group). Note that, prior to any normalization, all values were divided through by the amount of protein loaded (as determined by the Coomassie stained gel). UCP3 Tg AL mice possessed an ~ 250% increase in UCP3 protein as compared to Wt AL mice (***$P<0.0005$; t-test, two-tailed, unpaired).

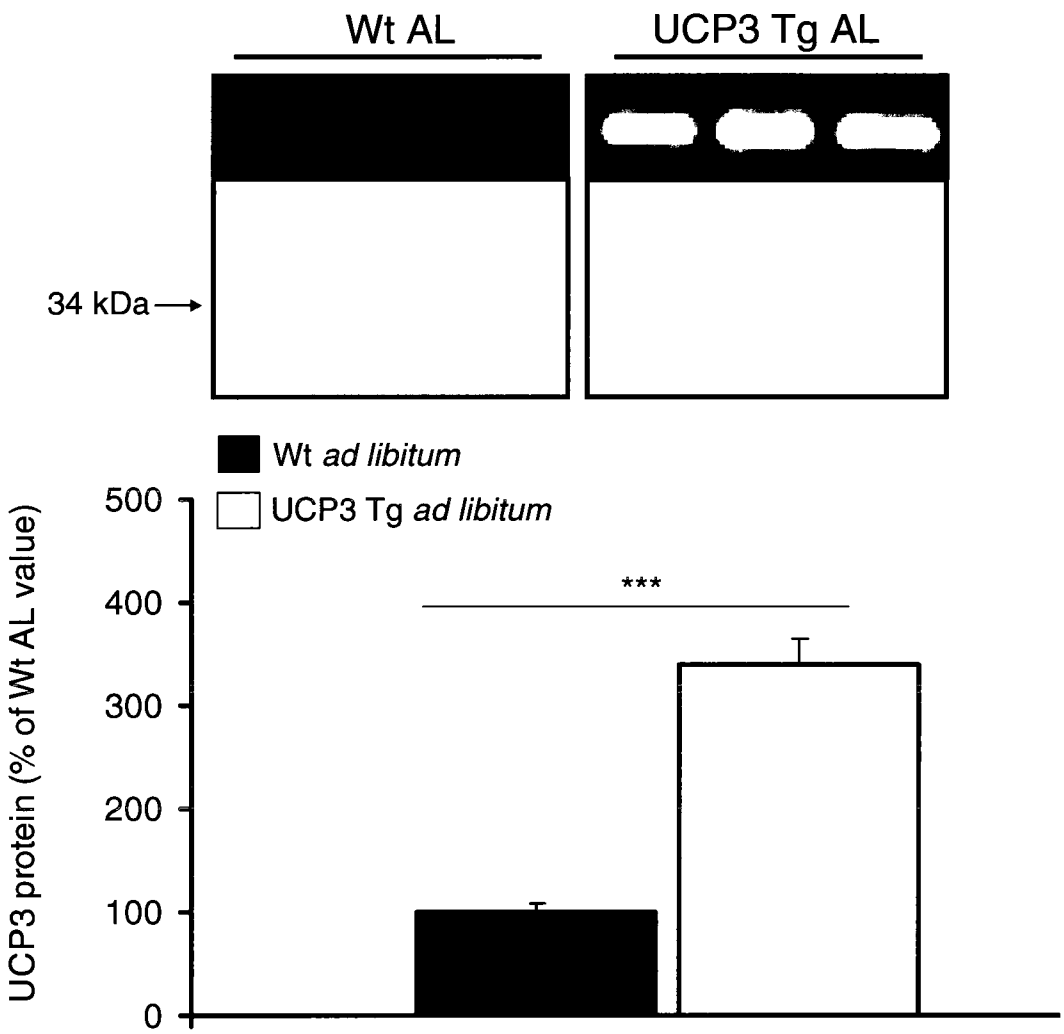
Wt AL
UCP3 Tg AL
34 kDa
Wt ad libitum
UCP3 Tg ad libitum
***
UCP3 protein (% of Wt AL value)
500
400
300
200
100
0

Tg AL mice at 16 wks of age is presented in Figure 12. In mitochondria from Wt and UCP3 Tg mice, oxygen consumption was plotted as a function of PMF in order to assess differences in mitochondrial proton leak kinetics (Figure 12 (A)). The furthest point on the right of each curve represents state 4 respiration; no differences were observed between genotypes. Compared to Wt, the UCP3 Tg curve was displaced leftward; in other words, at any given PMF, the rate of oxygen consumption was greater in UCP3 Tg compared to Wt mitochondria. At a common PMF (~ 3000 arbitrary units (A.U.)), the oxygen consumption rate was significantly higher in UCP3 Tg compared to Wt mitochondria ($P<0.05$, Figure 12 (B)). Therefore, mitochondria from UCP3 Tg mice had increased proton leak compared to mitochondria from Wt mice.

Maximal phosphorylating oxygen consumption (state 3), and leak-dependant (non-phosphorylating) oxygen consumption (state 4) were determined in mitochondria supplied with pyruvate/malate (5/2.5 mM) (Figure 13). Only data from 16 wk old Wt AL and UCP3 Tg AL mice are presented because daily calibrations of the oxygen electrode were not carried out for assays performed on mitochondria from 14 wk old mice. Note that on each experimental day, an AL-fed and one CR-fed mouse was paired; thus, comparisons between days could not be made unless daily calibrations were performed. State 4 respiration was similar in mitochondria from Wt and UCP3 Tg AL mice (Figure 13 (A)). There was, however, a trend for lower state 3 respiration in mitochondria from UCP3 Tg mice ($P=0.098$, Figure 13 (B)). Interestingly, the maximal uncoupled respiration rate was higher in UCP3 Tg compared to Wt mitochondria ($P<0.05$, Figure 13 (C)).

Figure 12. Mitochondrial proton leak in isolated skeletal muscle mitochondria from Wt AL and UCP3 Tg AL mice at 16 wks of age. Values are presented as means ± SEM (n=3–4/group). (A) Oxygen consumption and protonmotive force (PMF) were determined using a Clark-type electrode and a fluorescent dye, safranin (5 μM), respectively. Mitochondria (0.25 mg/mL) were supplied with succinate (10 mM), and determinations were performed in the presence of nigericin (0.4 μg/mL), rotenone (5 μM), oligomycin (8 μg/mg protein), and 5 successive 1 mM additions of malonate. The furthest point on the right represents state 4 respiration. Compared to Wt, the UCP3 Tg curve was displaced leftward; therefore, at any given PMF, the rate of oxygen consumption was increased compared to Wt controls. (B) The oxygen consumption rate was determined at a common PMF (~ 3000 arbitrary units (A.U.)) and UCP3 Tg mitochondria had an increased oxygen consumption rate compared to Wt (*$P<0.05$; t–test, two–tailed, unpaired).

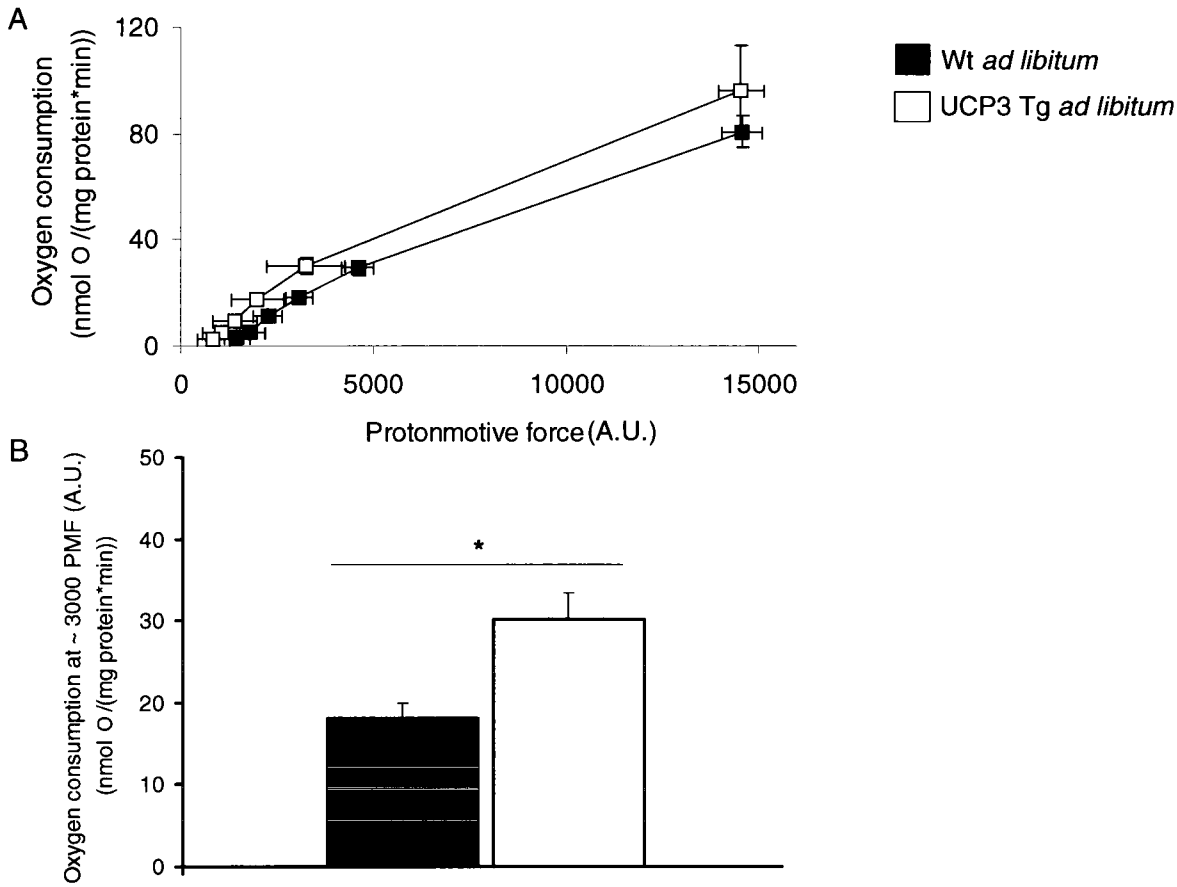
A
Oxygen consumption (nmol O /(mg protein*min))
120
80
40
0
0
5000
10000
15000
Protonmotive force (A.U.)
Wt ad libitum
UCP3 Tg ad libitum
B
Oxygen consumption at ~ 3000 PMF (A.U.) (nmol O /(mg protein*min))
50
40
30
20
10
0
*

Figure 13. Bioenergetic determinations in isolated skeletal muscle mitochondria from Wt AL and UCP3 Tg AL mice at 16 wks of age. Pyruvate (5 mM) and malate (2.5 mM) were used as the substrates. Values are shown as means ± SEM (n=4–5/group). (A) Non–phosphorylating respiration (state 4), as induced using oligomycin (8 μg/mg mitochondria). (B) Maximal phosphorylating respiration (state 3), as induced using saturating [ADP] (200 μM). (C) Maximal flux through the ETC with FCCP (3 μM) as a chemical uncoupler. There was no detectable difference in state 4 oxygen consumption between genotypes; however, mitochondria from UCP3 Tg mice had a higher maximal uncoupled respiration rate (*$P<0.05$; t-test, two-tailed, unpaired) and a tendency for lower state 3 oxygen consumption compared to mitochondria from Wt mice.

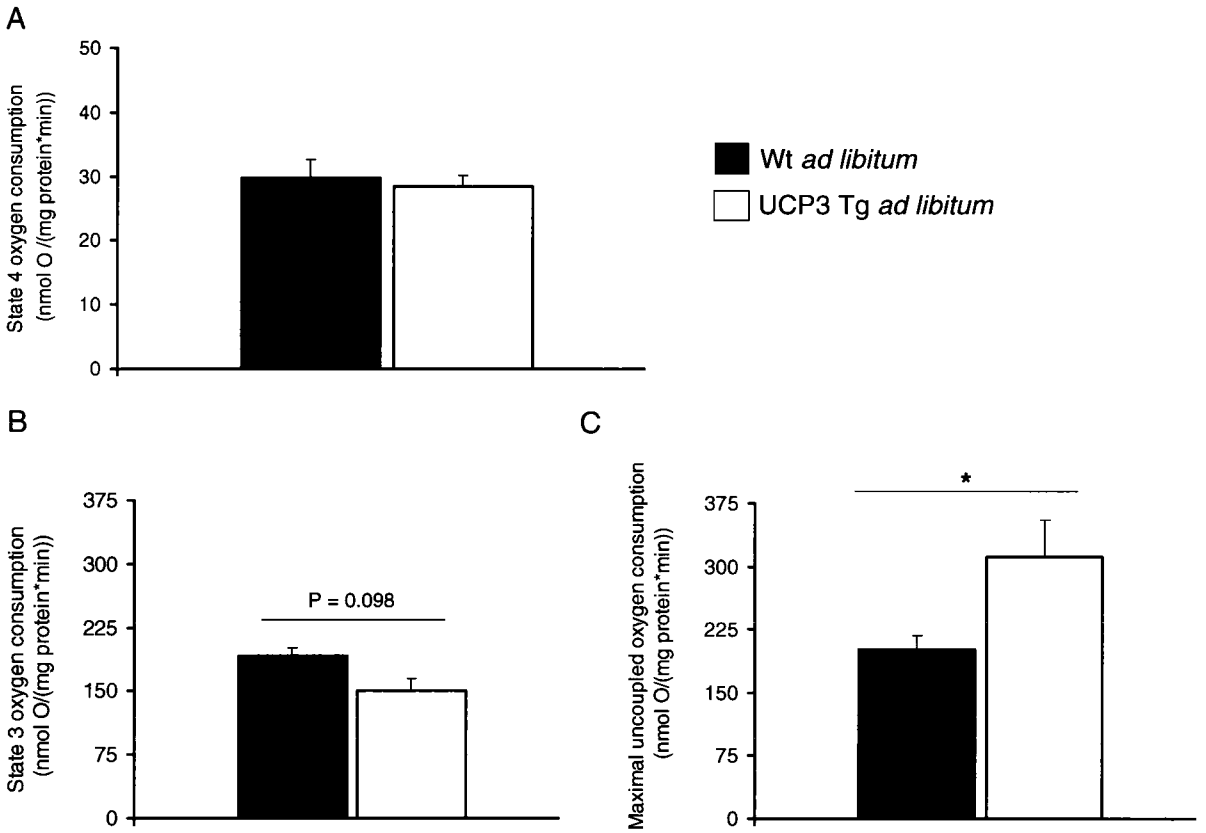
A
State 4 oxygen consumption (nmol O /(mg protein*min))
50
40
30
20
10
0
Wt ad libitum
UCP3 Tg ad libitum
B
State 3 oxygen consumption (nmol O/(mg protein*min))
375
300
225
150
75
0
P = 0.098
C
Maximal uncoupled oxygen consumption (nmol O/(mg protein*min))
375
300
225
150
75
0
*

3.1.6 Mitochondrial ROS production

Based on the increased 'leakiness' of skeletal muscle mitochondria from UCP3 Tg mice (Figure 12), it was of interest to determine mitochondrial ROS production capacity. Measures were performed under a number of conditions in order to investigate ROS production from different sites within the mitochondrial matrix. Figure 14 shows the capacity for mitochondrial ROS production in both genotypes under non-phosphorylating conditions (Figure 14 (A)), in the presence of the complex I inhibitor, rotenone (Figure 14 (B)), and in the presence of the complex III inhibitor, antimycin (Figure 14 (C)), with either a non-lipid (right panel) or fatty acid substrate (left panel). Under almost all conditions, mitochondria from UCP3 Tg mice generated less ROS than mitochondria from Wt mice.

3.1.7 Expression of mitochondrial antioxidant proteins

Because ROS production is highly dependant on levels of antioxidant proteins, it was of interest to determine the level of MnSOD and ANT in mitochondria from Wt and UCP3 Tg mice, especially in light of the decreased ROS production in mitochondria from UCP3 Tg mice (Figure 14). Figure 15 shows UCP3, ANT and MnSOD protein expression in isolated skeletal muscle mitochondria from Wt AL and UCP3 Tg AL mice. ANT and MnSOD protein levels were similar in mitochondria from 14 wk old Wt and UCP3 Tg mice (Figure 15 (B) and (C), respectively).

Figure 14. ROS production in isolated skeletal muscle mitochondria from Wt AL and UCP3 Tg AL mice at 14 wks of age. Values are shown as means ± SEM (n=4–6/group). (A) ROS production under non-phosphorylating conditions, as induced by the ATP synthase inhibitor oligomycin (oligo; 8 μg/mg mitochondria). (B) ROS production in the presence of the complex I inhibitor, rotenone (rot; 5 μM). (C) ROS production in the presence of the complex III inhibitor, antimycin (anti; 5 μM). Under almost all conditions mitochondria from UCP3 Tg mice produced less ROS than mitochondria from Wt mice (*$P<0.05$ and **$P<0.005$; t-test, two-tailed, unpaired). Abbreviations: P/M; pyruvate/malate (5/2.5 mM), SOD; superoxide dismutase (20 units/0.3 mL), PC; palmitoylcarnitine (18 μM), succ; succinate (10 mM).

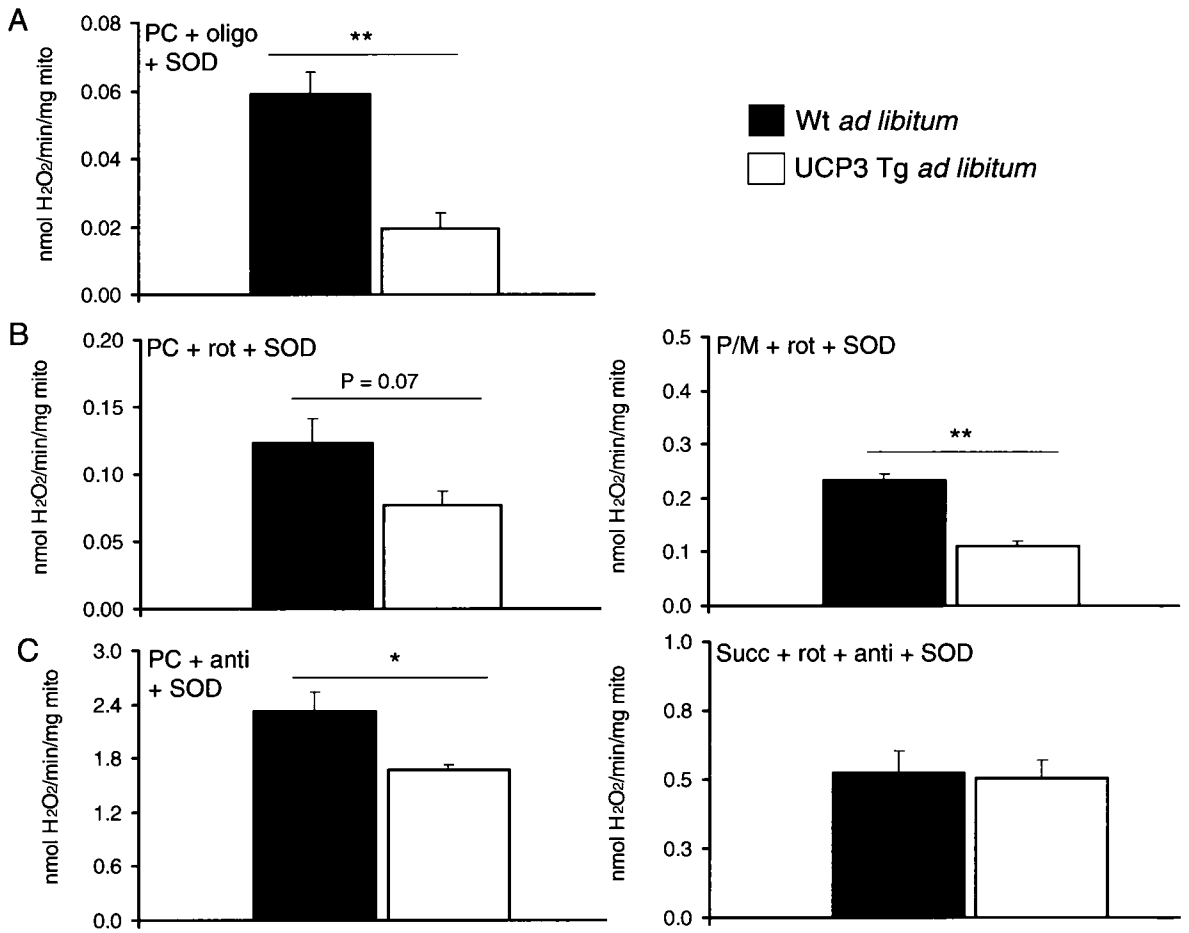
A
B
C
PC + oligo + SOD
**
nmol H2O2/min/mg mito
0.08
0.06
0.04
0.02
0.00
Wt ad libitum
UCP3 Tg ad libitum
PC + rot + SOD
P = 0.07
0.20
0.15
0.10
0.05
0.00
P/M + rot + SOD
**
0.5
0.4
0.3
0.2
0.1
0.0
PC + anti + SOD
*
3.0
2.4
1.8
1.2
0.6
0.0
Succ + rot + anti + SOD
1.0
0.8
0.5
0.3
0.0

Figure 15. UCP3, ANT and MnSOD protein expression in isolated skeletal muscle mitochondria from Wt AL/CR and UCP3 Tg AL/CR mice (2 wk CR treatment). Representative Western blot and corresponding Coomassie stained gel (top panel) for (A) UCP3, 34 kDa, (B) ANT, 33 kDa and (C) MnSOD, 25 kDa. Each lane corresponds to mitochondria from a different mouse and protein was loaded at 30 μg for UCP3, or 15 μg for ANT and MnSOD. For each protein, all samples were run on the same gel; the breaks represent different areas of the same blot/gel. Protein bands were quantified by densitometry (bottom panel) and are presented as means ± SEM for (A) UCP3; n=7–8/group, (B) ANT; n=5–7/group and (C) MnSOD; n=5–7/group. All values were divided through by the amount of protein loaded (as determined by the Coomassie stained gel). CR caused an increase in UCP3 protein in Wt mice and a decrease in ANT protein in UCP3 Tg mice (*$P<0.05$; two–way ANOVA, bonferroni post test).

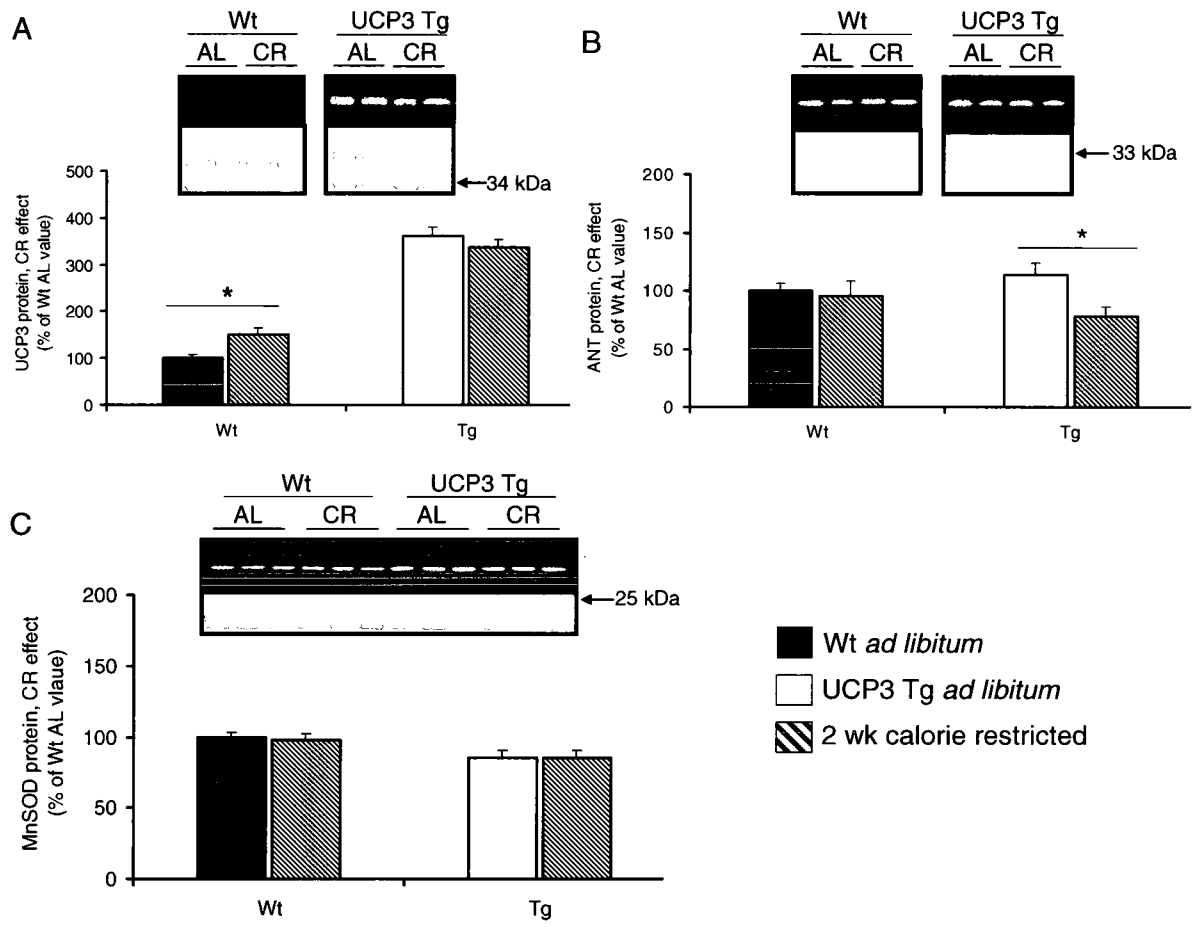
A
Wt
UCP3 Tg
AL
CR
AL
CR
34 kDa
UCP3 protein, CR effect
(% of Wt AL value)
500
400
300
200
100
0
*
Wt
Tg
B
Wt
UCP3 Tg
AL
CR
AL
CR
33 kDa
ANT protein, CR effect
(% of Wt AL value)
200
150
100
50
0
*
Wt
Tg
C
Wt
UCP3 Tg
AL
CR
AL
CR
25 kDa
MnSOD protein, CR effect
(% of Wt AL vlaue)
200
150
100
50
0
Wt
Tg
Wt ad libitum
UCP3 Tg ad libitum
2 wk calorie restricted

3.1.8 Oxidative stress of mitochondrial proteins

Due to the lower ROS production in mitochondria from UCP3 Tg mice compared to that of Wt mice (Figure 14), it was of interest to examine oxidative stress of mitochondrial proteins. Oxidative stress was determined immunologically using an antibody against 4–HNE modified proteins; thus, mitochondrial protein samples were electrophoresed on a denaturing gel, then probed with antibody (Figure 16). Comparison between Wt AL and UCP3 Tg AL mitochondria unexpectedly revealed a tendency for higher levels of 4–HNE modified proteins in UCP3 Tg mitochondria ($P=0.11$). This tendency was significant in mitochondria from 16 wk old Wt and UCP3 Tg mice ($P<0.05$, see Figure 31).

3. 2 EFFECT OF 2 WEEKS CR IN UCP3 TG AND WT MICE

3.2.1 Body and organ weights and body composition

The effect of 2 wk CR treatment on BW and individual tissue weights in both Wt and UCP3 Tg mice is presented in Table 2. In both genotypes, CR caused the loss of approximately 25% of total BW ($P<0.001$). In terms of individual tissue weight, the kidneys, liver, heart, gWAT, iBAT and skeletal muscle were all highly affected by the 2 wk CR treatment in both genotypes. In both Wt and UCP3 Tg mice, CR had the least effect on the heart, decreasing its weight by ~ 8% ($P<0.05$) and ~ 15% ($P<0.01$) in Wt and UCP3 Tg mice, respectively. CR decreased skeletal muscle and kidney weight by ~ 12% ($P<0.05$) and ~ 19% ($P<0.001$) respectively in

Figure 16. Levels of 4-HNE modified proteins in isolated skeletal muscle mitochondria from Wt AL/CR and UCP3 Tg AL/CR mice (2 wk CR treatment). Left: representative Western blot and corresponding Coomassie stained gel. Each lane corresponds to mitochondria from a different mouse and protein was loaded at 30 µg. All samples were run on the same gel. Right: 4–HNE protein adduct bands were quantified by densitometry. The regions that were assessed are denoted by brackets in both the coomassie stained gel and the corresponding Western blot. UCP3 protein (34 kDa) was omitted from the analysis. Values are presented as means ± SEM (n=5–7/group). All values were divided through by the amount of protein loaded (as determined by the Coomassie stained gel). There was a tendency for increased 4–HNE protein adduct levels in mitochondria from UCP3 Tg mice compared to that of Wt mice (P=0.11; two–way ANOVA, bonferroni post test). There was no detectable CR effect on 4–HNE protein adduct levels in either genotype.

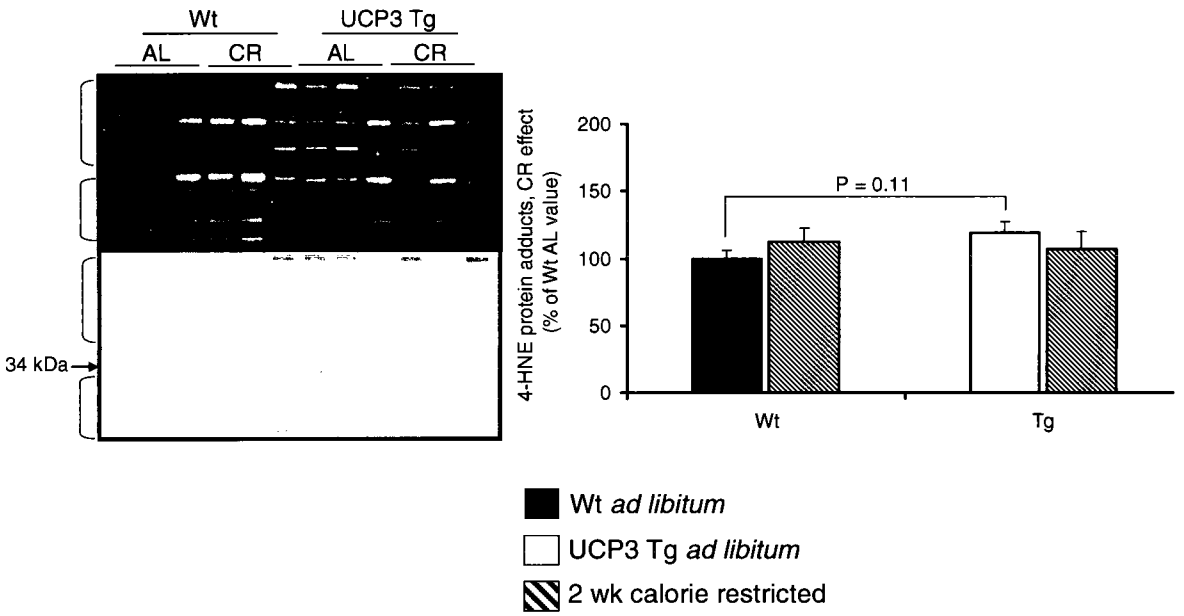
Wt
UCP3 Tg
AL
CR
AL
CR
34 kDa
4-HNE protein adducts, CR effect
(% of Wt AL value)
200
150
100
50
0
P = 0.11
Wt
Tg
Wt ad libitum
UCP3 Tg ad libitum
2 wk calorie restricted

Wt mice and by ~ 16% ($P<0.01$) and ~ 23% ($P<0.001$) respectively in UCP3 Tg mice. CR had a large effect on the liver in both Wt and UCP3 Tg mice, which decreased in weight by ~ 38% and ~ 35% in Wt and UCP3 Tg mice, respectively ($P<0.001$, for both genotypes). Of the tissues measured, the fat pads (gWAT and iBAT) in both genotypes were affected to the greatest extent by CR, decreasing in weight by ~ 56% (gWAT) and ~ 39% (iBAT) in Wt mice, and by ~ 75% (gWAT) and ~ 47% (iBAT) in UCP3 Tg mice ($P<0.001$, for both gWAT and iBAT in both Wt and UCP3 Tg mice).

The effect of 2 wk CR treatment on individual tissue weights in both Wt and UCP3 Tg mice expressed as a percentage of total BW is presented in Table 3. In Wt mice, the proportional contributions of liver ($P<0.01$, AL *vs.* CR) and gWAT ($P<0.001$, AL *vs.* CR) weight to total BW decreased with 2 wk CR; however, the proportional contributions of kidney, heart and iBAT weight were unchanged. On the other hand, the proportional contribution of muscle weight to total BW increased ($P<0.01$, AL *vs.* CR). In UCP3 Tg mice, 2 wk CR caused a decrease in the proportion of liver ($P<0.001$, AL *vs.* CR), kidney ($P<0.001$, AL *vs.* CR), gWAT ($P<0.001$, AL *vs.* CR), iBAT ($P<0.001$, AL *vs.* CR), as well as of muscle ($P<0.05$, AL *vs.* CR) weight. Only the proportion of heart weight was unchanged. Thus, after 2 wk CR, body composition was different between Wt and UCP3 Tg mice. Specifically, decreases in the proportional contributions of gWAT ($P<0.05$, Wt *vs.* UCP3 Tg) and iBAT ($P<0.001$, Wt *vs.* UCP3 Tg) to total BW were more pronounced in UCP3 Tg mice. Interestingly, the proportion of muscle weight increased in Wt but decreased in UCP3 Tg mice ($P<0.001$, Wt *vs.* UCP3 Tg).

3.2.2 Whole body energetics

The effect of 2 wk CR treatment on whole body $\dot{V}O_2$ in Wt and UCP3 Tg mice is shown in Figure 17 (A) and (B), respectively. On a per mouse basis, $\dot{V}O_2$ was greatly decreased at all timepoints over the 24 h period. Indeed, $\dot{V}O_2$/mouse was significantly decreased in CR mice of both genotypes, during both phases of the day ($P<0.001$, AL *vs.* CR for both Wt and UCP3 Tg) (Figure 17 (C) and (D)). Note that the extent of the decrease was similar for both genotypes.

The $\dot{V}O_2$ data from each mouse was expressed relative to BW; average values are plotted over 24 h (Figure 18 (A) and (B)). At almost all timepoints, and especially in the dark phase, CR induced a decrease in $\dot{V}O_2$/g in both Wt and UCP3 Tg mice. For analysis, mass–adjusted $\dot{V}O_2$ in Wt and UCP3 Tg AL/CR mice was averaged over each of the light and dark phases (Figure 18 (C) and (D), respectively). In the light phase, no differences in $\dot{V}O_2$ were detected in either genotype. In the dark phase, $\dot{V}O_2$ decreased with CR in both genotypes ($P<0.05$), and to the same extent.

The effect of 2 wk CR treatment on RER in Wt and UCP3 Tg mice is shown in Figure 19 (A) and (B), respectively. In both genotypes, RER in CR mice quickly decreased from ~ 1.0 to ~ 0.7 during the second half of the dark phase; whereas, RER in AL control mice remained at ~ 1.0. During the light phase, RER was maintained at ~ 0.7 in Wt CR and UCP3 Tg CR mice; however, in AL controls, RER remained at ~ 0.9.

Figure 17. The effect of 2 wk CR treatment on whole body oxygen consumption ($\dot{V}O_2$) in Wt and UCP3 Tg mice. Values are expressed per mouse and are presented as means ± SEM. (A) Mean $\dot{V}O_2$ in Wt AL (n=9) and Wt CR (n=8) mice plotted over a 24 h period (16:00-16:00). Some error bars are within the symbol. (B) Same as (A), for UCP3 Tg AL (n=9) and UCP3 Tg CR (n=10) mice. Mean $\dot{V}O_2$ in the light (06:00-18:00) phase (C) and dark (18:00-06:00) phase (D) for Wt AL/CR and UCP3 Tg AL/CR mice. In both genotypes CR decreased $\dot{V}O_2$ during the light and dark phase (***$P<0.001$; two–way ANOVA, bonferroni post test).

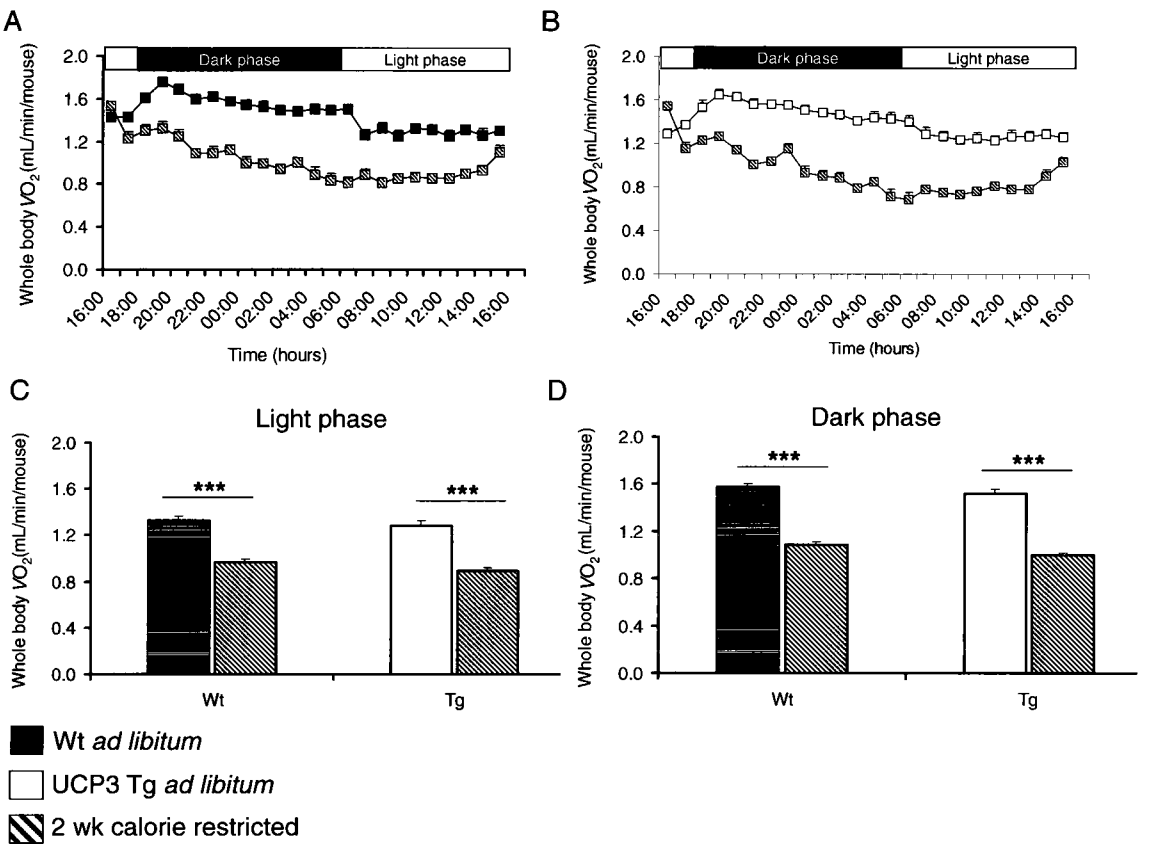
A
B
Dark phase
Light phase
Whole body VO_2 (mL/min/mouse)
2.0
1.6
1.2
0.8
0.4
0.0
16:00
18:00
20:00
22:00
00:00
02:00
04:00
06:00
08:00
10:00
12:00
14:00
16:00
Time (hours)
C
D
Light phase
Dark phase
***
Wt
Tg
Wt *ad libitum*
UCP3 Tg *ad libitum*
2 wk calorie restricted

Figure 18. The effect of 2 wk CR treatment on whole body oxygen consumption ($\dot{V}O_2$) in Wt and UCP3 Tg mice expressed per gram (g) of total body weight. Values are presented as means ± SEM. (A) Mean $\dot{V}O_2$ in Wt AL (n=9) and Wt CR (n=8) mice plotted over a 24 h period (16:00-16:00). Some error bars are within the symbol. (B) Same as (A), for UCP3 Tg AL (n=9) and UCP3 Tg CR (n=10) mice. Mean $\dot{V}O_2$ in the light (06:00-18:00) phase (C) and dark (18:00-06:00) phase (D) for Wt AL/CR and UCP3 Tg AL/CR mice. In both genotypes CR decreased $\dot{V}O_2$ only during the dark phase (*$P<0.05$; two–way ANOVA, bonferroni post test).

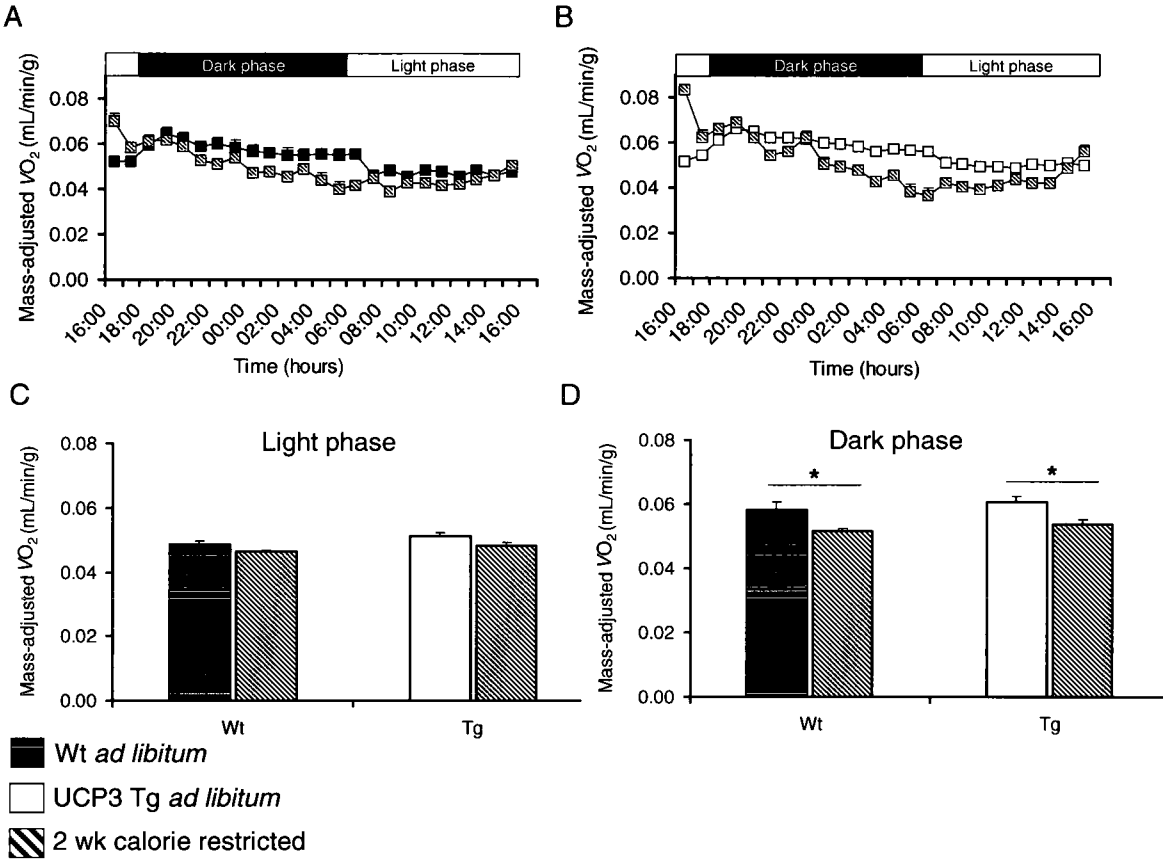
A
B
Dark phase
Light phase
Mass-adjusted VO_2 (mL/min/g)
0.08
0.06
0.04
0.02
0.00
16:00
18:00
20:00
22:00
00:00
02:00
04:00
06:00
08:00
10:00
12:00
14:00
16:00
Time (hours)
C
D
Light phase
Dark phase
*
Wt
Tg
Wt *ad libitum*
UCP3 Tg *ad libitum*
2 wk calorie restricted

Figure 19. The effect of 2 wk CR treatment on respiratory exchange ratio (RER) in Wt and UCP3 Tg mice. Values are presented as means ± SEM. (A) Mean RER data over a 24 h period (16:00-16:00) for Wt AL (n=9) and Wt CR (n=8) mice. Some error bars are within the symbol. (B) Same as (A), for UCP3 Tg AL (n=9) and UCP3 Tg CR (n=10) mice. In both genotypes, the chow provided at ~ 16:00 was rapidly consumed and the dietary carbohydrates were oxidized during the first half of the dark phase. Both genotypes then switched to fatty acid oxidation until the next feeding (~ 16:00). Therefore, Wt and UCP3 Tg CR mice spent a greater proportion of the day (~ 16 out of 24 h) oxidizing fatty acids.

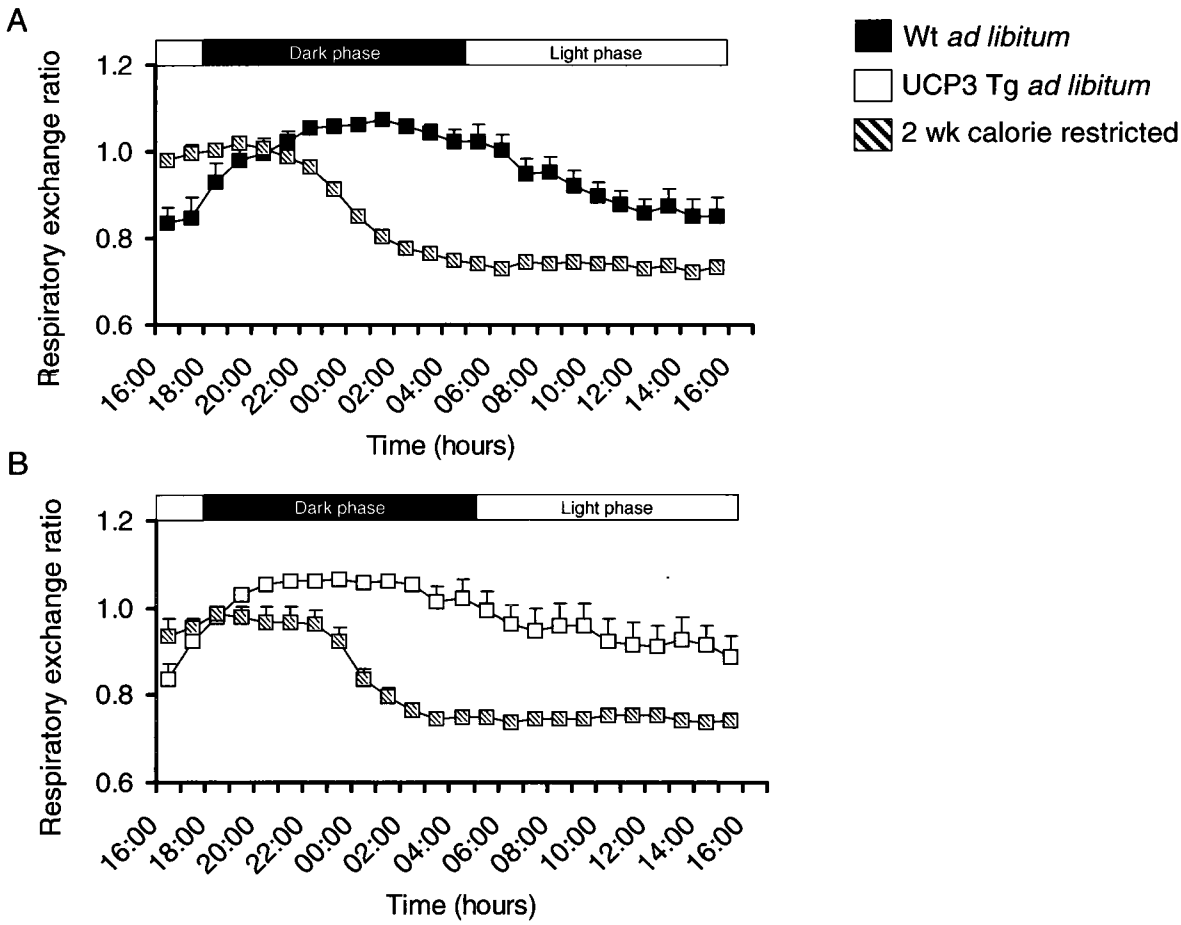
A
Dark phase
Light phase
Respiratory exchange ratio
1.2
1.0
0.8
0.6
16:00
18:00
20:00
22:00
00:00
02:00
04:00
06:00
08:00
10:00
12:00
14:00
16:00
Time (hours)
B
Dark phase
Light phase
Respiratory exchange ratio
1.2
1.0
0.8
0.6
16:00
18:00
20:00
22:00
00:00
02:00
04:00
06:00
08:00
10:00
12:00
14:00
16:00
Time (hours)
Wt ad libitum
UCP3 Tg ad libitum
2 wk calorie restricted

3.2.3 Mitochondrial content

The effect of 2 wk CR on mitochondrial content in skeletal muscle mitochondria from Wt and UCP3 Tg mice is shown in Figure 20. No CR-induced changes in COX activity were detected in either genotype. Therefore, 2 wk CR did not seem to affect mitochondrial content in Wt and UCP3 Tg mice.

3.2.4 Mitochondrial bioenergetics

The effects of 2 wk CR on state 3, state 4 and maximal uncoupled respiration rates were determined in skeletal muscle mitochondria from Wt and UCP3 Tg mice (Figure 21). Daily calibrations of the oxygen electrode were not carried out for mitochondria from 14 wk old mice. However, on each experimental day, an AL-fed and one CR-fed mouse were paired; thus, by applying an average calibration the CR-effect could be presented. State 4 and maximal uncoupled respiration were both unchanged with CR in mitochondria from both genotypes (Figure 21 (A) and (C), respectively). Conversely, state 3 tended to decrease with CR only in mitochondria from UCP3 Tg mice ($P=0.13$).

3.2.5 Mitochondrial ROS production

Because CR has been shown to decrease ROS production (*e.g.,* Bevilacqua et al., 2004, 2005), it was expected that we would indeed observe this in mitochondria from Wt mice. On the other hand, since mitochondria from UCP3 Tg

Figure 20. The effect of 2 wk CR treatment on mitochondrial content in skeletal muscle from Wt and UCP3 Tg mice. Values are presented as means ± SEM. Mitochondrial content was determined by histochemical activity of cytochrome c oxidase (COX). Left panel: example of COX activity in muscle sections from Wt AL/CR and UCP3 Tg AL/CR. Right panel: quantification of COX activity in Wt AL/CR and UCP3 Tg AL/CR muscle sections (n=5/group). No CR-induced differences in mitochondrial content were detected in either genotype. Abbreviations: OD; optical density.

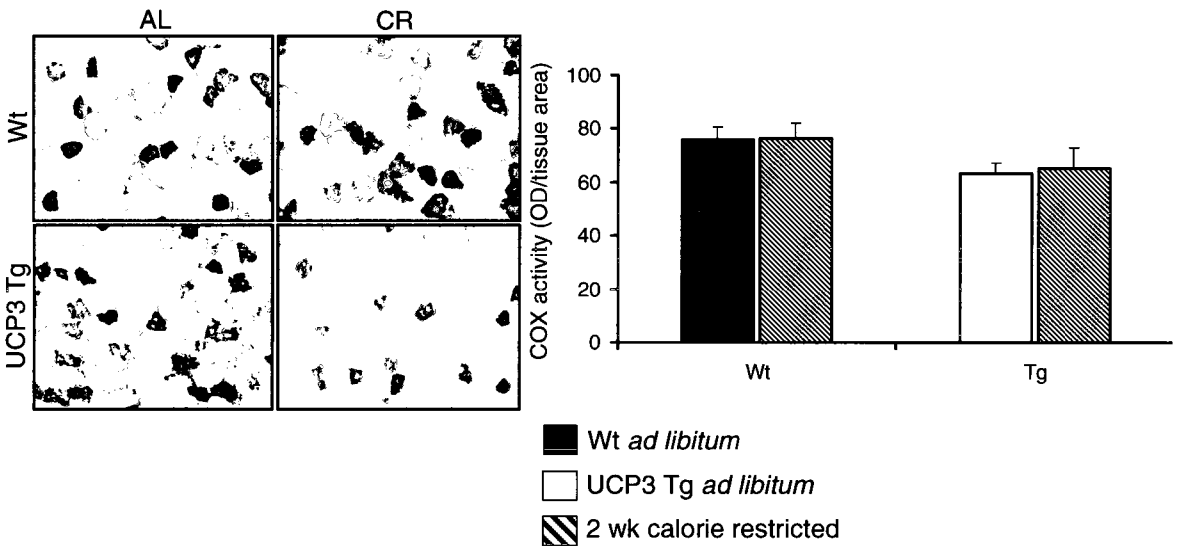
AL
CR
Wt
UCP3 Tg
COX activity (OD/tissue area)
100
80
60
40
20
0
Wt
Tg
Wt ad libitum
UCP3 Tg ad libitum
2 wk calorie restricted

Figure 21. The effect of 2 wk CR treatment on bioenergetics in isolated skeletal muscle mitochondria from Wt and UCP3 Tg mice. Pyruvate (5 mM) and malate (2.5 mM) were used as the substrate. Values are shown as means ± SEM. (A) Non–phosphorylating respiration (state 4), as induced by oligomycin (8 μg/mg mitochondria) (n=6–10/group). (B) Maximal phosphorylating respiration (state 3), as induced using saturating [ADP] (200 μM) (n=7–10/group). (C) Maximal flux through the ETC was obtained using FCCP (3 μM) as a chemical uncoupler (n=7–9/group). There were no detectable CR effects on state 4 oxygen consumption or maximal uncoupled oxygen consumption in either genotype. Conversely, there was a trend for a CR–induced decrease in state 3 oxygen consumption in UCP3 Tg mice (P=0.13; two–way ANOVA, bonferroni post test).

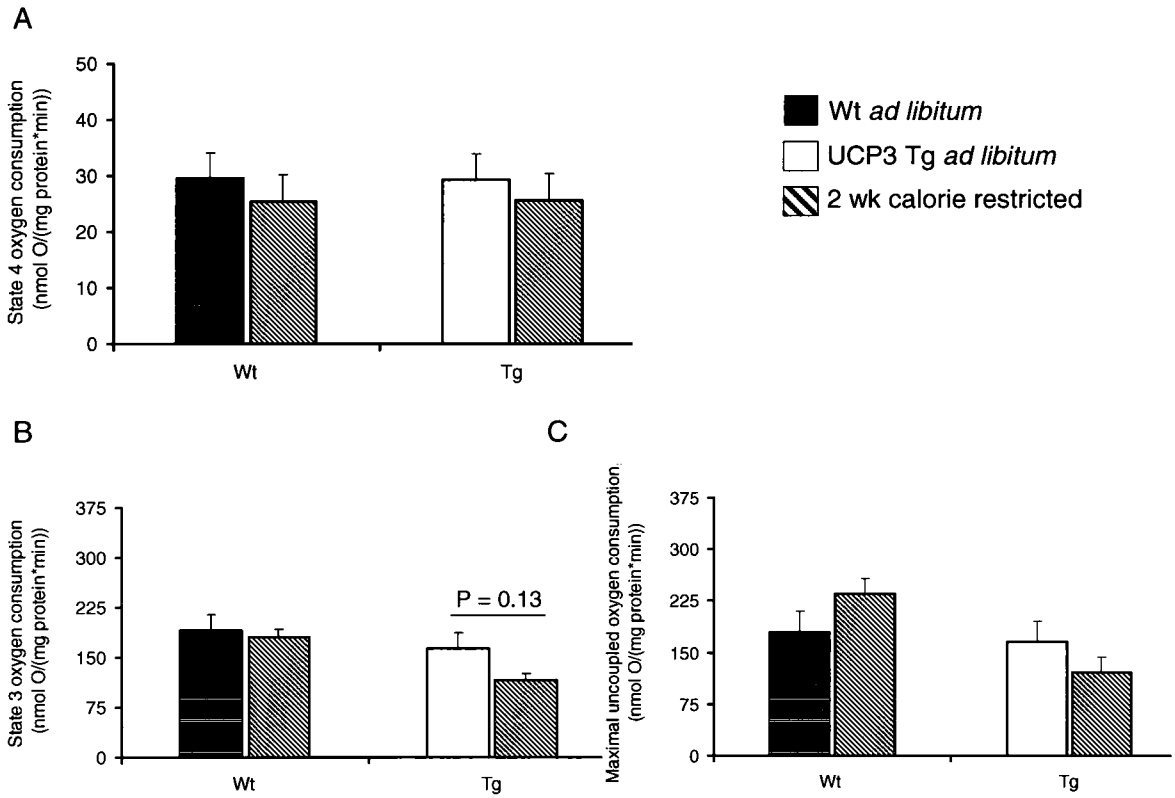
A
State 4 oxygen consumption (nmol O/(mg protein*min))
50
40
30
20
10
0
Wt
Tg
Wt ad libitum
UCP3 Tg ad libitum
2 wk calorie restricted
B
State 3 oxygen consumption (nmol O/(mg protein*min))
375
300
225
150
75
0
P = 0.13
Wt
Tg
C
Maximal uncoupled oxygen consumption (nmol O/(mg protein*min))
375
300
225
150
75
0
Wt
Tg

mice already had lowered ROS production compared to Wt (see Figure 14), it was hypothesized that CR would have no further effect on ROS production in mitochondria from UCP3 Tg mice.

Figure 22 shows the effect of 2 wk CR treatment on mitochondrial ROS production in skeletal muscle mitochondria from Wt and UCP3 Tg mice under non–phosphorylating conditions (Figure 22 (A)), in the presence of rotenone (Figure 22 (B)) or antimycin (Figure 22 (C)), with either a non-lipid substrate (right panel) or a fatty acid substrate (left panel). Surprisingly, CR had little effect on ROS production in Wt mitochondria under any of the conditions tested. Interestingly, ROS production tended to be increased with CR in mitochondria from UCP3 Tg mice. This tendency was most apparent with fatty acid substrate in the presence of antimycin ($P=0.12$, Figure 22 (C)), but other conditions followed this same trend (see Figure 22 (A) and (B)).

3.2.6 Expression of mitochondrial antioxidant proteins

Given the trend for higher ROS production in mitochondria from UCP3 Tg mice exposed to 2 wk CR, it was of interest to investigate levels of antioxidant proteins. Figure 15 (A) shows that CR induced an ~ 50% increase in UCP3 protein in mitochondria from Wt mice ($P<0.05$) but was without effect on UCP3 protein levels in mitochondria from UCP3 Tg mice. Conversely, CR had little effect on ANT protein expression in mitochondria from Wt mice, but actually lowered ANT protein expression in UCP3 Tg mitochondria ($P<0.05$, Figure 15 (B)). In both genotypes, levels of MnSOD were unaffected by CR (Figure 15 (C)).

Figure 22. The effect of 2 wk CR treatment on ROS production in isolated skeletal muscle mitochondria from Wt and UCP3 Tg mice. Values are presented as means ± SEM (n=4–7/group). (A) ROS production under non-phosphorylating conditions, as induced by the ATP synthase inhibitor oligomycin (oligo; 8 μg/mg mito). (B) ROS production in the presence of the complex I inhibitor, rotenone (rot; 5 μM). (C) ROS production in the presence of the complex III inhibitor, antimycin (anti; 5 μM). There was a trend for a CR-induced increase in ROS production in UCP3 Tg mice (P=0.12; two–way ANOVA, bonferroni post test). Abbreviations: P/M; pyruvate/malate (5/2.5 mM), SOD; superoxide dismutase (20 units/0.3 mL), PC; palmitoylcarnitine (18 μM), succ; succinate (10 mM).

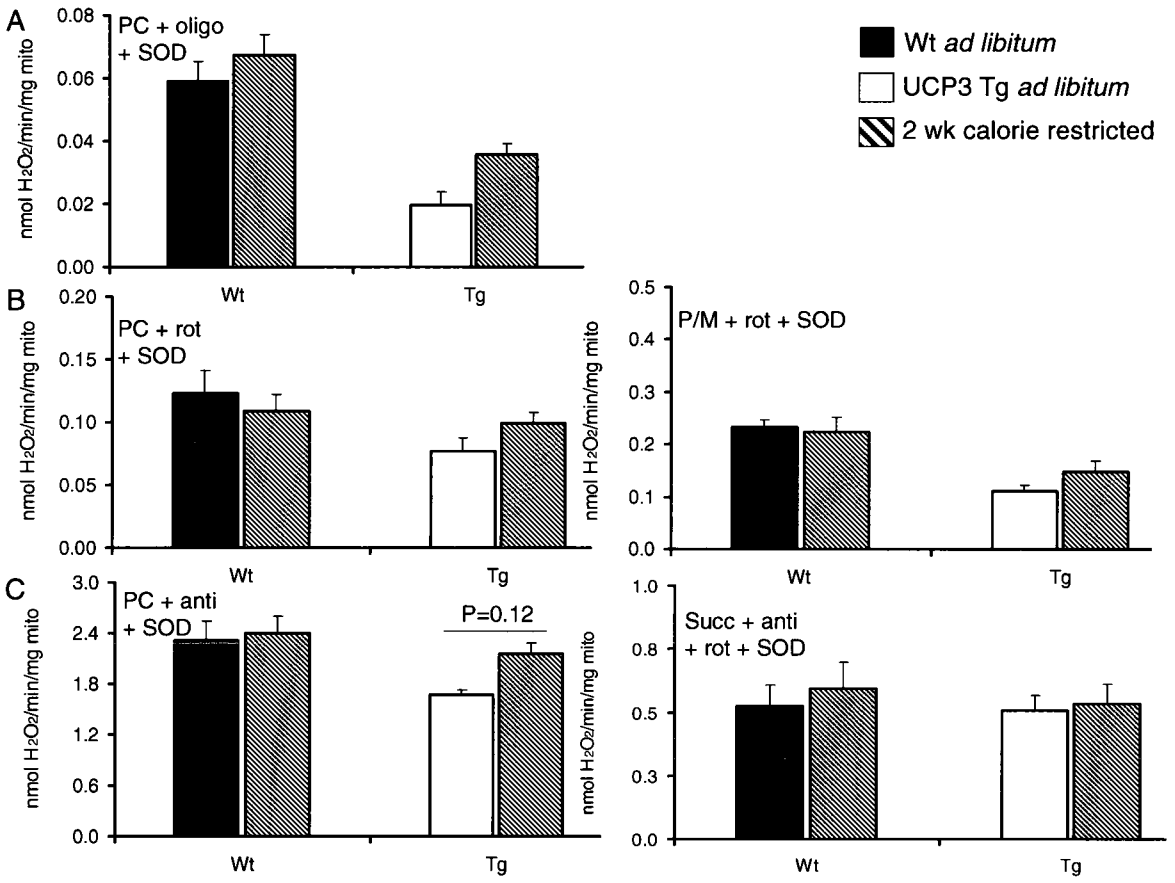
A
PC + oligo
+ SOD
nmol H2O2/min/mg mito
0.08
0.06
0.04
0.02
0.00
Wt
Tg
Wt ad libitum
UCP3 Tg ad libitum
2 wk calorie restricted
B
PC + rot
+ SOD
0.20
0.15
0.10
0.05
0.00
P/M + rot + SOD
0.5
0.4
0.3
0.2
0.1
0.0
C
PC + anti
+ SOD
P=0.12
3.0
2.4
1.8
1.2
0.6
0.0
Succ + anti
+ rot + SOD
1.0
0.8
0.5
0.3
0.0

3.2.7 Oxidative stress of mitochondrial proteins

It was thought that, although the 2 wk CR treatment did not decrease ROS production in Wt mice, the increased levels of UCP3 may lead to lower levels of oxidatively modified mitochondrial proteins (Figure 16). Thus, levels of 4-HNE protein adducts were determined in skeletal muscle mitochondria from Wt AL/CR and UCP3 Tg AL/CR mice (Figure 16). CR had little effect on this measure of oxidative stress in either genotype.

3. 3 EFFECT OF 1 MONTH CR IN UCP3 TG AND WT MICE

As outlined in section 3.2.5 and 3.2.7, the 2 wk CR treatment did not cause detectable changes in ROS production or oxidative stress in skeletal muscle mitochondria from Wt mice. It was therefore hypothesized that the 2 wk CR treatment was not long enough to lower ROS levels and oxidative damage, at least in mitochondria from Wt mice. Consequently, the duration of CR was extended to 1 mo.

3.3.1 Body and organ weights and body composition

The effects of 1 mo CR treatment on BW and individual tissue weights in both Wt and UCP3 Tg mice are presented in Table 4. In Wt and UCP3 Tg mice, CR caused the loss of ~ 38% and ~ 34% of total BW respectively ($P<0.001$, for both Wt and UCP3 Tg mice). In terms of individual tissue weight, the kidneys, liver, heart,

Table 4. Body weight and weights of individual tissues from Wt AL/CR and UCP3 Tg AL/CR at 16 wks of age (1 mo CR treatment). Values are presented as means ± SEM (n=6/group). Food intake values are based on the average daily food intake of Wt and UCP3 Tg mice during the 1 mo food intake period (n=18–20/group). The percent decrease with 1 mo CR treatment compared to AL for body weight and individual tissue weights from Wt and UCP3 Tg mice are also shown. UCP3 Tg AL mice weighed less then Wt controls due to less muscle mass. CR caused a decrease in body weight and in the weight of all tissues measured. *P<0.05, **P<0.01, ***P<0.001; two–way ANOVA, bonferroni post test (diet-effect). $^{\#\#}$P<0.01; two–way ANOVA, bonferroni post test (genotype-effect). Abbreviations: gWAT; gonadal white adipose tissue, iBAT; interscapular brown adipose tissue.

1 mo CR						
Organ (g)	Wt			UCP3 Tg		
	AL	CR	% decrease (CR *vs.* AL)	AL	CR	% decrease (CR *vs.* AL)
Liver	1.21 ± 0.09	0.75 ± 0.04***	38	1.15 ± 0.11	0.74 ± 0.06**	36
Kidney	0.34 ± 0.01	0.24 ± 0.01***	29	0.33 ± 0.02	0.25 ± 0.02**	24
Heart	0.12 ± 0.00	0.10 ± 0.00*	17	0.12 ± 0.01	0.10 ± 0.00**	17
gWAT	1.25 ± 0.19	0.15 ± 0.03***	88	0.86 ± 0.05	0.21 ± 0.05**	76
iBAT	0.17 ± 0.03	0.08 ± 0.01**	53	0.18 ± 0.02	0.07 ± 0.01**	61
Muscle	2.13 ± 0.05	1.56 ± 0.05***	27	1.84 ± 0.05##	1.46 ± 0.07***	21
Body weight	31.4 ± 1.05	19.5 ± 0.58***	38	27.3 ± 0.93##	18.1 ± 0.34***	34
Food intake (g/day)	2.98 ± 0.05			2.92 ± 0.05		

gWAT, iBAT and skeletal muscle were all highly affected by the 1 mo CR treatment in both genotypes. In both Wt and UCP3 Tg mice, CR had the least effect on the heart, which decreased in weight by ~ 17% in both genotypes ($P<0.05$ for Wt and $P<0.01$ for UCP3 Tg mice). CR decreased skeletal muscle and kidney weight by ~ 27% and ~ 29% respectively in Wt mice ($P<0.001$, for both tissues) and by ~ 21% ($P<0.001$) and ~ 24% ($P<0.01$) respectively in UCP3 Tg mice. As with 2 wk CR, 1 mo CR had a large effect on the liver in both Wt and UCP3 Tg mice, which decreased in weight by ~ 38% ($P<0.001$) and ~ 36% ($P<0.01$) in Wt and UCP3 Tg mice, respectively. Of the tissues measured, the fat pads (gWAT and iBAT) in both genotypes were affected to the greatest extent by CR, decreasing in weight by ~ 88% (gWAT, $P<0.001$) and ~ 53% (iBAT, $P<0.01$) in Wt mice, and by ~ 76% (gWAT, $P<0.01$) and ~ 61 % (iBAT, $P<0.01$) in UCP3 Tg mice.

To determine the effect of 1 mo CR on body composition, tissue weights were expressed as a percentage of total BW (Table 5). In Wt mice, liver, kidney and iBAT weight was unchanged, gWAT weight was decreased ($P<0.001$) and heart ($P<0.001$) and muscle ($P<0.05$) weight increased with CR. In UCP3 Tg mice, CR had no effect on the liver or kidneys, caused a decrease in gWAT ($P<0.01$) and iBAT ($P<0.05$) weight and increased heart and muscle weight ($P<0.01$, for both tissues). Thus, differently from the 2 wk CR intervention, body composition was similar between Wt and UCP3 Tg CR mice following 1 mo CR.

3.3.2 Whole body energetics

The effect of 1 mo CR treatment on whole body $\dot{V}O_2$ in Wt and UCP3 Tg mice

Table 5. Weights of individual tissues from Wt AL/CR and UCP3 Tg AL/CR at 16 wks of age (1 mo CR treatment) expressed as a percentage of total body weight. Values are presented as means ± SEM (n=5–6/group). After 1 mo CR, body composition between Wt and UCP3 Tg CR mice was the same. *P<0.05, **P<0.01, ***P<0.001; two–way ANOVA, bonferroni post test (diet-effect). Abbreviations: gWAT; gonadal white adipose tissue, iBAT; interscapular brown adipose tissue.

1 mo CR				
Organ (% of body weight)	Wt		UCP3 Tg	
	AL	CR	AL	CR
Liver	3.8 ± 0.10	3.8 ± 0.19	4.2 ± 0.42	4.0 ± 0.29
Kidney	1.1 ± 0.05	1.3 ± 0.04	1.2 ± 0.03	1.4 ± 0.09
Heart	0.4 ± 0.02	0.5 ± 0.01***	0.4 ± 0.02	0.5 ± 0.02**
gWAT	3.9 ± 0.63	0.8 ± 0.17***	3.1 ± 0.35	1.1 ± 0.24**
iBAT	0.5 ± 0.05	0.4 ± 0.03	0.6 ± 0.05	0.4 ± 0.07*
Muscle	6.9 ± 0.27	8.1 ± 0.21*	6.7 ± 0.30	8.0 ± 0.25**

is shown in Figure 23 (A) and (B), respectively. As with 2 wk CR, $\dot{V}O_2$ on a per mouse basis was greatly decreased at each timepoint over the 24 h period, in both Wt and UCP3 Tg CR mice. In both genotypes this decrease was highly significant in both the light and dark phase ($P<0.001$, Figure 23 (C) and (D), respectively).

Whole body $\dot{V}O_2$ results were divided through by BW (Figure 24). In contrast to the 2 wk CR intervention, mass-adjusted $\dot{V}O_2$ in both Wt and UCP3 Tg mice following 1 mo CR was similar to the respective AL values in both light and dark phases (Figure 24 (C) and (D), respectively).

As with 2 wk CR, the RER was reduced to ~ 0.7 for most of the day in Wt and UCP3 Tg mice subjected to 1 mo CR. In the 1 mo CR mice, RER rose to ~ 1.0 only for several hours after eating (Figure 25 (A) and (B)).

3.3.3 Mitochondrial content

The effect of 1 mo CR on mitochondrial content in skeletal muscle mitochondria from Wt and UCP3 Tg mice is shown in Figure 26. CR induced a decrease in COX activity in both Wt ($P<0.05$) and UCP3 Tg ($P<0.01$) mice. Therefore, mitochondrial content was decreased with 1 mo CR in both genotypes.

3.3.4 Mitochondrial bioenergetics

The effects of 1 mo CR on state 3, state 4 and maximal uncoupled respiration rates were determined in skeletal muscle mitochondria isolated from Wt and UCP3

Figure 23. The effect of 1 mo CR treatment on whole body oxygen consumption ($\dot{V}O_2$) in Wt and UCP3 Tg mice. Values are expressed per mouse and presented as means ± SEM (n=5/group). (A) Mean $\dot{V}O_2$ in Wt AL and Wt CR mice plotted over a 24 h period (16:00-16:00). Some error bars are within the symbol. (B) Same as (A), for UCP3 Tg AL and UCP3 Tg CR mice. Mean $\dot{V}O_2$ in the light (06:00-18:00) phase (C) and dark (18:00-06:00) phase (D) for Wt AL/CR and UCP3 Tg AL/CR mice. In both genotypes CR decreased $\dot{V}O_2$ during the light and dark phase (***$P<0.001$; two–way ANOVA, bonferroni post test).

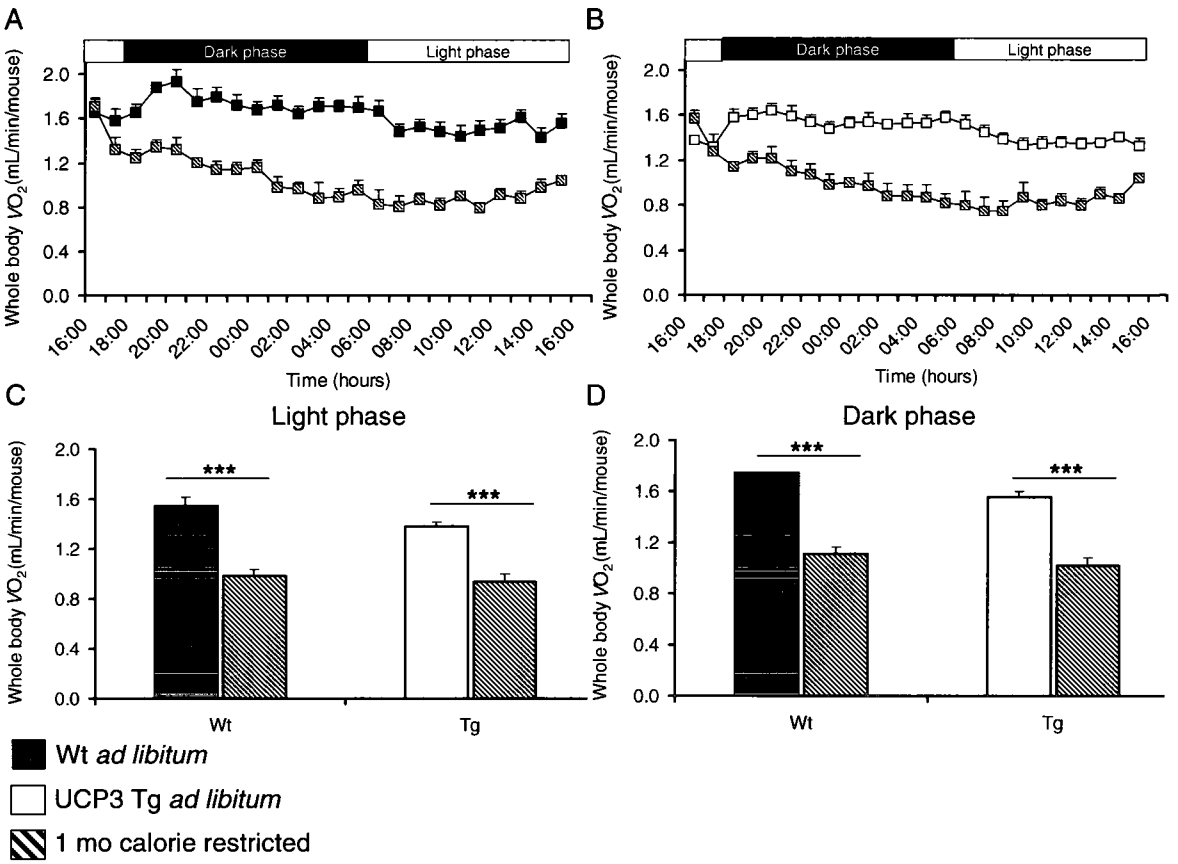
A
Dark phase
Light phase
Whole body VO_2 (mL/min/mouse)
2.0
1.6
1.2
0.8
0.4
0.0
16:00
18:00
20:00
22:00
00:00
02:00
04:00
06:00
08:00
10:00
12:00
14:00
16:00
Time (hours)
B
Dark phase
Light phase
Whole body VO_2 (mL/min/mouse)
Time (hours)
C
Light phase
Whole body VO_2 (mL/min/mouse)
***
***
Wt
Tg
D
Dark phase
Whole body VO_2 (mL/min/mouse)
***
***
Wt
Tg
Wt *ad libitum*
UCP3 Tg *ad libitum*
1 mo calorie restricted

Figure 24. The effect of 1 mo CR treatment on whole body oxygen consumption ($\dot{V}O_2$) in Wt and UCP3 Tg mice expressed per gram (g) of total body weight. Values are presented as means ± SEM (n=5/group). (A) Mean $\dot{V}O_2$ in Wt AL and Wt CR mice plotted over a 24 h period (16:00-16:00). Some error bars are within the symbol. (B) Same as (A), for UCP3 Tg AL and UCP3 Tg CR mice. Mean $\dot{V}O_2$ in the light (06:00-18:00) phase (C) and dark (18:00-06:00) phase (D) for Wt AL/CR and UCP3 Tg AL/CR mice. In both genotypes there were no detectable CR-effects on $\dot{V}O_2$ during the light and dark phase.

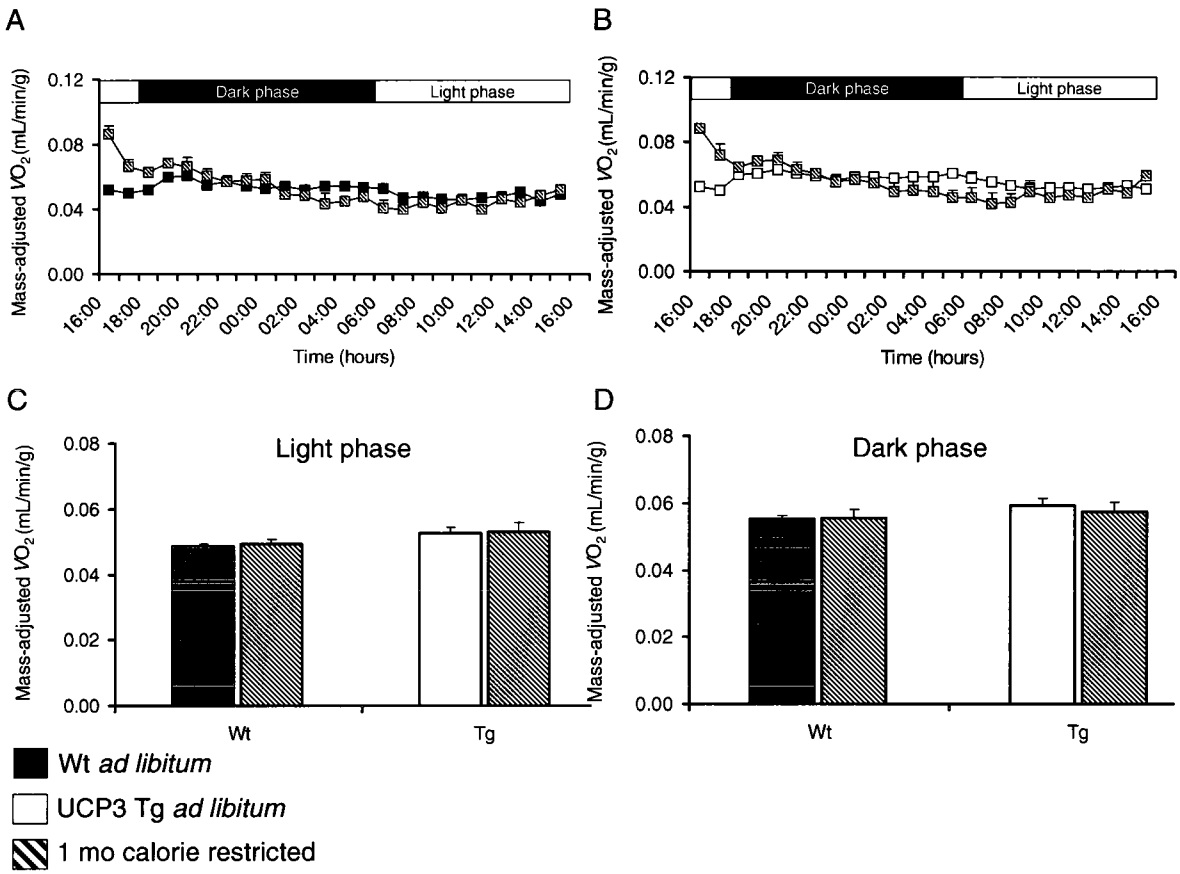
A
B
C
D
Dark phase
Light phase
Mass-adjusted VO_2 (mL/min/g)
Time (hours)
Light phase
Dark phase
Wt
Tg
Wt *ad libitum*
UCP3 Tg *ad libitum*
1 mo calorie restricted

Figure 25. The effect of 1 mo CR treatment on respiratory exchange ratio (RER) in Wt and UCP3 Tg mice. Values are presented as means ± SEM (n=5/group). (A) Mean RER data over a 24 h period (16:00-16:00) for Wt AL and Wt CR mice. Some error bars are within the symbol. (B) Same as (A), for UCP3 Tg AL and UCP3 Tg CR mice. As with 2 wk CR, 1 mo CR was associated with a greater proportion of the day oxidizing fatty acids (*i.e.* values nearing 0.7).

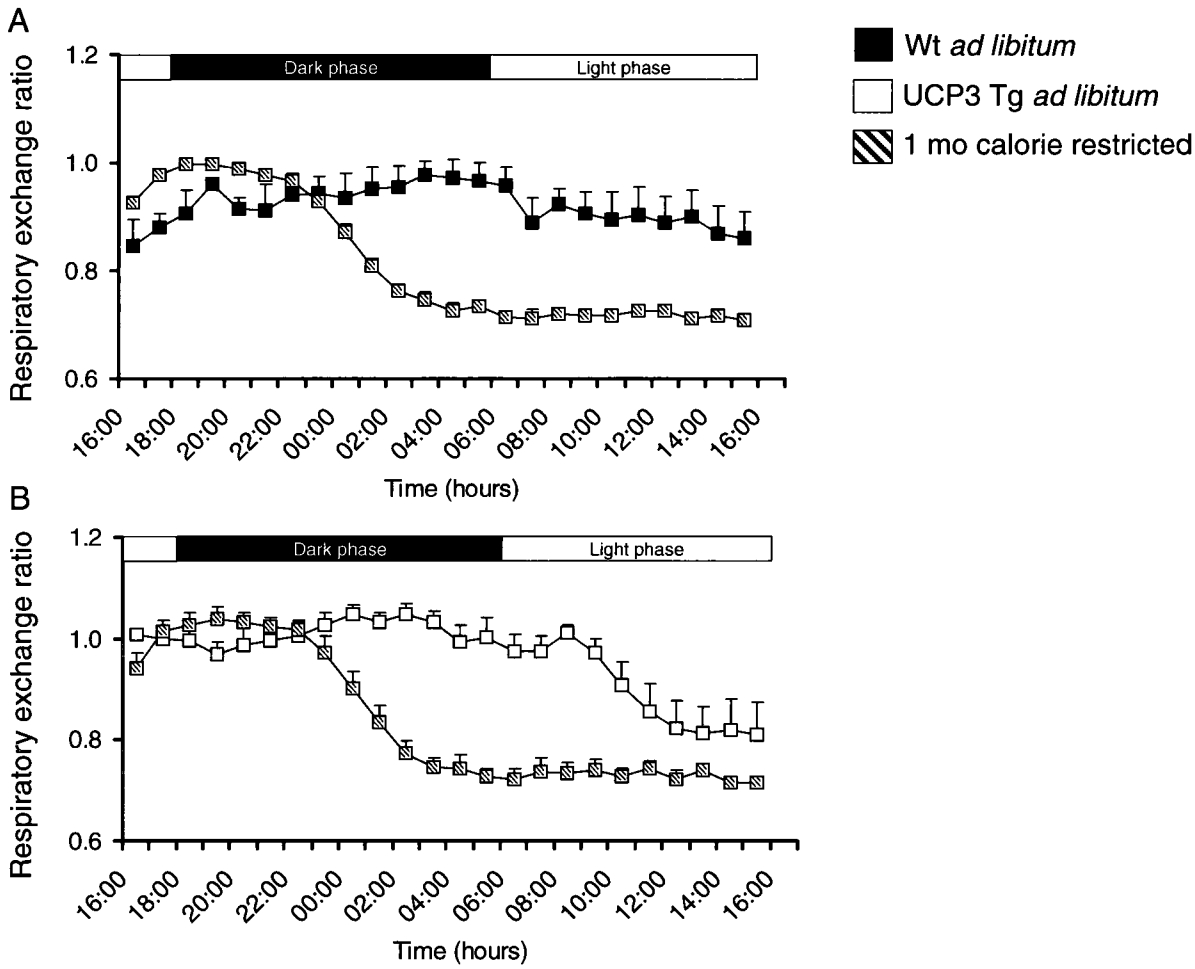
A
Respiratory exchange ratio
1.2
1.0
0.8
0.6
Dark phase
Light phase
16:00
18:00
20:00
22:00
00:00
02:00
04:00
06:00
08:00
10:00
12:00
14:00
16:00
Time (hours)
B
Respiratory exchange ratio
1.2
1.0
0.8
0.6
Dark phase
Light phase
16:00
18:00
20:00
22:00
00:00
02:00
04:00
06:00
08:00
10:00
12:00
14:00
16:00
Time (hours)
Wt ad libitum
UCP3 Tg ad libitum
1 mo calorie restricted

Figure 26. The effect of 1 mo CR treatment on mitochondrial content in skeletal muscle from Wt and UCP3 Tg mice. Values are presented as means ± SEM. Mitochondrial content was determined by histochemical staining of cytochrome c oxidase (COX). Left panel: example of COX activity in Wt AL/CR and UCP3 Tg AL/CR muscle sections. Right panel: quantification of COX activity in Wt AL/CR and UCP3 Tg AL/CR muscle sections (n=3-6/group). CR induced a decrease in mitochondrial content in both genotypes (*$P<0.05$ and **$P<0.01$; two–way ANOVA, bonferroni post test). Abbreviations: OD; optical density.

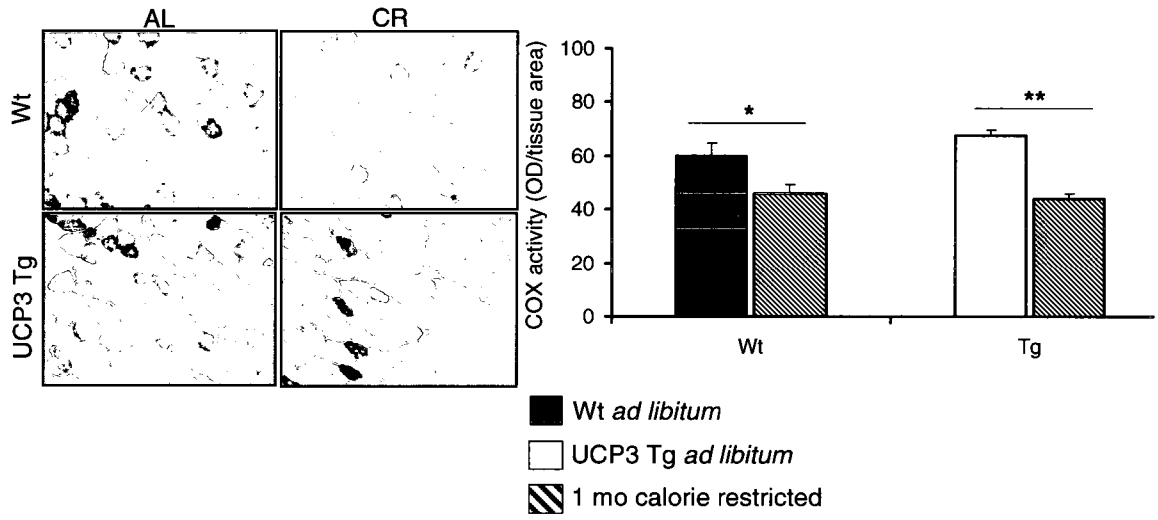
AL
CR
Wt
UCP3 Tg
COX activity (OD/tissue area)
100
80
60
40
20
0
*
**
Wt
Tg
Wt ad libitum
UCP3 Tg ad libitum
1 mo calorie restricted

Tg mice (Figure 27). State 4 respiration rate and the maximal uncoupled respiration rate were unchanged in mitochondria from Wt CR and UCP3 Tg CR mice compared to AL controls (Figure 27 (A) and (C), respectively). Conversely, state 3 respiration was decreased with 1 mo CR only in mitochondria from Wt mice ($P<0.01$, Figure 27 (B)).

3.3.5 Mitochondrial ROS production

Figure 28 shows the effect of 1 mo CR on ROS production in skeletal muscle mitochondria from Wt and UCP3 Tg mice under non-phosphorylating conditions (Figure 28 (A)), in the presence of rotenone to inhibit complex I (Figure 28 (B)), or of antimycin to inhibit complex III (Figure 28 (C)), with either a non-lipid (right panel) or fatty acid substrate (left panel). Differently from the 2 wk CR treatment, 1 mo CR lowered ROS production in Wt mitochondria. In particular, CR induced a decrease in ROS production in Wt mitochondria oxidizing fatty acid substrate in the presence of antimycin ($P<0.05$, Figure 28 (C)). In contrast, there were no CR-induced changes in ROS production in mitochondria from UCP3 Tg mice.

3.3.6 Mitochondrial proton leak

Due to the CR–induced decrease in ROS production in mitochondria from Wt mice, it was of interest to determine the effects of CR on mitochondrial proton leak. Findings are presented in Figure 29 (A) and (B). Oxygen consumption is plotted as a function of PMF in order to determine proton leak (top panel). The furthest point

Figure 27. The effect of 1 mo CR treatment on bioenergetics in isolated skeletal muscle mitochondria from Wt and UCP3 Tg mice. Pyruvate (5 mM) and malate (2.5 mM) were used as the substrate. Values are shown as means ± SEM. (A) Non–phosphorylating respiration (state 4), as induced by oligomycin (8 μg/mg mitochondria) (n=4–5/group). (B) Maximal phosphorylating respiration (state 3), as induced using saturating [ADP] (200 μM) (n=4–5/group). (C) Maximal flux through the ETC was obtained using FCCP (3 μM) as a chemical uncoupler (n=3–5/group). There were no detectable CR effects on state 4 oxygen consumption or on the maximal uncoupled oxygen consumption rate in either genotype. Conversely, CR decreased state 3 oxygen consumption in Wt mice (**$P<0.01$; two–way ANOVA, bonferroni post test).

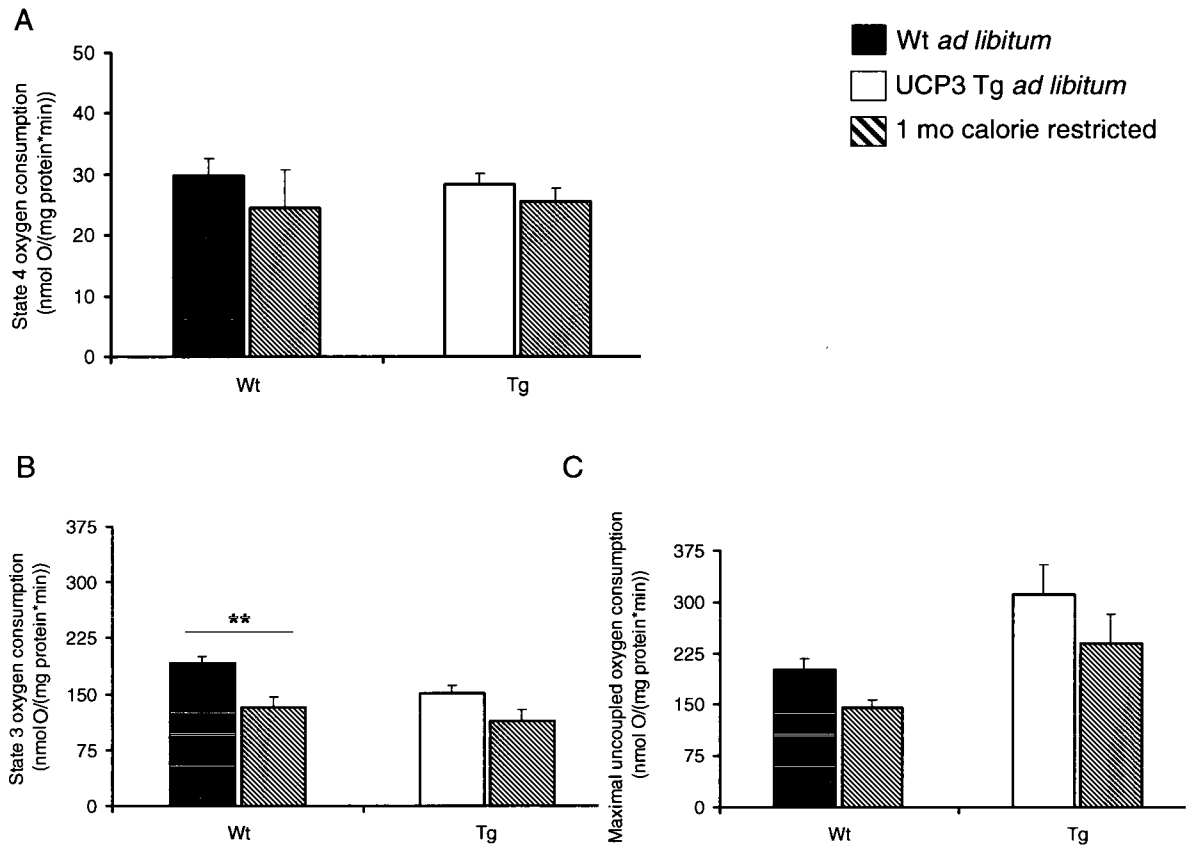
A
Wt ad libitum
UCP3 Tg ad libitum
1 mo calorie restricted
State 4 oxygen consumption (nmol O/(mg protein*min))
50
40
30
20
10
0
Wt
Tg
B
State 3 oxygen consumption (nmol O/(mg protein*min))
375
300
225
150
75
0
**
Wt
Tg
C
Maximal uncoupled oxygen consumption (nmol O/(mg protein*min))
375
300
225
150
75
0
Wt
Tg

Figure 28. The effect of 1 mo CR treatment on ROS production in isolated skeletal muscle mitochondria from Wt and UCP3 Tg mice. Values are presented as means ± SEM (n=6/group). (A) ROS production under non-phosphorylating conditions, as induced by the ATP synthase inhibitor oligomycin (oligo; 8 μg/mg mitochondria). (B) ROS production in the presence of the complex I inhibitor, rotenone (rot; 5 μM). (C) ROS production in the presence of the complex III inhibitor, antimycin (anti; 5 μM). CR induced a decrease in ROS production in Wt mice with antimycin and PC as the substrate (*$P<0.05$; two–way ANOVA, bonferroni post test). Abbreviations: P/M; pyruvate/malate (5/2.5 mM), SOD; superoxide dismutase (20 units/0.3 mL), PC; palmitoylcarnitine (18 μM), succ; succinate (10 mM).

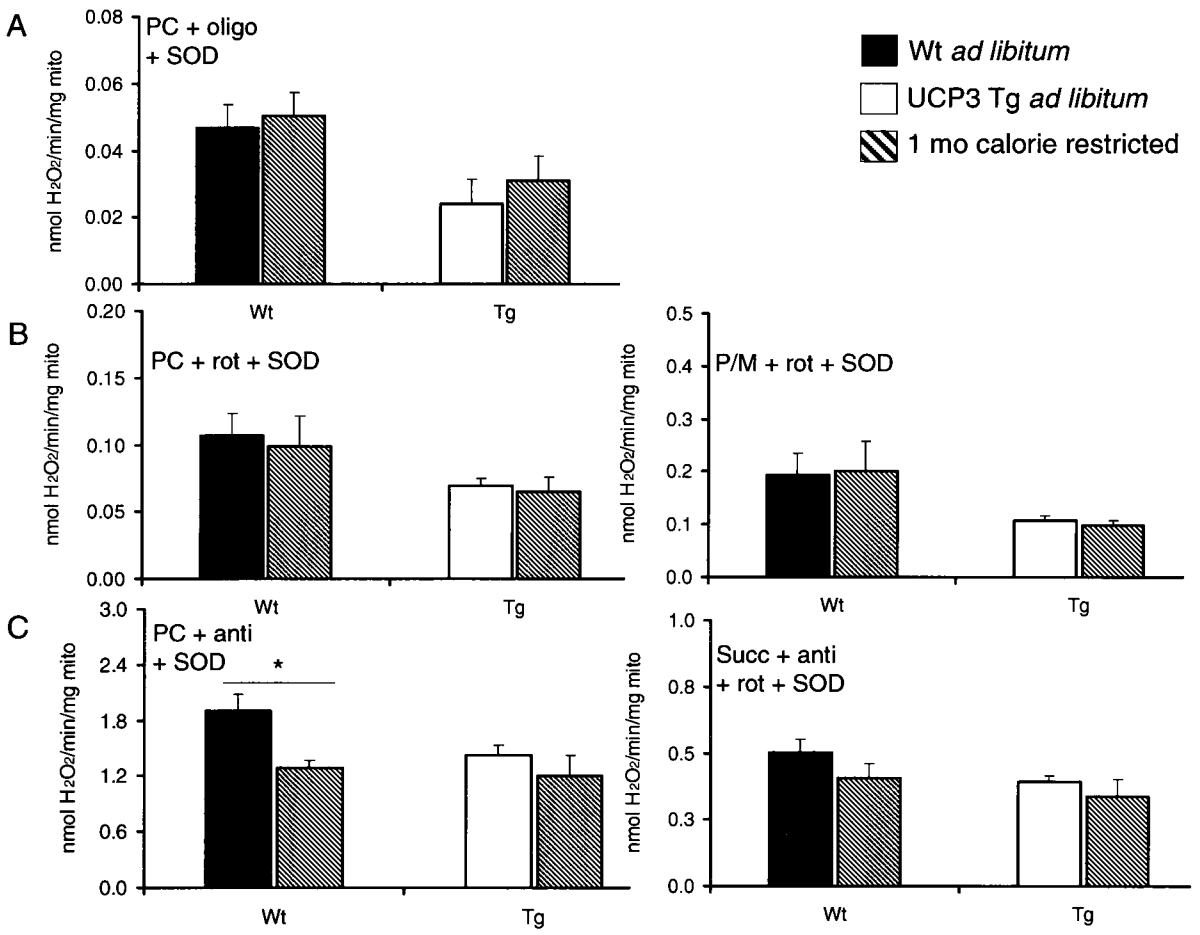
A
PC + oligo
+ SOD
nmol H2O2/min/mg mito
0.08
0.06
0.04
0.02
0.00
Wt
Tg
Wt ad libitum
UCP3 Tg ad libitum
1 mo calorie restricted
B
PC + rot + SOD
0.20
0.15
0.10
0.05
0.00
P/M + rot + SOD
0.5
0.4
0.3
0.2
0.1
0.0
C
PC + anti
+ SOD
*
3.0
2.4
1.8
1.2
0.6
0.0
Succ + anti
+ rot + SOD
1.0
0.8
0.5
0.3

Figure 29. The effect of 1 mo CR treatment on mitochondrial proton leak in isolated skeletal muscle mitochondria from Wt and UCP3 Tg mice. Values are presented as means ± SEM (n=3–4/group). (A) Top panel: oxygen consumption and protonmotive force (PMF) in mitochondria from Wt AL and Wt CR mice were determined as previously described (Figure 12). The furthest point on the right represents state 4 respiration. Compared to Wt AL, the Wt CR curve is slightly displaced leftward; therefore, at any given PMF, the rate of oxygen consumption was slightly increased compared to controls. Bottom panel: the oxygen consumption rate was determined at a common PMF (~ 2500 arbitrary units (A.U.)) and Wt CR mitochondria had increased oxygen consumption compared to Wt AL (*$P<0.05$; t–test, two–tailed, unpaired). (B) Same as (A), for UCP3 Tg AL and UCP3 Tg CR mice. The leak curves from UCP3 Tg AL and CR mice essentially overlapped and no differences in the rate of oxygen consumption were detected at a common PMF (~ 3000 arbitrary units (A.U.)). Therefore, in UCP3 Tg mice, CR had no effect on mitochondrial proton leak.

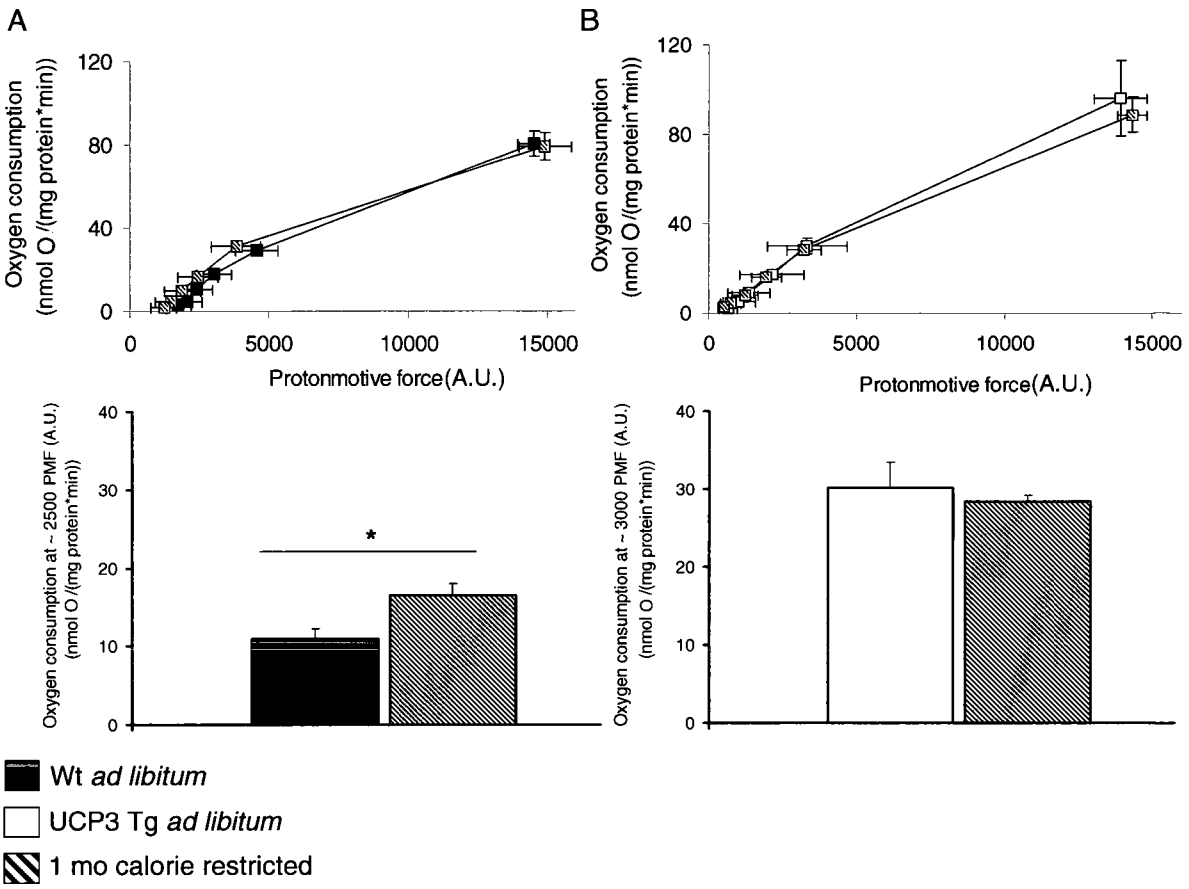
A
B
Oxygen consumption (nmol O /(mg protein*min))
120
80
40
0
0
5000
10000
15000
Protonmotive force(A.U.)
Oxygen consumption at ~ 2500 PMF (A.U.) (nmol O /(mg protein*min))
Oxygen consumption at ~ 3000 PMF (A.U.) (nmol O /(mg protein*min))
40
30
20
10
0
*
Wt ad libitum
UCP3 Tg ad libitum
1 mo calorie restricted

on the right of each curve represents state 4 respiration; no CR-induced differences were observed in state 4 respiration in either genotype. Compared to the Wt AL curve, the Wt CR leak curve was slightly displaced leftward; therefore, at any given PMF, the rate of oxygen consumption was slightly higher in mitochondria from CR mice (Figure 29 (A), top panel). Comparison of oxygen consumption between Wt AL and Wt CR, at the same PMF, revealed that oxygen consumption was significantly higher in mitochondria from Wt CR mice ($P<0.05$, Figure 29 (A), bottom panel). In contrast, the leak curves from UCP3 Tg AL and UCP3 Tg CR essentially overlapped one another (Figure 29 (B), top panel), and comparison of oxygen consumption at a common PMF yielded no difference (Figure 29 (B), bottom panel). Therefore, in UCP3 Tg mice, CR had no effect on mitochondrial proton leak.

3.3.7 Expression of mitochondrial antioxidant proteins

In light of the decreased mitochondrial ROS production and increased proton leak in mitochondria from Wt mice, levels of UCP3, ANT, and MnSOD protein were assessed in mitochondria from Wt AL/CR and UCP3 Tg AL/CR mice (Figure 30). CR induced an ~ 100% increase in UCP3 protein in mitochondria from Wt mice ($P<0.05$) but not in mitochondria from UCP3 Tg mice (Figure 30 (A)). Conversely, ANT protein expression was unaffected by CR in mitochondria from either genotype (Figure 30 (B)). Interestingly, CR induced an ~ 20% increase in the level of MnSOD protein in mitochondria from Wt mice ($P=0.074$); however, in UCP3 Tg mice, MnSOD protein levels were unchanged with CR (Figure 30 (C)).

Figure 30. UCP3, ANT and MnSOD protein expression in isolated skeletal muscle mitochondria from Wt AL/CR and UCP3 Tg AL/CR mice (1 mo CR treatment). Representative Western blot and corresponding Coomassie stained gel (top panel) for (A) UCP3, (B) ANT, and (C) MnSOD. Each lane corresponds to mitochondria from a different mouse and protein was loaded at 30 μg for UCP3, or 15 μg for ANT and MnSOD. For UCP3, all samples were run on the same gel. For ANT and MnSOD, Wt AL/CR samples were run together on one gel and UCP3 Tg AL/CR samples were run together on another gel. The breaks represent different areas of the same blot/gel. Protein bands were quantified by densitometry (bottom panel) and are presented as means ± SEM for (A) UCP3; n=4–8/group, (B) ANT; n=5–7/group, and (C) MnSOD; n=5–7/group. All values were divided through by the amount of protein loaded (as determined by the Coomassie stained gel). CR caused a significant increase in UCP3 protein and tended to increase MnSOD protein in mitochondria from Wt mice (*$P<0.05$, $P=0.074$, respectively; two–way ANOVA, bonferroni post test). ANT protein levels were unchanged with CR in mitochondria from both genotypes.

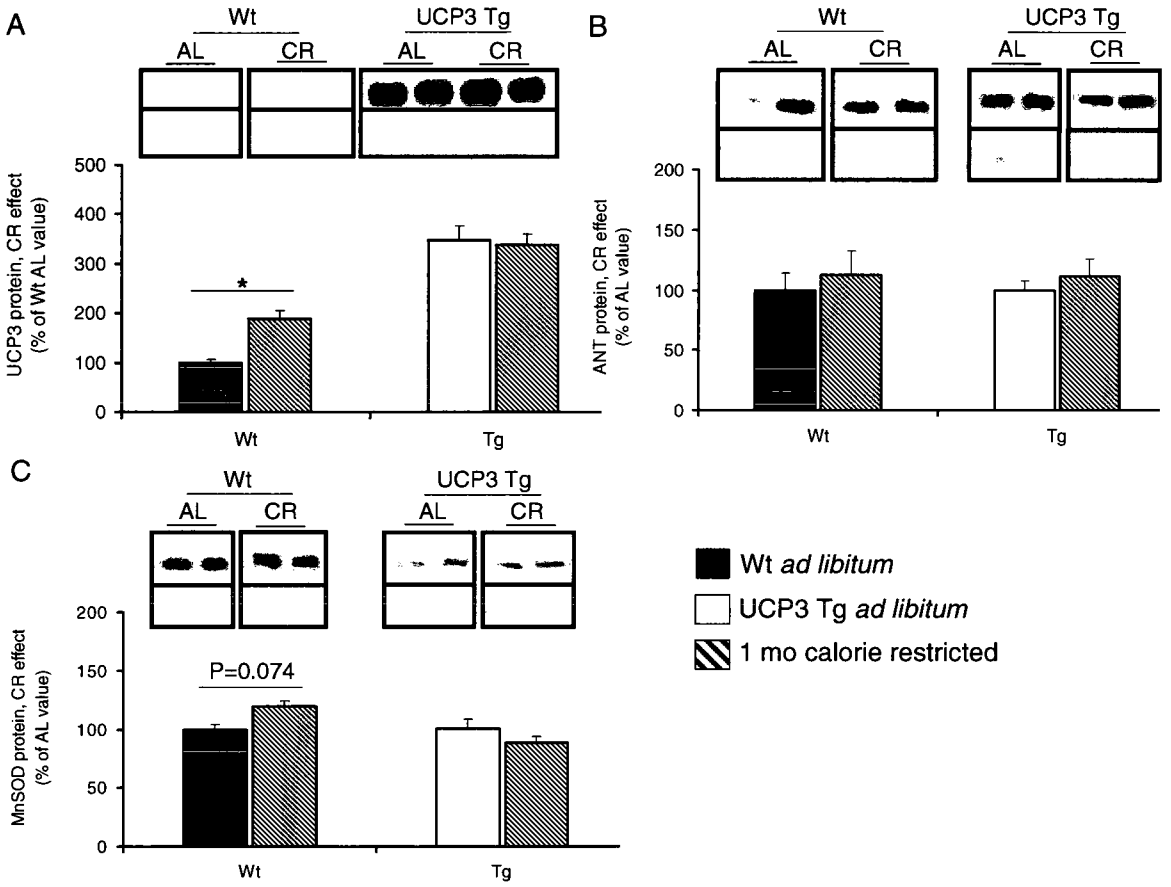
A
Wt
UCP3 Tg
AL
CR
AL
CR
UCP3 protein, CR effect
(% of Wt AL value)
500
400
300
200
100
0
*
Wt
Tg
B
Wt
UCP3 Tg
AL
CR
AL
CR
ANT protein, CR effect
(% of AL value)
200
150
100
50
0
Wt
Tg
C
Wt
UCP3 Tg
AL
CR
AL
CR
MnSOD protein, CR effect
(% of AL value)
200
150
100
50
0
P=0.074
Wt
Tg
Wt ad libitum
UCP3 Tg ad libitum
1 mo calorie restricted

3.3.8 Oxidative stress of mitochondrial proteins

Due to the finding of decreased ROS production in mitochondria from Wt mice, levels of oxidative damage were assessed in skeletal muscle mitochondria isolated from Wt AL/CR and UCP3 Tg AL/CR mice (Figure 31). Levels of 4–HNE protein adducts were unchanged in mitochondria from Wt and UCP3 Tg CR mice compared to AL controls, suggesting that oxidative stress was the same in mitochondria from AL and CR mice in both genotypes.

Figure 31. Levels of 4-HNE modified proteins in isolated skeletal muscle mitochondria from Wt AL/CR and UCP3 Tg AL/CR mice (1 mo CR treatment). Top: representative Western blot and corresponding Coomassie stained gel. Each lane corresponds to mitochondria from a different mouse and protein was loaded at 30 μg. Samples were run on the same gel; the breaks represent different areas of the same blot/gel. Bottom: 4–HNE protein adduct bands were quantified by densitometry. Values are presented as means ± SEM (n=4-9/group). All values were divided through by the amount of protein loaded (as determined by the Coomassie stained gel). Mitochondria from UCP3 Tg AL mice had increased levels of 4-HNE modified proteins compared to Wt AL controls ($^{\#}P<0.05$; two-way ANOVA, bonferroni post test). There was no detectable CR effect on 4–HNE protein adduct levels in either genotype.

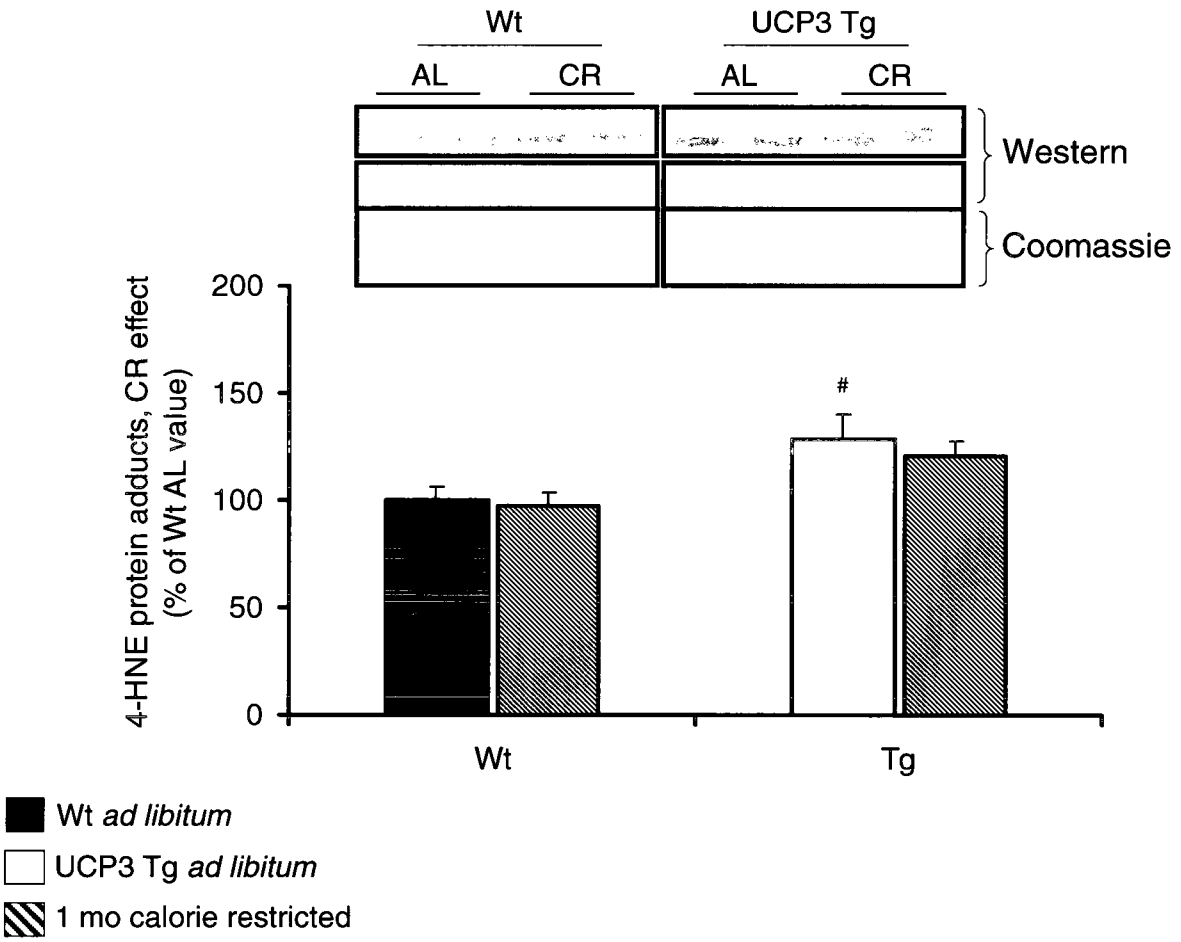
Wt
UCP3 Tg
AL
CR
AL
CR
Western
Coomassie
4-HNE protein adducts, CR effect
(% of Wt AL value)
200
150
100
50
0
#
Wt
Tg
Wt ad libitum
UCP3 Tg ad libitum
1 mo calorie restricted

CHAPTER 4
DISCUSSION AND CONCLUSION

4.1 SUMMARY OF KEY FINDINGS

The beneficial effects of CR on age-related pathologies (Austad, 1989; Colman et al., 2009; Comfort, 1963; Fontana et al., 2004; Heilbronn et al., 2006; Kemnitz et al., 1994; Klass, 1977; Lane et al., 1996; Lane et al., 1995; Walford et al., 1999; Weindruch et al., 1986) have been associated with a lowering of ROS production and oxidative stress (Asami et al., 2008; Bevilacqua et al., 2004, 2005; Lass et al., 1998; Pamplona et al., 2002) which has lent support to the *oxidative stress theory of aging* (see section 1.2.1). That increased uncoupled mitochondrial respiration may, in part, account for the lower ROS production forms the basis for the '*uncoupling to survive*' theory of aging (see section 1.4.1). We reasoned that, if the '*uncoupling to survive*' theory has any merit, then short-term CR should have little effect on ROS production and oxidative stress in muscle mitochondria from UCP3 Tg mice which already, under AL conditions, possess lower ROS production and a higher uncoupled respiration rate. Specifically, we investigated the effects of a 2 wk and 1 mo 40% CR treatment in Wt and UCP3 Tg mice on whole body energetics and composition, and on skeletal muscle mitochondrial energetics and ROS metabolism.

Figure 32 and 33 summarize the main findings of this study from the 2 wk and 1 mo CR treatments, respectively. Please note that only the key outcome measures have been included in these figures; other observations are discussed later, in the

Figure 32. Schematic representation of the most important findings with 2 wk CR in Wt and UCP3 Tg mice. In skeletal muscle mitochondria from Wt mice, CR had no effect on the levels of ROS production or oxidative stress and induced an increase in muscle weight per gram body weight. UCP3 Tg mice possessed uncoupled mitochondria and decreased ROS production. With 2 wk CR, mitochondrial ROS production tended to be increased, oxidative stress levels were unaffected and muscle weight per gram body weight was decreased in UCP3 Tg mice. Abbreviations: ox stress; oxidative stress, BW; body weight.

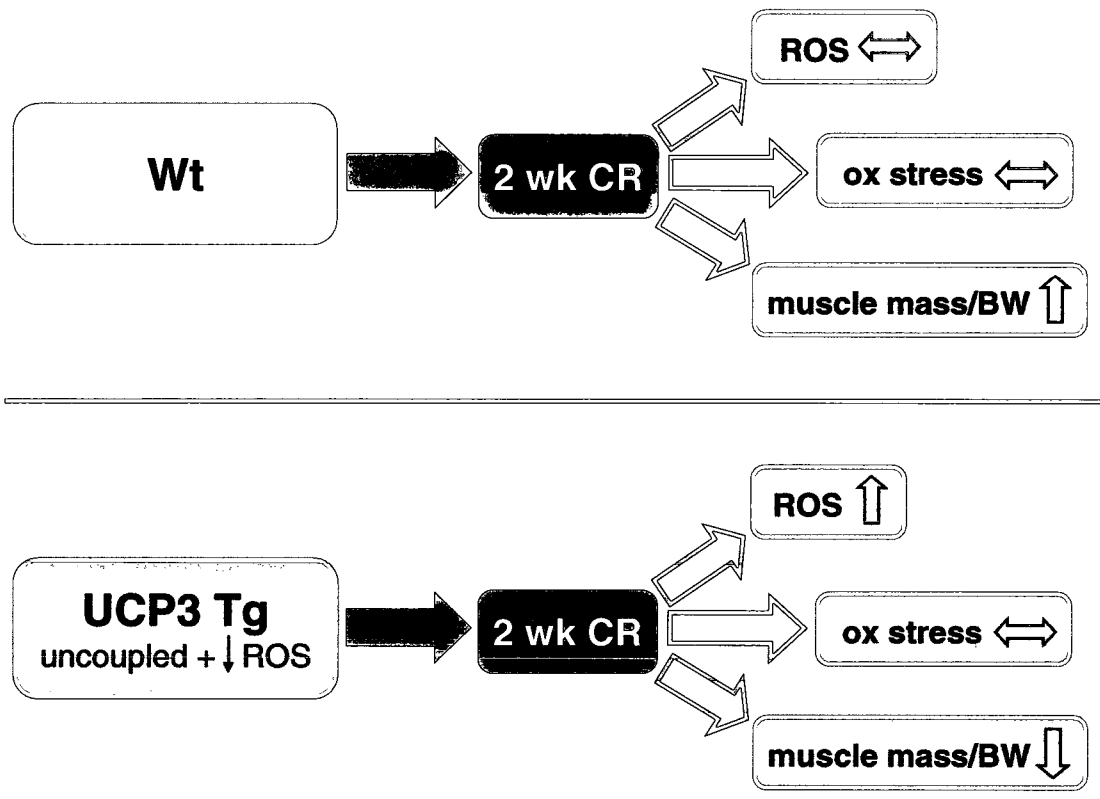
Wt
2 wk CR
ROS ⇔
ox stress ⇔
muscle mass/BW ⇧
UCP3 Tg
uncoupled + ↓ ROS
2 wk CR
ROS ⇧
ox stress ⇔
muscle mass/BW ⇩

Figure 33. Schematic representation of the most important findings with 1 mo CR in Wt and UCP3 Tg mice. In Wt mice, CR induced a decrease in mitochondrial ROS production and an increase in muscle weight per gram body weight. Mitochondrial oxidative stress levels were unaffected in Wt mice subjected to 1 mo CR. In UCP3 Tg mice, mitochondrial ROS production and oxidative stress levels were unaffected with 1 mo CR treatment. As with Wt mice, CR induced an increase in muscle weight per gram body weight in UCP3 Tg mice. Abbreviations: ox stress; oxidative stress, BW; body weight.

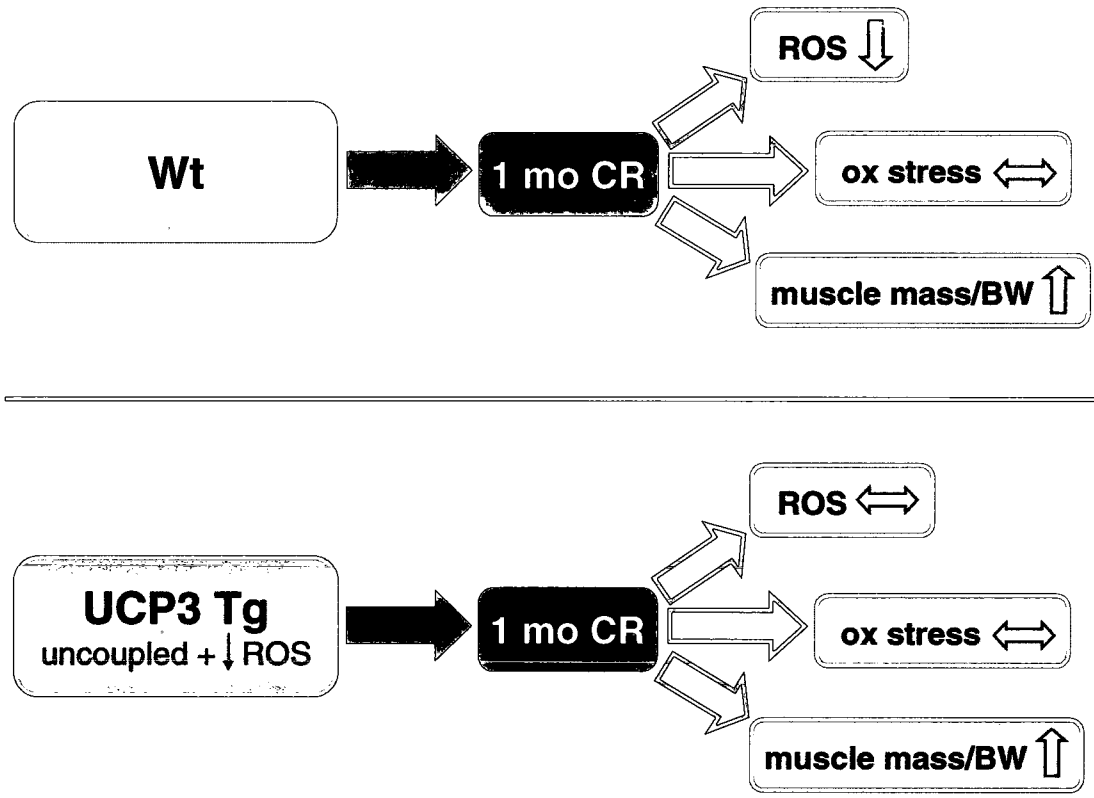
Wt
1 mo CR
ROS ⇩
ox stress ⇔
muscle mass/BW ⇧
UCP3 Tg
uncoupled + ↓ ROS
1 mo CR
ROS ⇔
ox stress ⇔
muscle mass/BW ⇧

context of possible explanations for any changes in these key outcome variables. The main finding with 2 wk CR was the trend for greater ROS production in skeletal muscle mitochondria from UCP3 Tg mice; decreased ANT protein expression was associated with this observation. In contrast, ROS production and ANT expression were unchanged in mitochondria from Wt CR mice. Another important finding was the decrease in the proportional contribution of muscle weight to total BW in UCP3 Tg mice subjected to 2 wk CR. This was compared to a higher proportion of muscle weight in Wt mice subjected to the same intervention. Extending CR to 1 mo resulted in decreased ROS production in skeletal muscle mitochondria from Wt mice, along with increased proton leak. However, ROS production and proton leak were unchanged with 1 mo CR in mitochondria from UCP3 Tg mice. The proportional contribution of muscle weight to total BW was increased in both genotypes following 1 mo CR treatment. Overall these findings show that muscle from UCP3 Tg mice was not neutral to the 2 wk CR intervention. Rather, the adaptation of skeletal muscle mitochondria, as well as muscle as a whole, to short-term CR was delayed in UCP3 Tg mice. In fact, our findings show that their muscle which, under AL-conditions, possesses phenotypic characteristics of CR-adapted muscle, responds to CR in a deleterious manner. In other words, although mitochondria from UCP3 Tg AL mice exhibit higher proton leak, this phenotype is not necessarily beneficial to muscle health.

4.2 CHARACTERISTICS OF AL-FED UCP3 TG MICE

Previous studies from our laboratory have investigated some metabolic

characteristics of UCP3 Tg mice (Bezaire et al., 2005; Costford et al., 2008; Costford et al., 2006); however, characteristics of mitochondrial energetics were not studied. Of particular interest were mitochondrial proton leak, ROS production and oxidative stress, all of which have been investigated in the present study. In particular, previous studies of UCP3 Tg mice have found increased proton leak in skeletal muscle mitochondria (Clapham et al., 2000; Tiraby et al., 2007). Inspection of the Westerns blots in these latter studies from other laboratories suggests that the level of UCP3 overexpression in our mice was between the levels in the mice used in those two studies. Therefore, it is not surprising that increased uncoupling was observed in mitochondria from our UCP3 Tg mice. What follows in this subsection is a discussion of the impact this increased mitochondrial proton leak has on whole body energetics and on mitochondrial ROS production and oxidative stress.

4.2.1 Whole body implications of having a mitochondrial proton leak in skeletal muscle

Isolated skeletal muscle mitochondria from UCP3 Tg mice were shown to possess increased proton leak compared to Wt mice. Because of this, it was expected that this genotype would have increased whole body $\dot{V}O_2$. This is because skeletal muscle makes up a significant portion of total BW (~ 10% shown here in mice) and at the whole body level, proton leak has been estimated to account for 20-25% of the resting metabolic rate of a rat (Rolfe and Brand, 1997). Therefore, due to its size and relative contribution, differences in muscle proton leak should have an impact at the whole body level. The increased whole body $\dot{V}O_2$ (mass-adjusted) was clear but small, yet did not reach significance when data from 14 and 16 wk old

mice were combined (Figure 8). Clapham and colleagues reported that energy expenditure was greatly increased, by 25%, in their UCP3 Tg mice (Clapham et al., 2000). However, other studies have reported no difference in energy expenditure in UCP3 Tg mice (Bezaire et al., 2005; Costford et al., 2006; Tiraby et al., 2007) with even smaller sample sizes than was used in the present study. It is important to note the levels of UCP3 protein overexpression in the F1 generation mice used in the Clapham study were ~ 20-fold higher than in Wt mice (Clapham et al., 2000). However, the levels of UCP3 overexpression used in the present study were ~ 250% higher in UCP3 Tg mice than in Wt mice (Figure 11). There is a normal degree of error associated with all indirect calorimetry equipment, estimated at ~ 7-10% (Livesey and Elia, 1988). Therefore, small differences in whole body $\dot{V}O_2$ due to reduced coupling efficiency of oxidative phosphorylation in skeletal muscle may be difficult to detect by indirect calorimetry.

The possibility that increased locomotor activity could explain the greater energy expenditure does not seem likely. Although, in this study, activity levels were not measured directly, similar variability in the indirect calorimetry data was seen in both UCP3 Tg and Wt mice (data not shown). This observation was especially evident during the dark phase when mice are more active, suggesting that activity levels were similar in these two genotypes. Other studies have directly measured activity and found no differences between Wt and UCP3 Tg mice (Choi et al., 2007; Clapham et al., 2000). Instead, the trend for higher whole body $\dot{V}O_2$ seen in UCP3 Tg mice was most likely caused by the increased mitochondrial proton leak present in their skeletal muscle (Figure 12).

The finding of lower BW in UCP3 Tg AL compared to Wt AL mice has previously been reported by our laboratory and in other studies (Clapham et al., 2000; Costford et al., 2008; Costford et al., 2006). In the present study, this phenotype was mainly due to decreased muscle mass and was not due to differences in food intake (Table 2). Interestingly, the lack of a BW phenotype in UCP3 Tg mice compared to Wt mice has also been reported (Bezaire et al., 2005; Tiraby et al., 2007). These discrepant findings may be due to differences in the genetic background of the mice (Tiraby et al., 2007), or the use of young mice in which the phenotype may not have yet become apparent (Bezaire et al., 2005). We cannot determine at this time whether the different BW results are due to differences in the degree of muscle mitochondrial uncoupled respiration, as proton leak was not always measured. However, based on reported levels of UCP3 overexpression, it is predicted that proton leak in UCP3 Tg mice studied by Tiraby and colleagues (Tiraby et al., 2007) would be even lower, which could explain the absence of a BW phenotype in their mice.

Interestingly, UCP3 knockout (KO) mice do not have a greater BW than Wt mice, nor do they have decreased whole body energy expenditure (Bezaire et al., 2005; Costford et al., 2006; Gong et al., 2000; Hoeks et al., 2006). This absence of an energy-balance phenotype likely reflects similar 'basal' proton leak respiration in muscle mitochondria from UCP3 KO and Wt mice (Bezaire et al., 2001; Echtay et al., 2003; Echtay et al., 2002) (see section below for further discussion).

UCP3 Tg mice tended to have higher RER values than Wt mice, primarily in the hours after feeding at 16:00, suggesting that UCP3 Tg mice more rapidly switched to carbohydrate oxidization. However, UCP3 Tg and Wt mice had similar

RER values at the end of the dark phase and during the light phase (before feeding). Therefore, UCP3 Tg and Wt mice oxidized the same mix of fuels during the inactive phase of the day, when food consumption was minimal. Indeed, previous findings in UCP3 Tg mice found similar RER values (Choi et al., 2007; Costford et al., 2006) or slightly lower RER values (Bezaire et al., 2005; Tiraby et al., 2007) compared to Wt mice. In the present study, the higher RER observed in UCP3 Tg mice after feeding could reflect a greater rate of consumption or assimilation of food; regardless of the cause, the higher RER seems to be associated with feeding.

4.2.2 Does the existence of a mitochondrial proton leak in skeletal muscle protect against ROS production and oxidative stress?

The increased mitochondrial proton leak observed in skeletal muscle of UCP3 Tg mice was associated with decreased ROS production (Figure 14). The lower ROS was not surprising because studies which have experimentally manipulated mitochondrial PMF have demonstrated that ROS is very sensitive to PMF (Miwa et al., 2003); ROS production can be reduced by 70% if PMF is decreased by only 10 mV. Theoretically, other explanations for the lower ROS production in UCP3 Tg mice would be increased abundance of detoxifying enzymes and/or decreased substrate oxidation. However, there were no differences in MnSOD or ANT protein levels in UCP3 Tg mitochondria (Figure 15). Also, ETC capacity was increased in mitochondria from UCP3 Tg mice as assessed by FCCP–induced respiration (Figure 13), which argues against lower substrate oxidation as an explanation for the

decreased ROS. Thus, the likely cause of this lower H_2O_2 emission rate in mitochondria from UCP3 Tg mice is increased proton conductance.

Based on the lower ROS production observed in mitochondria from UCP3 Tg mice, it was expected that oxidative damage would also be lower. To assess oxidative damage to mitochondrial proteins, we measured levels of 4-HNE protein adducts because 4-HNE is the primary by-product of lipid peroxidation (see Figure 4). It was therefore surprising that our results were inconsistent with this notion, as mitochondria from UCP3 Tg mice tended to have increased levels of oxidative damage compared to those of Wt mice (Figures 16 and 31). Theoretically, the levels of 4-HNE modified proteins would be determined by the rate of lipid peroxidation, which in turn would depend on ROS production as well as on the membrane lipid composition (*i.e.* poly-unsaturated lipids are more susceptible to peroxidation) (see Figure 4). Also, the level of oxidatively modified proteins could depend on mitochondrial turnover rate ('mitophagy') (Tolkovsky, 2009). Since ROS production was shown to be lower in mitochondria from UCP3 Tg mice, then either differences in membrane lipid composition or organelle turnover rate would explain the slightly higher oxidatively modified protein levels in UCP3 Tg mitochondria.

4.2.3 Mechanisms of UCP3-mediated proton leak

Uncoupled respiration in mitochondria has been classified as basal or inducible (see section 1.4.1). Briefly, ~ 50% of basal proton leak is mediated by ANT, and this basal leak has been defined as leak that is not sensitive to the specific ANT inhibitor, CAT (Brand and Esteves, 2005). Inducible proton leak has been

defined as that which can be activated; fatty acids, AMP, and alkenals have all been identified as activators of UCP3 and/or ANT (Andreyev et al., 1989; Andreyev et al., 1988; Brand et al., 2005; Cadenas et al., 2000; Echtay et al., 2003; Shabalina et al., 2006). One problem with this definition is that basal leak is often measured under conditions where activators are likely present. For example, although BSA is added to the incubation medium to bind fatty acids, it is usually only added at 0.3% (w/v) (*e.g.,* present study; (Brand et al., 2005; Echtay et al., 2003; Echtay et al., 2002)). However, increasing BSA to 1% decreases the proton leak (Parker et al., 2008). Therefore, the definition of 'basal' seems quite arbitrary. It is thought that UCP3, like UCP1, needs to be activated (Brand and Esteves, 2005). This conclusion is based on observations in which proton leak, measured under 'basal' conditions (*i.e.*, in the presence of 0.3% BSA and in the absence of CAT) was similar in muscle mitochondria from UCP3 KO and Wt mice (Echtay et al., 2003; Echtay et al., 2002). The uncoupled respiration rate then increased when palmitate (at a very high concentration; 300 μM) or 4-HNE was added to the incubation medium (Echtay et al., 2003; Echtay et al., 2002). However, in the present study, and in that of Clapham and colleagues (Clapham et al., 2000), the increased proton leak observed in mitochondria from UCP3 Tg mice was determined under 'basal' conditions. It has also been reported that GDP and CAT, which inhibit 'activated' uncoupling, also inhibit uncoupling by UCP3 and ANT under 'basal' conditions (Bevilacqua et al., submitted) (Talbot and Brand, 2005). Altogether, these observations lead us to question the definitions of 'basal' and 'inducible' proton leak, and more specifically the idea that UCP3 is only involved in activated proton leak.

4.3 WHOLE BODY RESPONSE TO SHORT–TERM CR IN WT AND UCP3 TG MICE

4.3.1 Body and organ weights and body composition

In Wt and UCP3 Tg mice, both 2 wk and 1 mo CR interventions had large effects on total BW and individual tissue weights (Tables 2 and 4). BW was affected to the same extent in both genotypes with either 2 wk or 1 mo CR. After both CR treatments, fat weight (gWAT and iBAT) was decreased to the greatest extent, followed by liver, kidney and muscle weight; heart weight decreased the least. Findings here are qualitatively and quantitatively similar to those from a previous study from our laboratory that challenged mice with 2 wk CR, although, muscle weight was not assessed (Bevilacqua et al., submitted). In further support, Bevilacqua and colleagues demonstrated that increased duration of CR was associated with a greater reduction in BW (Bevilacqua et al., 2004, 2005). We also found a larger reduction in BW with 1 mo CR compared to 2 wk CR, in both genotypes. In rats, only CR of ≥ 6 mo duration resulted in the same tissue weight reduction pattern seen with mice in the present study (Bevilacqua et al., 2005).

Glucose is stored as glycogen primarily in the liver, and to a lesser extent in muscle (*i.e.* on a percentage tissue weight basis). Liver glycogen is the primary fuel source used to maintain normal blood glucose levels (5 mM); therefore, when blood glucose levels are low, liver glycogen is catabolised and glucose is released into the blood. Therefore, with CR, the significant reduction in liver weight observed was partially due to depletion of glycogen and its associated water weight. During CR, the carbohydrate supply (from food and stored glycogen) is limited, thus fats

become an increasingly important fuel source. Indeed, with both CR interventions, the chow provided to Wt and UCP3 Tg mice at ~ 16:00 was rapidly consumed and dietary carbohydrates were subsequently oxidized during the first half of the dark phase, evidenced by the increase in RER to ~ 1 (Figures 19 and 25). Both genotypes then switched to fatty acid oxidation and spent ~ 16 out of 24 h oxidizing stored fats (Figures 19 and 25). Because of triglyceride mobilization to support energy demands, fat depots became smaller (Tables 2 and 4).

It is also important to consider body composition since this has been shown to change with CR (Ramsey et al., 2000). In Wt mice, 2 wk CR had no effect on the proportional contributions of heart, iBAT or kidney weight to total BW; however, the proportional contribution of both liver and gWAT weight was decreased (Table 3). Such observations are consistent with previous findings in mice and rats (Bevilacqua et al., submitted) (Ramsey et al., 2000). Interestingly, CR increased the proportional contribution of muscle weight to total BW in Wt mice, which is consistent with previous findings in monkeys, mice and humans (Colman et al., 2009; Faulks et al., 2006; Heilbronn et al., 2006). It has previously been shown that rhesus monkeys subjected to 30% CR for 17 years possessed a much slower rate of muscle weight loss relative to BW compared to normally fed controls (Colman et al., 2008). Similar results have also been shown in rats (McKiernan et al., 2004; Payne et al., 2003). These observations support a protective effect of CR against sarcopenia (Evans, 1995; Marzetti et al., 2008). In summary, for the purposes of the present study, comparison with previous findings indicates that the Wt mice responded to CR with the expected changes in body composition.

A striking difference in the whole body response of UCP3 Tg mice to CR was a decrease in the proportional contribution of muscle weight to total BW with the 2 wk CR intervention (Table 3). Since skeletal muscle is an important site of glucose disposal and is essential for strength and locomotion, a reduction in muscle mass in relation to BW could be deleterious to the organism. Thus, the greater proton leak in skeletal muscle mitochondria was associated with a maladaptive response of muscle to the 2 wk CR intervention.

After 1 mo CR, body composition was the same in Wt and UCP3 Tg mice and only the proportional contribution of fat weight to total BW was decreased in both genotypes; the proportional contribution of lean tissue weight was either unchanged or increased (Table 5). Thus, with the addition of 2 wk CR, UCP3 Tg mice were able to adapt to the CR treatment, at least at the level of whole body characteristics. It seems therefore, that UCP3 Tg mice took longer than Wt mice to reach a steady state with respect to proportional tissue weight changes.

4.3.2 Whole body energetics

CR has been associated with a lower than normal level of energy expenditure, termed hypometabolism (Ramsey et al., 2000). One idea is that a hypometabolic state, induced by CR, may favour a reduction in overall ROS production and oxidative stress, thereby slowing the aging process (Ramsey et al., 2000). At first glance, this notion appears to run counter to the overall hypothesis that CR will induce mitochondrial proton leak, which on its own would cause an increase in energy expenditure. However, it is important to note that our

assessments and hypotheses of leak are at the isolated mitochondrial level and are expressed per mg mitochondrial protein. It is most likely that mitochondria are significantly 'remodelled' by CR and reach a new functional steady-state in which they operate at a lower PMF.

In the present study, it was shown that 2 wk and 1 mo CR treatments induced a decrease in whole body $\dot{V}O_2$ in both genotypes when expressed per mouse (Figures 17 and 23). Such results are consistent with previous findings from our laboratory, in which 2 wk CR decreased whole body $\dot{V}O_2$ per animal (*i.e.* not mass-adjusted) in Wt mice (Bevilacqua et al., submitted) and in rats subjected to short, medium and long term CR treatment periods (Bevilacqua et al., 2004, 2005). It is common practise to normalize whole body $\dot{V}O_2$ to BW, as in the present study as well as in previous ones (*e.g.,* (Bevilacqua et al., 2004, 2005)). However, the normalization of $\dot{V}O_2$ to BW must be carried out with caution (Himms-Hagen, 1997). In particular, if there are significant differences in body composition, especially in tissues that have very low ATP demands, such as white adipose tissue (WAT), then it is inappropriate to rely exclusively on BW-normalized data as the basis for concluding whether or not energy expenditure has changed. After normalization to BW, differences in $\dot{V}O_2$ were only apparent in the dark phase in both genotypes subjected to 2 wk CR (Figure 18). Lean tissue mass refers to internal organs and muscle. These tissues have high energy requirements and largely contribute to BMR. In particular, muscle contributes ~ 20-33% to BMR whereas WAT contributes ~ 1-12% (Ramsey et al., 2000). Thus, changes in whole body $\dot{V}O_2$ in response to 2 wk CR need to be interpreted in light of the differential effect of the 2 wk CR intervention on proportional muscle and WAT weights in Wt and UCP3 Tg mice;

neither the per mouse nor the per g BW representation of $\dot{V}O_2$ takes the latter into account. Thus, while mass-adjusted $\dot{V}O_2$ was similar in 2 wk CR Wt and UCP3 Tg mice, the proportional decrease in muscle in 2 wk CR UCP3 Tg mice indicates that $\dot{V}O_2$ *per lean tissue mass* was greater with 2 wk CR in UCP3 Tg mice compared to Wt mice.

With 1 mo CR, differences in whole body $\dot{V}O_2$ disappeared upon normalization to BW (Figure 24). From here, concluding that CR did not have an effect on whole body $\dot{V}O_2$ would not be correct, as body composition changed, consistent with other studies (Ramsey et al., 2000). In both Wt and UCP3 Tg mice, 1 mo CR caused a decrease in the proportional contribution of fat weight to total BW and had no effect, or increased the proportional contribution of lean tissue weight. Therefore, Wt and UCP3 Tg CR mice had a larger proportion of metabolically active tissue compared to AL controls. Thus, in this respect, mass-adjusted $\dot{V}O_2$ was decreased with 1 mo CR in both genotypes.

4.4 MITOCHONDRIAL REMODELLING WITH SHORT-TERM CR IN WT MICE

'Mitochondrial remodelling' refers to any changes in mitochondrial content, composition, function or dynamics. As outlined in section 1.4, evidence increasingly supports the idea that mitochondrial remodelling plays an important role in the mechanisms activated by CR (Barazzoni et al., 2005; Bevilacqua et al., 2004, 2005; Bua et al., 2004; Civitarese et al., 2007; Guarente, 2008; Marzetti et al., 2008; Pamplona et al., 2002). Indeed, CR consistently decreases ROS production and oxidative stress in a number of species (Asami et al., 2008; Bevilacqua et al., 2004,

2005; Lass et al., 1998; Pamplona et al., 2002), consistent with the *oxidative stress theory of aging* (Finkel and Holbrook, 2000). One potential mechanism by which CR decreases ROS production is by increasing proton leak, consistent with the '*uncoupling to survive*' theory (see section 1.4.1). In the present study, levels of ROS production were unchanged in Wt mitochondria subjected to 2 wk CR, despite an ~ 50% increase in UCP3 protein content (Figures 15 and 22). ANT levels were unchanged with 2 wk CR (Figure 22). These findings have been replicated in a separate study of skeletal muscle mitochondria (Bevilacqua et al., submitted). The lack of a CR–induced effect on mitochondrial ROS production in Wt mice was surprising and inconsistent with previous studies from our laboratory where 2 wk CR treatment in rats resulted in marked decreases in ROS production and oxidative damage in skeletal muscle mitochondria (Bevilacqua et al., 2004); neither UCP3 nor ANT protein content was determined. As outlined in sections 1.4.1 and 1.4.3, UCP3 and ANT can mediate proton leak, therefore, a CR-induced increase in expression should decrease ROS production and oxidative stress. Thus, the increase in UCP3 protein levels with CR may not have been sufficient to decrease ROS production. It is theoretically possible that other antioxidant mechanisms decreased in expression; however, protein levels of MnSOD and ANT were unchanged with CR in Wt mice (Figure 15). ROS production also depends on substrate oxidation; thus, an increase in substrate oxidation could also theoretically explain the lack of a decrease in ROS with CR. However, such an increase in substrate oxidation was not detected.

We were surprised to find the differences between mice (present study; Bevilacqua et al., submitted) and rats (Bevilacqua et al., 2004) in the effect of 2 wk CR on ROS production and oxidative stress. In our study and in that of Bevilacqua

et al., the methods used to determine ROS production were identical. Therefore, differences in methodological procedures cannot account for this difference. There have been reports of differences in the capacity for ROS generation with different muscle fiber types (Anderson et al., 2007); however, the selection of muscles for mitochondrial isolations in both studies were composed primarily of type II fibers. Therefore, differences in muscle fiber types cannot account for this difference either. Thus, at this point an explanation for the species difference remains unknown. Overall, these observations suggest that the effects of CR in one mammalian species cannot necessarily be extrapolated to another.

It was thought that although the 2 wk CR treatment did not decrease ROS production in Wt mice, perhaps CR was still able to mitigate oxidative damage. Indeed, UCP3 has been linked to decreased levels of oxidative stress (Bezaire et al., 2007; Brand and Esteves, 2005). However, levels of oxidative damage, as determined by 4–HNE modified proteins, were unchanged in mitochondria from Wt CR mice compared to mitochondria from AL controls (Figure 16). Thus, overall, our findings indicate that CR is not always associated with decreased ROS production and oxidative stress.

Because the 2 wk CR treatment did not lower mitochondrial ROS production, the duration of CR was extended by 2 wks. Indeed, the 1 mo CR intervention was associated with lowered ROS production. Specifically, ROS production decreased with CR in Wt mice only, and only with provisioning of a fatty acid substrate in the presence of the complex III inhibitor antimycin (Figure 28). Under such conditions, ROS production primarily occurs at complex III, as well as at upstream sites such

as, at the electron transfer flavoprotein (ETF) and ETF–ubiquinone oxidoreductase (St-Pierre et al., 2002).

However, CR did not induce a change in the levels of oxidative damage in mitochondria from Wt mice (Figure 31). This finding was not expected based on the decreased ROS production observed, and is inconsistent with previous findings from our laboratory where lowered ROS production was accompanied by decreased oxidative damage in rat skeletal muscle (Bevilacqua et al., 2004, 2005). Our results are also inconsistent with other studies in mouse skeletal muscle where CR was associated with decreased oxidative stress; however the duration of CR was greater than 1 mo (Asami et al., 2008; Lass et al., 1998). 4–HNE protein adduct levels were assessed as the marker of mitochondrial oxidative damage (Tsai et al., 1998). Since only the levels of lipid peroxidation were measured, it is possible that we missed an effect of CR to lower other forms of oxidative stress. Therefore, it would be of interest, in future studies, to assess, for example, the level of mitochondrial DNA damage or protein carbonyls.

In Wt mice, 1 mo CR lead to two very interesting findings that could explain the observed decrease in ROS production. First, UCP3 protein was increased to a greater extent in mitochondria from Wt mice subjected to 1 mo CR as compared to only 2 wk CR (Figures 15 and 30). With 2 wk CR, UCP3 protein levels were increased ~ 50%; whereas, with 1 mo CR, levels rose by ~ 100%. On the other hand, ANT protein expression was unchanged with both the 2 wk and 1 mo CR interventions. Thus, it is possible that the greater level of UCP3 protein associated with 1 mo CR induced a greater mitochondrial proton leak compared to 2 wk CR, thereby decreasing ROS production only in the former. Therefore, the level of UCP3

protein and the associated proton leak may determine whether mitigation of ROS production occurs. Accordingly, it was deemed important to assess mitochondrial proton leak, with the expectation that 1 mo CR in Wt mice would increase mitochondrial proton leak compared to controls. Our results support this hypothesis (Figure 29). Although, in this study, mitochondrial proton leak was not assessed in Wt mice subjected to 2 wk CR, another study from our laboratory has shown that 2 wk CR does not alter proton leak in skeletal muscle mitochondria of Wt mice even with a CR–induced increase in UCP3 protein content (Bevilacqua *et al.*, submitted). Overall, our findings of increased proton leak and decreased ROS production with 1 mo CR in mice are consistent with previous studies from our laboratory which have shown that short–term CR (2 wk or 2 mo CR) in rat skeletal muscle mitochondria resulted in lowered PMF, increased oxygen consumption and marked decreases in ROS production and oxidative stress (Bevilacqua et al., 2004). However, UCP3 protein content was not consistently assessed in the study of Bevilacqua and colleagues. In further support, rats exposed to a 4–mo CR treatment also possessed increased proton leak in liver mitochondria compared to controls; this was also associated with decreased ROS production (Lambert and Merry, 2004). It seems therefore that CR in Wt mice upregulates UCP3 protein, and only at a certain threshold does mitochondrial proton leak increase. Once proton leak is activated, the production of mitochondrial ROS is subsequently attenuated.

The second interesting finding that may explain the decreased ROS production associated with 1 mo CR is the lowered state 3 respiration rate (Figure 27); suggestive of a decrease in mitochondrial oxidative capacity. Interestingly, with 2 wk CR, ROS production was unchanged in mitochondria from Wt mice, as was

state 3 respiration (Figures 21 and 22). Therefore, this suggests that the decreased mitochondrial oxidative capacity observed with 1 mo CR in Wt mice could explain the decrease in ROS production. Theoretically, a decrease in mitochondrial oxidative capacity could arise if levels of ETC complexes are reduced. Specifically, a decrease in the amount of complex I and/or complex III would result in decreased ROS production, as superoxide is primarily produced at these two complexes (see section 1.2.2.2). However, studies in rat muscle have shown that a significant lowering of the activity of ETC complexes is required before an overall impact on mitochondrial respiratory flux or ATP synthesis is observed (Mazat et al., 2001). For example, oxygen consumption remained unchanged until complex IV (COX) was inhibited by ~ 80-90% at which point the respiration rate decreased dramatically. Similar results have been reported with each of the other ETC complexes (Rossignol et al., 2000; Rossignol et al., 1999). Therefore, normal oxidative phosphorylation can occur even when mitochondria are significantly deficient in ETC complexes. Given this, it is unlikely that the decreased oxidative capacity observed in the present study was due to a reduced abundance of ETC complexes. Nonetheless, Western blotting and/or enzyme activity assays could be used to verify that the content of the ETC complexes and their activity (Vmax) are not greatly decreased by 1 mo CR. Although not significant, 1 mo CR tended to decrease the maximal uncoupled respiration rate in Wt mice, as determined through the use of FCCP. FCCP causes mitochondrial uncoupling in a 'non-regulated' manner. Therefore, because CR tended to decrease this rate as well as the maximum respiration rate (state 3), it can be hypothesized that the decrease in overall mitochondrial oxidative capacity was not due to CR-induced changes in the components of the ETC.

Rather, results point to factors upstream of the ETC. Interestingly, citrate synthase activity has been shown to decrease with CR in rat skeletal muscle (Zangarelli et al., 2006). Citrate synthase is localized to the mitochondrial matrix and catalyzes the first step of the Krebs cycle. Thus, it is possible that the decreased maximal capacity observed here was due to lower citrate synthase activity.

In skeletal muscle, many enzymes exist to help scavenge ROS, thereby dampening pathological effects associated with high levels of ROS (see sections 1.2.2.4-5). Higher levels of antioxidant enzymes have been associated with decreased levels of ROS in mice (Hu et al., 2007; Schriner et al., 2005). MnSOD is located in the mitochondrial matrix and is the primary enzyme responsible for converting superoxide produced into H_2O_2 (Halliwell, 1999; Okado-Matsumoto and Fridovich, 2001). With 1 mo CR, there was a trend for increased MnSOD protein levels in skeletal muscle mitochondria from Wt mice (Figure 30). Other studies have assessed the levels of antioxidant enzymes with CR and results have been inconsistent. For example, gene transcript levels were assessed in skeletal muscle mitochondria isolated from rats (Sreekumar et al., 2002). It was found that messenger RNA (mRNA) levels of ROS scavenging enzymes including, CuZnSOD, MnSOD and Gpx, were upregulated in mitochondria from CR rats compared to normally-fed controls. Our finding of increased MnSOD protein with CR in Wt mice is consistent with this study. However, in mouse skeletal muscle mitochondria, Gpx and SOD activities were not increased following 4 mo of CR in mice, compared to controls (Lass et al., 1998). Similarly, HeLa and FaO cells treated with serum isolated from rats exposed to CR possessed similar levels of Cu/ZnSOD and catalase protein compared to controls (Lopez-Lluch et al., 2006). Despite

inconsistent findings, our study revealed that 1 mo CR in Wt mice was associated with a tendency for increased MnSOD protein. The trend for increased MnSOD protein induced by 1 mo CR in the present study was associated with decreased ROS production. However, the increase in MnSOD protein observed cannot explain the decrease in ROS because our measurements of ROS production specifically assessed H_2O_2 emission. A CR-induced increase in MnSOD protein could result in the increased conversion of superoxide to H_2O_2, which would increase the H_2O_2 emission rate. Overall, the induction of antioxidant enzymes to decrease ROS production may be a mechanism activated by CR; however, in this study, increased MnSOD protein was not responsible for the decrease in ROS production observed.

Interestingly, a decrease in skeletal muscle mitochondrial content was observed in Wt mice only with the 1 mo CR intervention (Figures 20 and 26). In agreement with our finding, Baker and colleagues, using enzyme activities in whole muscle homogenates, demonstrated that CR of ≥ 5 mo duration in mice resulted in decreased mitochondrial content in skeletal muscle (Baker et al., 2006). Also consistent with our finding is that of Lambert and colleagues who reported a decrease in mitochondrial yield in heart with CR of 4.5 mo duration in rats (Lambert et al., 2004). In human muscle, mitochondrial content was reported to be increased with CR, based on increased mtDNA (Civitarese et al., 2007). However, when the activities of key mitochondrial enzymes were measured, no differences were found with CR. Therefore, the Civitarese study does not convincingly show an increase in mitochondrial content with CR in muscle. Overall, it seems clear that CR can in fact be associated with decreased mitochondrial biogenesis, despite reports indicating

that mitochondrial biogenesis is stimulated (Civitarese et al., 2007; Nisoli et al., 2005).

In the present study, 1 mo CR induced an ~ 45% increase in mitochondrial proton leak in Wt mice (Figure 29). Interestingly, this was accompanied by an ~ 25% decrease in mitochondrial content (Figure 26). The CR-induced increase in proton leak observed was also associated with decreased ROS production. Therefore, at the mitochondrial level, the increase in proton leak would be advantageous because it could mitigate the production of ROS. However, at the level of the muscle, an increase in proton leak would, theoretically, result in an increase in energy expenditure which could be disadvantageous in the context of CR. However, it seems that muscle from Wt mice was able to significantly compensate for the CR-induced increase in uncoupling by decreasing the amount of total mitochondria.

4.5 DOES SHORT–TERM CR PROVIDE UCP3 TG MICE WITH ADDITIONAL PROTECTION AGAINST OXIDATIVE STRESS?

Skeletal muscle mitochondria from UCP3 Tg mice were characterized by decreased ROS production and increased proton leak. It was hypothesized that short–term CR in skeletal muscle mitochondria from UCP3 Tg mice would not enhance the existing proton leak and therefore, would not provide any further protection against ROS production and oxidative stress. Together, such results would provide support for the overall hypothesis that CR causes mitochondrial proton leak which becomes responsible for CR–induced decreases in ROS production and oxidative stress.

2 wk CR did not lower ROS production in mitochondria from UCP3 Tg mice. Instead, ROS production tended to increase (Figure 22). To our knowledge, this is the first report of increased ROS with CR. It therefore appears that CR was acting as a stressor in this genotype, resulting in increased ROS production. Interestingly, this was associated with a decrease in ANT protein content; UCP3 protein content was unaltered (Figure 15). ANT has been shown to mediate up to 50% of proton leak in muscle (Brand et al., 2005); therefore, it would be expected that decreased ANT protein content would dampen proton conductance, thereby increasing PMF and the likelihood of ROS production. Therefore, it is possible that the increased ROS production observed with 2 wk CR in mitochondria from UCP3 Tg mice was due to decreased ANT protein content. Future studies should assess the kinetics of skeletal muscle mitochondrial proton leak in UCP3 Tg mice subjected to 2 wk CR, to determine whether the decrease in ANT protein content was associated with decreased proton conductance. Given the above, it would be expected that the UCP3 Tg mice would have greater levels of mitochondrial oxidative damage with 2 wk CR. However, we demonstrate that the level of 4–HNE modified proteins was unchanged (Figure 16). In future studies, it would be of interest to assess levels of oxidative stress using another indicator, such as formation of protein carbonyls.

Interestingly, ROS production in mitochondria from UCP3 Tg mice was not increased with 1 mo CR as seen with 2 wk CR; levels were unchanged (Figure 28). Also different from 2 wk CR, ANT protein levels were unchanged in mitochondria from UCP3 Tg mice subjected to 1 mo CR. Together, these results further support the hypothesis that the trend for increased ROS production following 2 wk CR was caused by the CR–induced decrease in ANT protein content. It was expected that

proton leak would be unaffected with 1 mo CR in mitochondria from UCP3 Tg mice. Results support this prediction (Figure 29). Furthermore, due to the lack of a CR-induced effect on ROS production in mitochondria from UCP3 Tg mice, it was expected that levels of oxidative damage would also be unaltered. Results also support this prediction (Figure 31). Thus, mitochondria from UCP3 Tg mice were better adapted to the effects of CR when the duration of treatment was extended from 2 wks to 1 mo. That being said, short–term CR in skeletal muscle mitochondria from mice overexpressing UCP3 protein did not enhance the existing proton leak and therefore, did not provide any further protection against ROS production and oxidative stress. Overall, these observations in UCP3 Tg mice support the hypothesis that CR causes a UCP3–mediated mitochondrial proton leak which is responsible for the CR–induced decrease in ROS production observed with 1 mo CR in Wt mice.

Interestingly, 1 mo CR induced an ~ 55% decrease in mitochondrial content in UCP3 Tg mice (Figure 26). This genotype already possessed enhanced levels of mitochondrial uncoupling within their muscle (see Figure 11). Since mitochondrial proton leak was not affected by the 1 mo CR intervention in this genotype, UCP3 Tg CR mice would have lower levels of uncoupling at the whole muscle level compared to AL-fed controls. It seems therefore, that energy restriction within this genotype provokes a compensatory effect that offsets the increased energy expenditure due to proton leak processes. Thus, CR would induce an overall decrease in energy expenditure in the UCP3 Tg mice.

4.6 IMPLICATIONS OF INCREASED MITOCHONDRIAL PROTON LEAK IN SKELETAL MUSCLE

Studies that have directly manipulated mitochondrial proton leak in skeletal muscle, or have correlated the degree of uncoupling with functional measurements have concluded that increased proton leak is in fact protective against age-related disease. Specifically, ectopic expression of UCP1 in mouse skeletal muscle was accompanied by increased median survival, and decreased markers of lymphoma, atherosclerosis, diabetes and hypertension (Gates et al., 2007). Additionally, mild uncoupling in human muscle was correlated with a reduction in age-induced decreases in mitochondrial function (Amara et al., 2007). Furthermore, increased uncoupling in skeletal muscle has been shown to be less susceptible to the development of diabetes. For example, mice overexpressing UCP3 in muscle have improved glucose handling and insulin sensitivity, and accumulate less intramuscular triglyceride when fed a normal diet or challenged with a high fat diet (Costford et al., 2006). UCP3 Tg mice were also protected from the development of insulin resistance when challenged with a high fat diet (Choi et al., 2007). Overall, previous studies have implicated uncoupling in muscle as being beneficial to overall health. However, in the present study, we demonstrate a situation where increased mitochondrial proton leak in muscle does not necessarily benefit the organism. Therefore, our results are not consistent with previous studies and our findings show that increased proton leak in muscle can, in fact, be associated with deleterious effects in the context of a mild stress.

4.7 CONCLUSION

From the research presented herein, a number of conclusions can be drawn. First, physiological increases (*i.e.* 2-4 fold range) of UCP3 protein are associated with increased proton leak and decreased ROS production. Findings from Wt mice demonstrate that CR does not always mitigate ROS production and oxidative stress. When short-term CR does lower ROS production, this occurs in conjunction with mitochondrial remodelling and a generalized decrease in mitochondrial content. Specifically, we demonstrate that UCP3 and MnSOD proteins are upregulated and proton leak processes are induced along with decreases in mitochondrial oxidative capacity. Each of these changes would favour a decrease in ROS production. Mitochondrial uncoupling may be a mechanism activated by CR that underlies the beneficial effects of CR. However, muscle that already possesses greater mitochondrial uncoupling and lower ROS production prior to CR should not be considered to be 'pre-adapted' to CR, because the muscle of the UCP3 Tg mice responded to the 2 wk CR intervention. Importantly, the muscle phenotype of the UCP3 Tg mice predisposed the muscle to potentially deleterious effects in response to short-term CR. More generally, while increased proton leak in muscle leads to a phenotype, namely lower ROS production, that may protect muscle from age-related degeneration, the greater proton leak can lead to a maladaptive response to a mild stress. In this regard, increased uncoupling does not appear to be uniformly beneficial to skeletal muscle, and thus to the survival of the organism.

REFERENCES

Akerman, K.E., and Wikstrom, M.K. (1976). Safranine as a probe of the mitochondrial membrane potential. FEBS Lett *68*, 191-197.

Amara, C.E., Shankland, E.G., Jubrias, S.A., Marcinek, D.J., Kushmerick, M.J., and Conley, K.E. (2007). Mild mitochondrial uncoupling impacts cellular aging in human muscles in vivo. Proc Natl Acad Sci U S A *104*, 1057-1062.

Anderson, E.J., Yamazaki, H., and Neufer, P.D. (2007). Induction of endogenous uncoupling protein 3 suppresses mitochondrial oxidant emission during fatty acid-supported respiration. J Biol Chem *282*, 31257-31266.

Andreyev, A., Bondareva, T.O., Dedukhova, V.I., Mokhova, E.N., Skulachev, V.P., Tsofina, L.M., Volkov, N.I., and Vygodina, T.V. (1989). The ATP/ADP-antiporter is involved in the uncoupling effect of fatty acids on mitochondria. Eur J Biochem *182*, 585-592.

Andreyev, A., Bondareva, T.O., Dedukhova, V.I., Mokhova, E.N., Skulachev, V.P., and Volkov, N.I. (1988). Carboxyatractylate inhibits the uncoupling effect of free fatty acids. FEBS Lett *226*, 265-269.

Andreyev, A.Y., Kushnareva, Y.E., and Starkov, A.A. (2005). Mitochondrial metabolism of reactive oxygen species. Biochemistry (Mosc) *70*, 200-214.

Antier, D., Carswell, H.V., Brosnan, M.J., Hamilton, C.A., Macrae, I.M., Groves, S., Jardine, E., Reid, J.L., and Dominiczak, A.E. (2004). Increased levels of superoxide in brains from old female rats. Free Radic Res *38*, 177-183.

Asami, D.K., McDonald, R.B., Hagopian, K., Horwitz, B.A., Warman, D., Hsiao, A., Warden, C., and Ramsey, J.J. (2008). Effect of aging, caloric restriction, and uncoupling protein 3 (UCP3) on mitochondrial proton leak in mice. Exp Gerontol *43*, 1069-1076.

Austad, S.N. (1989). Life extension by dietary restriction in the bowl and doily spider, Frontinella pyramitela. Exp Gerontol *24*, 83-92.

Baker, D.J., Betik, A.C., Krause, D.J., and Hepple, R.T. (2006). No decline in skeletal muscle oxidative capacity with aging in long-term calorically restricted rats: effects are independent of mitochondrial DNA integrity. J Gerontol A Biol Sci Med Sci *61*, 675-684.

Bandy, B., and Davison, A.J. (1990). Mitochondrial mutations may increase oxidative stress: implications for carcinogenesis and aging? Free Radic Biol Med *8*, 523-539.

Barazzoni, R., Zanetti, M., Bosutti, A., Biolo, G., Vitali-Serdoz, L., Stebel, M., and Guarnieri, G. (2005). Moderate caloric restriction, but not physiological hyperleptinemia per se, enhances mitochondrial oxidative capacity in rat liver and skeletal muscle--tissue-specific impact on tissue triglyceride content and AKT activation. Endocrinology *146*, 2098-2106.

Barja, G. (1999). Mitochondrial oxygen radical generation and leak: sites of production in states 4 and 3, organ specificity, and relation to aging and longevity. J Bioenerg Biomembr *31*, 347-366.

Barja, G., Cadenas, S., Rojas, C., Perez-Campo, R., and Lopez-Torres, M. (1994). Low mitochondrial free radical production per unit O2 consumption can explain the simultaneous presence of high longevity and high aerobic metabolic rate in birds. Free Radic Res *21*, 317-327.

Bevilacqua, L., Ramsey, J.J., Hagopian, K., Weindruch, R., and Harper, M.E. (2004). Effects of short- and medium-term calorie restriction on muscle mitochondrial proton leak and reactive oxygen species production. Am J Physiol Endocrinol Metab *286*, E852-861.

Bevilacqua, L., Ramsey, J.J., Hagopian, K., Weindruch, R., and Harper, M.E. (2005). Long-term caloric restriction increases UCP3 content but decreases proton leak and reactive oxygen species production in rat skeletal muscle mitochondria. Am J Physiol Endocrinol Metab *289*, E429-438.

Bezaire, V., Hofmann, W., Kramer, J.K., Kozak, L.P., and Harper, M.E. (2001). Effects of fasting on muscle mitochondrial energetics and fatty acid metabolism in Ucp3(-/-) and wild-type mice. Am J Physiol Endocrinol Metab *281*, E975-982.

Bezaire, V., Seifert, E.L., and Harper, M.E. (2007). Uncoupling protein-3: clues in an ongoing mitochondrial mystery. FASEB J *21*, 312-324.

Bezaire, V., Spriet, L.L., Campbell, S., Sabet, N., Gerrits, M., Bonen, A., and Harper, M.E. (2005). Constitutive UCP3 overexpression at physiological levels increases mouse skeletal muscle capacity for fatty acid transport and oxidation. FASEB J *19*, 977-979.

Blackwell, K.A., Sorenson, J.P., Richardson, D.M., Smith, L.A., Suda, O., Nath, K., and Katusic, Z.S. (2004). Mechanisms of aging-induced impairment of endothelium-dependent relaxation: role of tetrahydrobiopterin. Am J Physiol Heart Circ Physiol *287*, H2448-2453.

Bluher, M., Kahn, B.B., and Kahn, C.R. (2003). Extended longevity in mice lacking the insulin receptor in adipose tissue. Science *299*, 572-574.

Boss, O., Samec, S., Paoloni-Giacobino, A., Rossier, C., Dulloo, A., Seydoux, J., Muzzin, P., and Giacobino, J.P. (1997). Uncoupling protein-3: a new member of the mitochondrial carrier family with tissue-specific expression. FEBS Lett *408*, 39-42.

Bouillaud, F., Ricquier, D., Thibault, J., and Weissenbach, J. (1985). Molecular approach to thermogenesis in brown adipose tissue: cDNA cloning of the mitochondrial uncoupling protein. Proc Natl Acad Sci U S A *82*, 445-448.

Bouillaud, F., Weissenbach, J., and Ricquier, D. (1986). Complete cDNA-derived amino acid sequence of rat brown fat uncoupling protein. J Biol Chem *261*, 1487-1490.

Brand, M.D. (1990). The proton leak across the mitochondrial inner membrane. Biochim Biophys Acta *1018*, 128-133.

Brand, M.D. (2000). Uncoupling to survive? The role of mitochondrial inefficiency in ageing. Exp Gerontol *35*, 811-820.

Brand, M.D., Affourtit, C., Esteves, T.C., Green, K., Lambert, A.J., Miwa, S., Pakay, J.L., and Parker, N. (2004). Mitochondrial superoxide: production, biological effects, and activation of uncoupling proteins. Free Radic Biol Med *37*, 755-767.

Brand, M.D., and Esteves, T.C. (2005). Physiological functions of the mitochondrial uncoupling proteins UCP2 and UCP3. Cell Metab *2*, 85-93.

Brand, M.D., Pakay, J.L., Ocloo, A., Kokoszka, J., Wallace, D.C., Brookes, P.S., and Cornwall, E.J. (2005). The basal proton conductance of mitochondria depends on adenine nucleotide translocase content. Biochem J *392*, 353-362.

Brand, M.D., Pamplona, R., Portero-Otin, M., Requena, J.R., Roebuck, S.J., Buckingham, J.A., Clapham, J.C., and Cadenas, S. (2002). Oxidative damage and phospholipid fatty acyl composition in skeletal muscle mitochondria from mice underexpressing or overexpressing uncoupling protein 3. Biochem J *368*, 597-603.

Brown, G.C. (1992). The leaks and slips of bioenergetic membranes. FASEB J *6*, 2961-2965.

Brunelle, J.K., Bell, E.L., Quesada, N.M., Vercauteren, K., Tiranti, V., Zeviani, M., Scarpulla, R.C., and Chandel, N.S. (2005). Oxygen sensing requires mitochondrial ROS but not oxidative phosphorylation. Cell Metab *1*, 409-414.

Brunet-Rossinni, A.K. (2004). Reduced free-radical production and extreme longevity in the little brown bat (Myotis lucifugus) versus two non-flying mammals. Mech Ageing Dev *125*, 11-20.

Bua, E., McKiernan, S.H., and Aiken, J.M. (2004). Calorie restriction limits the generation but not the progression of mitochondrial abnormalities in aging skeletal muscle. FASEB J *18*, 582-584.

Cadenas, S., Buckingham, J.A., Samec, S., Seydoux, J., Din, N., Dulloo, A.G., and Brand, M.D. (1999). UCP2 and UCP3 rise in starved rat skeletal muscle but mitochondrial proton conductance is unchanged. FEBS Lett *462*, 257-260.

Cadenas, S., Buckingham, J.A., St-Pierre, J., Dickinson, K., Jones, R.B., and Brand, M.D. (2000). AMP decreases the efficiency of skeletal-muscle mitochondria. Biochem J *351 Pt 2*, 307-311.

Canada, H. (2002). Canada's Aging Population, D.o.A.a. Seniors, ed. (Ottawa, Minister of Public Works and Government Services Canada), pp. 9-11.

Chance, B., Sies, H., and Boveris, A. (1979). Hydroperoxide metabolism in mammalian organs. Physiol Rev *59*, 527-605.

Chappell, J.B., and Perry, S.V. (1954). Biochemical and osmotic properties of skeletal muscle mitochondria. Nature *173*, 1094-1095.

Chavous, D.A., Jackson, F.R., and O'Connor, C.M. (2001). Extension of the Drosophila lifespan by overexpression of a protein repair methyltransferase. Proc Natl Acad Sci U S A *98*, 14814-14818.

Choi, C.S., Fillmore, J.J., Kim, J.K., Liu, Z.X., Kim, S., Collier, E.F., Kulkarni, A., Distefano, A., Hwang, Y.J., Kahn, M., *et al.* (2007). Overexpression of uncoupling protein 3 in skeletal muscle protects against fat-induced insulin resistance. J Clin Invest *117*, 1995-2003.

Civitarese, A.E., Carling, S., Heilbronn, L.K., Hulver, M.H., Ukropcova, B., Deutsch, W.A., Smith, S.R., and Ravussin, E. (2007). Calorie restriction increases muscle mitochondrial biogenesis in healthy humans. PLoS Med *4*, e76.

Clapham, J.C., Arch, J.R., Chapman, H., Haynes, A., Lister, C., Moore, G.B., Piercy, V., Carter, S.A., Lehner, I., Smith, S.A., *et al.* (2000). Mice overexpressing human uncoupling protein-3 in skeletal muscle are hyperphagic and lean. Nature *406*, 415-418.

Colman, R.J., Anderson, R.M., Johnson, S.C., Kastman, E.K., Kosmatka, K.J., Beasley, T.M., Allison, D.B., Cruzen, C., Simmons, H.A., Kemnitz, J.W., *et al.* (2009). Caloric restriction delays disease onset and mortality in rhesus monkeys. Science *325*, 201-204.

Colman, R.J., Beasley, T.M., Allison, D.B., and Weindruch, R. (2008). Attenuation of sarcopenia by dietary restriction in rhesus monkeys. J Gerontol A Biol Sci Med Sci *63*, 556-559.

Comfort, A. (1963). Effect of Delayed and Resumed Growth on the Longevity of a Fish (Lebistes Reticulatus, Peters) in Captivity. Gerontologia *49*, 150-155.

Costford, S.R., Chaudhry, S.N., Crawford, S.A., Salkhordeh, M., and Harper, M.E. (2008). Long-term high-fat feeding induces greater fat storage in mice lacking UCP3. Am J Physiol Endocrinol Metab *295*, E1018-1024.

Costford, S.R., Chaudhry, S.N., Salkhordeh, M., and Harper, M.E. (2006). Effects of the presence, absence, and overexpression of uncoupling protein-3 on adiposity and fuel metabolism in congenic mice. Am J Physiol Endocrinol Metab *290*, E1304-1312.

Csiszar, A., Ungvari, Z., Edwards, J.G., Kaminski, P., Wolin, M.S., Koller, A., and Kaley, G. (2002). Aging-induced phenotypic changes and oxidative stress impair coronary arteriolar function. Circ Res *90*, 1159-1166.

Droge, W. (2002). Free radicals in the physiological control of cell function. Physiol Rev *82*, 47-95.

Dubowitz, V., Sewry, CA. (2007). Muscle Biopsy: A practical Approach, Third edn (Elsevier Limited).

Echtay, K.S., Esteves, T.C., Pakay, J.L., Jekabsons, M.B., Lambert, A.J., Portero-Otin, M., Pamplona, R., Vidal-Puig, A.J., Wang, S., Roebuck, S.J., *et al.* (2003). A signalling role for 4-hydroxy-2-nonenal in regulation of mitochondrial uncoupling. EMBO J *22*, 4103-4110.

Echtay, K.S., Roussel, D., St-Pierre, J., Jekabsons, M.B., Cadenas, S., Stuart, J.A., Harper, J.A., Roebuck, S.J., Morrison, A., Pickering, S., *et al.* (2002). Superoxide activates mitochondrial uncoupling proteins. Nature *415*, 96-99.

Elchuri, S., Oberley, T.D., Qi, W., Eisenstein, R.S., Jackson Roberts, L., Van Remmen, H., Epstein, C.J., and Huang, T.T. (2005). CuZnSOD deficiency leads to persistent and widespread oxidative damage and hepatocarcinogenesis later in life. Oncogene *24*, 367-380.

Evans, W.J. (1995). What is sarcopenia? J Gerontol A Biol Sci Med Sci *50 Spec No*, 5-8.

Farmer, K.J., and Sohal, R.S. (1989). Relationship between superoxide anion radical generation and aging in the housefly, Musca domestica. Free Radic Biol Med *7*, 23-29.

Faulks, S.C., Turner, N., Else, P.L., and Hulbert, A.J. (2006). Calorie restriction in mice: effects on body composition, daily activity, metabolic rate, mitochondrial reactive oxygen species production, and membrane fatty acid composition. J Gerontol A Biol Sci Med Sci *61*, 781-794.

Finkel, T. (2003). Ageing: a toast to long life. Nature *425*, 132-133.

Finkel, T., and Holbrook, N.J. (2000). Oxidants, oxidative stress and the biology of ageing. Nature *408*, 239-247.

Fleury, C., Neverova, M., Collins, S., Raimbault, S., Champigny, O., Levi-Meyrueis, C., Bouillaud, F., Seldin, M.F., Surwit, R.S., Ricquier, D., *et al.* (1997). Uncoupling protein-2: a novel gene linked to obesity and hyperinsulinemia. Nat Genet *15*, 269-272.

Fontana, L. (2006). Excessive adiposity, calorie restriction, and aging. JAMA *295*, 1577-1578.

Fontana, L., and Klein, S. (2007). Aging, adiposity, and calorie restriction. JAMA *297*, 986-994.

Fontana, L., Meyer, T.E., Klein, S., and Holloszy, J.O. (2004). Long-term calorie restriction is highly effective in reducing the risk for atherosclerosis in humans. Proc Natl Acad Sci U S A *101*, 6659-6663.

Gates, A.C., Bernal-Mizrachi, C., Chinault, S.L., Feng, C., Schneider, J.G., Coleman, T., Malone, J.P., Townsend, R.R., Chakravarthy, M.V., and Semenkovich, C.F. (2007). Respiratory uncoupling in skeletal muscle delays death and diminishes age-related disease. Cell Metab *6*, 497-505.

Gimeno, R.E., Dembski, M., Weng, X., Deng, N., Shyjan, A.W., Gimeno, C.J., Iris, F., Ellis, S.J., Woolf, E.A., and Tartaglia, L.A. (1997). Cloning and characterization of an uncoupling protein homolog: a potential molecular mediator of human thermogenesis. Diabetes *46*, 900-906.

Gong, D.W., He, Y., Karas, M., and Reitman, M. (1997). Uncoupling protein-3 is a mediator of thermogenesis regulated by thyroid hormone, beta3-adrenergic agonists, and leptin. J Biol Chem *272*, 24129-24132.

Grigorieff, N. (1998). Three-dimensional structure of bovine NADH:ubiquinone oxidoreductase (complex I) at 22 A in ice. J Mol Biol *277*, 1033-1046.

Guarente, L. (2008). Mitochondria--a nexus for aging, calorie restriction, and sirtuins? Cell *132*, 171-176.

Guzy, R.D., Hoyos, B., Robin, E., Chen, H., Liu, L., Mansfield, K.D., Simon, M.C., Hammerling, U., and Schumacker, P.T. (2005). Mitochondrial complex III is required for hypoxia-induced ROS production and cellular oxygen sensing. Cell Metab *1*, 401-408.

Halliwell, B. (1999). Antioxidant defence mechanisms: from the beginning to the end (of the beginning). Free Radic Res *31*, 261-272.

Hamilton, C.A., Brosnan, M.J., McIntyre, M., Graham, D., and Dominiczak, A.F. (2001). Superoxide excess in hypertension and aging: a common cause of endothelial dysfunction. Hypertension *37*, 529-534.

Hansford, R.G., Hogue, B.A., and Mildaziene, V. (1997). Dependence of H2O2 formation by rat heart mitochondria on substrate availability and donor age. J Bioenerg Biomembr *29*, 89-95.

Harman, D. (1956). Aging: a theory based on free radical and radiation chemistry. J Gerontol *11*, 298-300.

Harris, N., Costa, V., MacLean, M., Mollapour, M., Moradas-Ferreira, P., and Piper, P.W. (2003). Mnsod overexpression extends the yeast chronological (G(0)) life span but acts independently of Sir2p histone deacetylase to shorten the replicative life span of dividing cells. Free Radic Biol Med *34*, 1599-1606.

Heilbronn, L.K., de Jonge, L., Frisard, M.I., DeLany, J.P., Larson-Meyer, D.E., Rood, J., Nguyen, T., Martin, C.K., Volaufova, J., Most, M.M., *et al.* (2006). Effect of 6-month calorie restriction on biomarkers of longevity, metabolic adaptation, and oxidative stress in overweight individuals: a randomized controlled trial. JAMA *295*, 1539-1548.

Hill, D.J., Hosking, C.S., Shelton, M.J., and Turner, M.W. (1981). Growing out of asthma: Clinical and immunological changes over 5 years. Lancet *2*, 1359-1362.

Himms-Hagen, J. (1997). On raising energy expenditure in ob/ob mice. Science *276*, 1132-1133.

Hirosumi, J., Tuncman, G., Chang, L., Gorgun, C.Z., Uysal, K.T., Maeda, K., Karin, M., and Hotamisligil, G.S. (2002). A central role for JNK in obesity and insulin resistance. Nature *420*, 333-336.

Holzenberger, M., Dupont, J., Ducos, B., Leneuve, P., Geloen, A., Even, P.C., Cervera, P., and Le Bouc, Y. (2003). IGF-1 receptor regulates lifespan and resistance to oxidative stress in mice. Nature *421*, 182-187.

Hu, D., Cao, P., Thiels, E., Chu, C.T., Wu, G.Y., Oury, T.D., and Klann, E. (2007). Hippocampal long-term potentiation, memory, and longevity in mice that

overexpress mitochondrial superoxide dismutase. Neurobiol Learn Mem *87*, 372-384.

Hulbert, A.J., Pamplona, R., Buffenstein, R., and Buttemer, W.A. (2007). Life and death: metabolic rate, membrane composition, and life span of animals. Physiol Rev *87*, 1175-1213.

Hyslop, P.A., and Sklar, L.A. (1984). A quantitative fluorimetric assay for the determination of oxidant production by polymorphonuclear leukocytes: its use in the simultaneous fluorimetric assay of cellular activation processes. Anal Biochem *141*, 280-286.

Iwata, S., Lee, J.W., Okada, K., Lee, J.K., Iwata, M., Rasmussen, B., Link, T.A., Ramaswamy, S., and Jap, B.K. (1998). Complete structure of the 11-subunit bovine mitochondrial cytochrome bc1 complex. Science *281*, 64-71.

Judge, S., Jang, Y.M., Smith, A., Hagen, T., and Leeuwenburgh, C. (2005). Age-associated increases in oxidative stress and antioxidant enzyme activities in cardiac interfibrillar mitochondria: implications for the mitochondrial theory of aging. FASEB J *19*, 419-421.

Jun, T., Ke-yan, F., and Catalano, M. (1996). Increased superoxide anion production in humans: a possible mechanism for the pathogenesis of hypertension. J Hum Hypertens *10*, 305-309.

Kemnitz, J.W., Roecker, E.B., Weindruch, R., Elson, D.F., Baum, S.T., and Bergman, R.N. (1994). Dietary restriction increases insulin sensitivity and lowers blood glucose in rhesus monkeys. Am J Physiol *266*, E540-547.

Kenyon, C., Chang, J., Gensch, E., Rudner, A., and Tabtiang, R. (1993). A C. elegans mutant that lives twice as long as wild type. Nature *366*, 461-464.

Klass, M.R. (1977). Aging in the nematode Caenorhabditis elegans: major biological and environmental factors influencing life span. Mech Ageing Dev *6*, 413-429.

Koc, A., Gasch, A.P., Rutherford, J.C., Kim, H.Y., and Gladyshev, V.N. (2004). Methionine sulfoxide reductase regulation of yeast lifespan reveals reactive oxygen species-dependent and -independent components of aging. Proc Natl Acad Sci U S A *101*, 7999-8004.

Korshunov, S.S., Skulachev, V.P., and Starkov, A.A. (1997). High protonic potential actuates a mechanism of production of reactive oxygen species in mitochondria. FEBS Lett *416*, 15-18.

Kugler, P., Vogel, S., Volk, H., and Schiebler, T.H. (1988). Cytochrome oxidase histochemistry in the rat hippocampus. A quantitative methodological study. Histochemistry *89*, 269-275.

Kushnareva, Y., Murphy, A.N., and Andreyev, A. (2002). Complex I-mediated reactive oxygen species generation: modulation by cytochrome c and NAD(P)+ oxidation-reduction state. Biochem J *368*, 545-553.

Lakatta, E.G. (2003). Arterial and cardiac aging: major shareholders in cardiovascular disease enterprises: Part III: cellular and molecular clues to heart and arterial aging. Circulation *107*, 490-497.

Lambert, A.J., and Merry, B.J. (2004). Effect of caloric restriction on mitochondrial reactive oxygen species production and bioenergetics: reversal by insulin. Am J Physiol Regul Integr Comp Physiol *286*, R71-79.

Lambert, A.J., Wang, B., Yardley, J., Edwards, J., and Merry, B.J. (2004). The effect of aging and caloric restriction on mitochondrial protein density and oxygen consumption. Exp Gerontol *39*, 289-295.

Lane, M.A., Baer, D.J., Rumpler, W.V., Weindruch, R., Ingram, D.K., Tilmont, E.M., Cutler, R.G., and Roth, G.S. (1996). Calorie restriction lowers body temperature in rhesus monkeys, consistent with a postulated anti-aging mechanism in rodents. Proc Natl Acad Sci U S A *93*, 4159-4164.

Lane, M.A., Ball, S.S., Ingram, D.K., Cutler, R.G., Engel, J., Read, V., and Roth, G.S. (1995). Diet restriction in rhesus monkeys lowers fasting and glucose-stimulated glucoregulatory end points. Am J Physiol *268*, E941-948.

Lass, A., Sohal, B.H., Weindruch, R., Forster, M.J., and Sohal, R.S. (1998). Caloric restriction prevents age-associated accrual of oxidative damage to mouse skeletal muscle mitochondria. Free Radic Biol Med *25*, 1089-1097.

Lillig, C.H., and Holmgren, A. (2007). Thioredoxin and related molecules--from biology to health and disease. Antioxid Redox Signal *9*, 25-47.

Lindeman, R.D., Tobin, J., and Shock, N.W. (1985). Longitudinal studies on the rate of decline in renal function with age. J Am Geriatr Soc *33*, 278-285.

Livesey, G., and Elia, M. (1988). Estimation of energy expenditure, net carbohydrate utilization, and net fat oxidation and synthesis by indirect calorimetry: evaluation of errors with special reference to the detailed composition of fuels. Am J Clin Nutr *47*, 608-628.

Longo, V.D., Gralla, E.B., and Valentine, J.S. (1996). Superoxide dismutase activity is essential for stationary phase survival in Saccharomyces cerevisiae. Mitochondrial production of toxic oxygen species in vivo. J Biol Chem *271*, 12275-12280.

Looker, A.C., Orwoll, E.S., Johnston, C.C., Jr., Lindsay, R.L., Wahner, H.W., Dunn, W.L., Calvo, M.S., Harris, T.B., and Heyse, S.P. (1997). Prevalence of low femoral bone density in older U.S. adults from NHANES III. J Bone Miner Res *12*, 1761-1768.

Lopez-Lluch, G., Hunt, N., Jones, B., Zhu, M., Jamieson, H., Hilmer, S., Cascajo, M.V., Allard, J., Ingram, D.K., Navas, P., *et al.* (2006). Calorie restriction induces mitochondrial biogenesis and bioenergetic efficiency. Proc Natl Acad Sci U S A *103*, 1768-1773.

MacLellan, J.D., Gerrits, M.F., Gowing, A., Smith, P.J., Wheeler, M.B., and Harper, M.E. (2005). Physiological increases in uncoupling protein 3 augment fatty acid oxidation and decrease reactive oxygen species production without uncoupling respiration in muscle cells. Diabetes *54*, 2343-2350.

Mannella, C.A., Marko, M., and Buttle, K. (1997). Reconsidering mitochondrial structure: new views of an old organelle. Trends Biochem Sci *22*, 37-38.

Martins Chaves, M., Prates Rodrigues, A.L., Pereira dos Reis, A., Gerzstein, N.C., and Nogueira-Machado, J.A. (2002). Correlation between NADPH oxidase and protein kinase C in the ROS production by human granulocytes related to age. Gerontology *48*, 354-359.

Marzetti, E., Lawler, J.M., Hiona, A., Manini, T., Seo, A.Y., and Leeuwenburgh, C. (2008). Modulation of age-induced apoptotic signaling and cellular remodeling by exercise and calorie restriction in skeletal muscle. Free Radic Biol Med *44*, 160-168.

Mazat, J.P., Rossignol, R., Malgat, M., Rocher, C., Faustin, B., and Letellier, T. (2001). What do mitochondrial diseases teach us about normal mitochondrial functions...that we already knew: threshold expression of mitochondrial defects. Biochim Biophys Acta *1504*, 20-30.

McKiernan, S.H., Bua, E., McGorray, J., and Aiken, J. (2004). Early-onset calorie restriction conserves fiber number in aging rat skeletal muscle. FASEB J *18*, 580-581.

Michael, M.D., Kulkarni, R.N., Postic, C., Previs, S.F., Shulman, G.I., Magnuson, M.A., and Kahn, C.R. (2000). Loss of insulin signaling in hepatocytes leads to severe insulin resistance and progressive hepatic dysfunction. Mol Cell *6*, 87-97.

Miwa, S., St-Pierre, J., Partridge, L., and Brand, M.D. (2003). Superoxide and hydrogen peroxide production by Drosophila mitochondria. Free Radic Biol Med *35*, 938-948.

Moskovitz, J., Bar-Noy, S., Williams, W.M., Requena, J., Berlett, B.S., and Stadtman, E.R. (2001). Methionine sulfoxide reductase (MsrA) is a regulator of antioxidant defense and lifespan in mammals. Proc Natl Acad Sci U S A *98*, 12920-12925.

Muller, F.L., Liu, Y., and Van Remmen, H. (2004). Complex III releases superoxide to both sides of the inner mitochondrial membrane. J Biol Chem *279*, 49064-49073.

Muller, F.L., Song, W., Liu, Y., Chaudhuri, A., Pieke-Dahl, S., Strong, R., Huang, T.T., Epstein, C.J., Roberts, L.J., 2nd, Csete, M., *et al.* (2006). Absence of CuZn superoxide dismutase leads to elevated oxidative stress and acceleration of age-dependent skeletal muscle atrophy. Free Radic Biol Med *40*, 1993-2004.

Nicholls, D.G. (1974). The influence of respiration and ATP hydrolysis on the proton-electrochemical gradient across the inner membrane of rat-liver mitochondria as determined by ion distribution. Eur J Biochem *50*, 305-315.

Nicholls, D.G., and Locke, R.M. (1984). Thermogenic mechanisms in brown fat. Physiol Rev *64*, 1-64.

Nisoli, E., Tonello, C., Cardile, A., Cozzi, V., Bracale, R., Tedesco, L., Falcone, S., Valerio, A., Cantoni, O., Clementi, E., *et al.* (2005). Calorie restriction promotes mitochondrial biogenesis by inducing the expression of eNOS. Science *310*, 314-317.

Okado-Matsumoto, A., and Fridovich, I. (2001). Subcellular distribution of superoxide dismutases (SOD) in rat liver: Cu,Zn-SOD in mitochondria. J Biol Chem *276*, 38388-38393.

Pamplona, R., Portero-Otin, M., Requena, J., Gredilla, R., and Barja, G. (2002). Oxidative, glycoxidative and lipoxidative damage to rat heart mitochondrial proteins is lower after 4 months of caloric restriction than in age-matched controls. Mech Ageing Dev *123*, 1437-1446.

Parker, N., Affourtit, C., Vidal-Puig, A., and Brand, M.D. (2008). Energization-dependent endogenous activation of proton conductance in skeletal muscle mitochondria. Biochem J *412*, 131-139.

Parkes, T.L., Elia, A.J., Dickinson, D., Hilliker, A.J., Phillips, J.P., and Boulianne, G.L. (1998). Extension of Drosophila lifespan by overexpression of human SOD1 in motorneurons. Nat Genet *19*, 171-174.

Payne, A.M., Dodd, S.L., and Leeuwenburgh, C. (2003). Life-long calorie restriction in Fischer 344 rats attenuates age-related loss in skeletal muscle-specific force and reduces extracellular space. J Appl Physiol *95*, 2554-2562.

Perez, V.I., Bokov, A., Remmen, H.V., Mele, J., Ran, Q., Ikeno, Y., and Richardson, A. (2009). Is the oxidative stress theory of aging dead? Biochim Biophys Acta.

Perez, V.I., Lew, C.M., Cortez, L.A., Webb, C.R., Rodriguez, M., Liu, Y., Qi, W., Li, Y., Chaudhuri, A., Van Remmen, H., *et al.* (2008). Thioredoxin 2 haploinsufficiency in mice results in impaired mitochondrial function and increased oxidative stress. Free Radic Biol Med *44*, 882-892.

Phillips, J.P., Campbell, S.D., Michaud, D., Charbonneau, M., and Hilliker, A.J. (1989). Null mutation of copper/zinc superoxide dismutase in Drosophila confers hypersensitivity to paraquat and reduced longevity. Proc Natl Acad Sci U S A *86*, 2761-2765.

Ramsey, J.J., Harper, M.E., and Weindruch, R. (2000). Restriction of energy intake, energy expenditure, and aging. Free Radic Biol Med *29*, 946-968.

Reveillaud, I., Phillips, J., Duyf, B., Hilliker, A., Kongpachith, A., and Fleming, J.E. (1994). Phenotypic rescue by a bovine transgene in a Cu/Zn superoxide dismutase-null mutant of Drosophila melanogaster. Mol Cell Biol *14*, 1302-1307.

Reynafarje, B., Costa, L.E., and Lehninger, A.L. (1985). O2 solubility in aqueous media determined by a kinetic method. Anal Biochem *145*, 406-418.

Ricci, R., Sumara, G., Sumara, I., Rozenberg, I., Kurrer, M., Akhmedov, A., Hersberger, M., Eriksson, U., Eberli, F.R., Becher, B., *et al.* (2004). Requirement of JNK2 for scavenger receptor A-mediated foam cell formation in atherogenesis. Science *306*, 1558-1561.

Rolfe, D.F., and Brand, M.D. (1997). The physiological significance of mitochondrial proton leak in animal cells and tissues. Biosci Rep *17*, 9-16.

Rossignol, R., Letellier, T., Malgat, M., Rocher, C., and Mazat, J.P. (2000). Tissue variation in the control of oxidative phosphorylation: implication for mitochondrial diseases. Biochem J *347 Pt 1*, 45-53.

Rossignol, R., Malgat, M., Mazat, J.P., and Letellier, T. (1999). Threshold effect and tissue specificity. Implication for mitochondrial cytopathies. J Biol Chem *274*, 33426-33432.

Roubenoff, R. (2000). Sarcopenic obesity: does muscle loss cause fat gain? Lessons from rheumatoid arthritis and osteoarthritis. Ann N Y Acad Sci *904*, 553-557.

Ruan, H., Tang, X.D., Chen, M.L., Joiner, M.L., Sun, G., Brot, N., Weissbach, H., Heinemann, S.H., Iverson, L., Wu, C.F., *et al.* (2002). High-quality life extension by the enzyme peptide methionine sulfoxide reductase. Proc Natl Acad Sci U S A *99*, 2748-2753.

Sanz, A., Pamplona, R., and Barja, G. (2006). Is the mitochondrial free radical theory of aging intact? Antioxid Redox Signal *8*, 582-599.

Schacterle, G.R., and Pollack, R.L. (1973). A simplified method for the quantitative assay of small amounts of protein in biologic material. Anal Biochem *51*, 654-655.

Schmidt, C.D., Dickman, M.L., Gardner, R.M., and Brough, F.K. (1973). Spirometric standards for healthy elderly men and women. 532 subjects, ages 55 through 94 years. Am Rev Respir Dis *108*, 933-939.

Schriner, S.E., Linford, N.J., Martin, G.M., Treuting, P., Ogburn, C.E., Emond, M., Coskun, P.E., Ladiges, W., Wolf, N., Van Remmen, H., *et al.* (2005). Extension of murine life span by overexpression of catalase targeted to mitochondria. Science *308*, 1909-1911.

Seidell, J.C., Oosterlee, A., Deurenberg, P., Hautvast, J.G., and Ruijs, J.H. (1988). Abdominal fat depots measured with computed tomography: effects of degree of obesity, sex, and age. Eur J Clin Nutr *42*, 805-815.

Seligman, A.M., Wasserkrug, H.L., Deb, C., and Hanker, J.S. (1968). Osmium-containing compounds with multiple basic or acidic groups as stains for ultrastructure. J Histochem Cytochem *16*, 87-101.

Shabalina, I.G., Kramarova, T.V., Nedergaard, J., and Cannon, B. (2006). Carboxyatractyloside effects on brown-fat mitochondria imply that the adenine nucleotide translocator isoforms ANT1 and ANT2 may be responsible for basal and fatty-acid-induced uncoupling respectively. Biochem J *399*, 405-414.

Silva, J.P., Shabalina, I.G., Dufour, E., Petrovic, N., Backlund, E.C., Hultenby, K., Wibom, R., Nedergaard, J., Cannon, B., and Larsson, N.G. (2005). SOD2 overexpression: enhanced mitochondrial tolerance but absence of effect on UCP activity. EMBO J *24*, 4061-4070.

Sohal, R.S., Agarwal, A., Agarwal, S., and Orr, W.C. (1995). Simultaneous overexpression of copper- and zinc-containing superoxide dismutase and catalase retards age-related oxidative damage and increases metabolic potential in Drosophila melanogaster. J Biol Chem *270*, 15671-15674.

Spencer, C.C., Howell, C.E., Wright, A.R., and Promislow, D.E. (2003). Testing an 'aging gene' in long-lived drosophila strains: increased longevity depends on sex and genetic background. Aging Cell *2*, 123-130.

Sreekumar, R., Unnikrishnan, J., Fu, A., Nygren, J., Short, K.R., Schimke, J., Barazzoni, R., and Nair, K.S. (2002). Effects of caloric restriction on mitochondrial function and gene transcripts in rat muscle. Am J Physiol Endocrinol Metab *283*, E38-43.

St-Pierre, J., Buckingham, J.A., Roebuck, S.J., and Brand, M.D. (2002). Topology of superoxide production from different sites in the mitochondrial electron transport chain. J Biol Chem *277*, 44784-44790.

Staron, R.S., Hagerman, F.C., Hikida, R.S., Murray, T.F., Hostler, D.P., Crill, M.T., Ragg, K.E., and Toma, K. (2000). Fiber type composition of the vastus lateralis muscle of young men and women. J Histochem Cytochem *48*, 623-629.

Sun, J., Folk, D., Bradley, T.J., and Tower, J. (2002). Induced overexpression of mitochondrial Mn-superoxide dismutase extends the life span of adult Drosophila melanogaster. Genetics *161*, 661-672.

Sun, J., Molitor, J., and Tower, J. (2004). Effects of simultaneous over-expression of Cu/ZnSOD and MnSOD on Drosophila melanogaster life span. Mech Ageing Dev *125*, 341-349.

Sun, J., and Tower, J. (1999). FLP recombinase-mediated induction of Cu/Zn-superoxide dismutase transgene expression can extend the life span of adult Drosophila melanogaster flies. Mol Cell Biol *19*, 216-228.

Talbot, D.A., and Brand, M.D. (2005). Uncoupling protein 3 protects aconitase against inactivation in isolated skeletal muscle mitochondria. Biochim Biophys Acta *1709*, 150-156.

Talbot, D.A., Lambert, A.J., and Brand, M.D. (2004). Production of endogenous matrix superoxide from mitochondrial complex I leads to activation of uncoupling protein 3. FEBS Lett *556*, 111-115.

Tantisira, K.G., Colvin, R., Tonascia, J., Strunk, R.C., Weiss, S.T., and Fuhlbrigge, A.L. (2008). Airway responsiveness in mild to moderate childhood asthma: sex influences on the natural history. Am J Respir Crit Care Med *178*, 325-331.

Tatar, M., Kopelman, A., Epstein, D., Tu, M.P., Yin, C.M., and Garofalo, R.S. (2001). A mutant Drosophila insulin receptor homolog that extends life-span and impairs neuroendocrine function. Science *292*, 107-110.

Thomas, D.R. (2007). Loss of skeletal muscle mass in aging: examining the relationship of starvation, sarcopenia and cachexia. Clin Nutr *26*, 389-399.

Tiraby, C., Tavernier, G., Capel, F., Mairal, A., Crampes, F., Rami, J., Pujol, C., Boutin, J.A., and Langin, D. (2007). Resistance to high-fat-diet-induced obesity and

sexual dimorphism in the metabolic responses of transgenic mice with moderate uncoupling protein 3 overexpression in glycolytic skeletal muscles. Diabetologia *50*, 2190-2199.

Tolkovsky, A.M. (2009). Mitophagy. Biochim Biophys Acta *1793*, 1508-1515.

Tsai, L., Szweda, P.A., Vinogradova, O., and Szweda, L.I. (1998). Structural characterization and immunochemical detection of a fluorophore derived from 4-hydroxy-2-nonenal and lysine. Proc Natl Acad Sci U S A *95*, 7975-7980.

Turrens, J.F. (1997). Superoxide production by the mitochondrial respiratory chain. Biosci Rep *17*, 3-8.

Turrens, J.F. (2003). Mitochondrial formation of reactive oxygen species. J Physiol *552*, 335-344.

Vidal-Puig, A., Solanes, G., Grujic, D., Flier, J.S., and Lowell, B.B. (1997). UCP3: an uncoupling protein homologue expressed preferentially and abundantly in skeletal muscle and brown adipose tissue. Biochem Biophys Res Commun *235*, 79-82.

Vidal-Puig, A.J., Grujic, D., Zhang, C.Y., Hagen, T., Boss, O., Ido, Y., Szczepanik, A., Wade, J., Mootha, V., Cortright, R., *et al.* (2000). Energy metabolism in uncoupling protein 3 gene knockout mice. J Biol Chem *275*, 16258-16266.

Votyakova, T.V., and Reynolds, I.J. (2001). DeltaPsi(m)-Dependent and -independent production of reactive oxygen species by rat brain mitochondria. J Neurochem *79*, 266-277.

Walford, R.L., Mock, D., MacCallum, T., and Laseter, J.L. (1999). Physiologic changes in humans subjected to severe, selective calorie restriction for two years in biosphere 2: health, aging, and toxicological perspectives. Toxicol Sci *52*, 61-65.

Wang, M.C., Bohmann, D., and Jasper, H. (2005). JNK extends life span and limits growth by antagonizing cellular and organism-wide responses to insulin signaling. Cell *121*, 115-125.

Wawryn, J., Krzepilko, A., Myszka, A., and Bilinski, T. (1999). Deficiency in superoxide dismutases shortens life span of yeast cells. Acta Biochim Pol *46*, 249-253.

Weindruch, R., Walford, R.L., Fligiel, S., and Guthrie, D. (1986). The retardation of aging in mice by dietary restriction: longevity, cancer, immunity and lifetime energy intake. J Nutr *116*, 641-654.

Weinert, B.T., and Timiras, P.S. (2003). Invited review: Theories of aging. J Appl Physiol *95*, 1706-1716.

Wiseman, H., and Halliwell, B. (1996). Damage to DNA by reactive oxygen and nitrogen species: role in inflammatory disease and progression to cancer. Biochem J *313 (Pt 1)*, 17-29.

Zangarelli, A., Chanseaume, E., Morio, B., Brugere, C., Mosoni, L., Rousset, P., Giraudet, C., Patrac, V., Gachon, P., Boirie, Y., *et al.* (2006). Synergistic effects of caloric restriction with maintained protein intake on skeletal muscle performance in 21-month-old rats: a mitochondria-mediated pathway. FASEB J *20*, 2439-2450.

Zhang, Z., Huang, L., Shulmeister, V.M., Chi, Y.I., Kim, K.K., Hung, L.W., Crofts, A.R., Berry, E.A., and Kim, S.H. (1998). Electron transfer by domain movement in cytochrome bc1. Nature *392*, 677-684.

CURRICULUM VITAE

CARMEN ESTEY

FORMAL EDUCATION

M.Sc.	**University of Ottawa, Faculty of Medicine, 2009** *Department of Biochemistry, Microbiology and Immunology (BMI)* Supervisor: Dr. Mary-Ellen Harper Thesis: Mitochondrial uncoupling and remodelling during caloric restriction: Implications for oxidative stress and ageing
B.Sc. (Honors)	**University of Ottawa, Faculty of Science, 2007** *Department of Biopharmaceutical Science (Genomics option)*
O.S.S.D	**St. Mark High School, 2003**

TEACHING AND RESEARCH EXPERIENCE

Sept 2007 – Present	**M.Sc. (Biochemistry) candidate** *University of Ottawa, Faculty of Medicine, Department of BMI* *Supervisor: Dr. Mary-Ellen Harper* *Thesis: Mitochondrial uncoupling and remodelling during caloric restriction: Implications for oxidative stress and ageing*
Jan – May 2009 Jan – May 2008	**Teaching Assistant** *University of Ottawa, Faculty of Science* - Responsible for answering students questions, marking exams and entering marks into spreadsheet for the 2nd year Introduction to Metabolism course
May 2007 – Aug 2007	**Summer student**

University of Ottawa, Faculty of Medicine, Department of BMI
Supervisor: Dr. Mary-Ellen Harper

- Conducted research for various projects on a daily basis
- Analyzed research data
- Attended and participated in weekly journal club sessions

Aug 2006 – May 2007 **Honors student**
University of Ottawa, Faculty of Medicine, Department of BMI
Supervisor: Dr. Mary-Ellen Harper
Thesis: The relationship between mitochondrial fatty acid supply and hydrogen peroxide generation: Does fat make you radical?

ACADEMIC AWARDS

Sept 2003 – Apr 2004 **University of Ottawa Entrance Scholarship**
- $1,500

Sept 2003 – Apr 2004 **Queen Elizabeth II aiming for the top scholarship**
- In recognition of outstanding academic achievement in OAC (~$1,000)

RESEARCH AWARDS

May 2008 **Dept. Biochemistry, Microbiology and Immunology**
Graduate Student Poster Day
- Best visual poster presentation

VOLUNTEER EXPERIENCE

SCIENCE PROMOTION

Sept 2008 – May 2009 **Let's Talk Science Representative**
University of Ottawa

POSTER PRESENTATIONS

October 2009 — **The North American Association for the Study of Obesity (NAASO)**
Annual Meeting; Washington, DC
Abstract: Uncoupling protein-3 can mitigate oxidative stress by a membrane potential-independent mechanism
- Co-author

Apr 2009 — **The 2009 Annual Meeting of the American Experimental Biology Societies**
Annual Meeting; New Orleans, LA
Abstract: Mitochondrial uncoupling and remodelling during caloric restriction: Implications for oxidative stress and aging.
- First author

Oct 2007 — **The North American Association for the Study of Obesity (NAASO)**
Annual Meeting; New Orleans, LA
Abstract: Effect of fatty acid supply on reactive oxygen species production in skeletal muscle mitochondria: Does fat make you radical?
- Co-author

May 2007 — **5th Meeting of the Canadian Oxidative Stress Consortium**
Montreal, QC
Abstract: Skeletal muscle mitochondria respiring under resting conditions generate matrix hydrogen peroxide when metabolizing high but not low levels of fatty acids
- Co-author

RESEARCH PUBLICATIONS

PEER REVIEWED ARTICLES

Seifert EL, **ESTEY C**, Xuan JY, Haper ME. Electron transport chain dependent and independent mechanisms of mitochondrial H_2O_2 emission during long-chain fatty acid oxidation. J Biol Chem. Epub 2009 Dec 23.

Seifert EL, Bézaire V, **ESTEY C**, Harper ME. Essential role for uncoupling protein-3 in mitochondrial adaptation to fasting but not in Fatty Acid oxidation or Fatty Acid anion export. J Biol Chem. 2008 Sep 12; 283(37): 25124-31. Epub 2008 Jul 14.

Boily G, Seifert EL, Bevilacqua L, He XH, Sabourin G, **ESTEY C**, Moffat C, Crawford S, Saliba S, Jardine K, Xuan J, Evans M, Harper ME, McBurney MW. SirT1 regulates energy metabolism and response to caloric restriction in mice. PLoS ONE. 2008 Mar 12; 3(3): e1759.

Submitted articles:

Bevilacqua L, Seifert EL, **ESTEY C**, Gerrits MF, Harper ME. Absence of uncoupling protein-3 leads to greater activation of an adenine nucleotide translocase-mediated proton conductance in skeletal muscle mitochondria from calorie restricted mice. Submitted to BBA Bioenergetics (MS#BBABIO-09-134R1) on January 15, 2010.